Climate Impact of Hydrogen Aviation

Research on the variations of surface temperature change caused by hydrogen and kerosene combustion aircraft.

Master's Thesis Report

Miguel Ángel Sáez Ortuño

Delft University of Technology

TU Delft

Climate Impact of Hydrogen Aviation

Research on the variations of surface temperature change caused by hydrogen and kerosene combustion aircraft.

by

Miguel Ángel Sáez Ortuño

Miguel Angel Saez Ortuno 4541235

Supervisor:	Dr. Feijia Yin
Chair:	Prof.dr.ir. Mirjam Snellen
Examiner:	Prof.dr.ir Arvind Gangoli Rao
Institution:	Delft University of Technology
Place:	Faculty of Aerospace Engineering, Delft
Project Duration:	November, 2021 - July, 2022

Cover Image: Image obtained from Roelof Vos, depicting the current Hydrogen Powered Flying-V. Included in the National Geographic's magazine of October.

TU Delft

Preface

I am one of those who believe that nothing can or should be done in isolation. What you are about to read right now may seem the work of one person, or four as I quote on the cover, but there is so much work behind it and so many people who have contributed that I would run out of space if I were to thank them all. First of all, I would like to thank my supervisor and colleague Feijia Yin, for so many hours of meetings and above all, for her generous wisdom. I would also like to thank Pieter-Jan and Roelof Vos, whose help has been second to none and I doubt I could have had better support during this study. I would also like to express my special gratitude to Arvind G. Rao for his inexplicable ability to find mistakes and making this research more interesting. To my parents and siblings, for making the transitions between work and everyday life so much more pleasant. To my girlfriend for believing in me as much as my family, even though her opinion is always a little biased. Finally, to my friends, for being my warmth and shelter, for making the bad times better and the good times even brighter.

Miguel Ángel Sáez Ortuño
Delft, June 2022

Executive Summary

Worried about the impact of climate change, international institutions, nations and other groups are promoting change to reduce emissions and hold the current global temperature increase below 2.0°C compared to pre-industrial times. Aircraft manufacturers must contribute to this effort because the improvements shown by the development trends in aerodynamic and propulsion performance and fleet operations have lead to an insufficient reduction of emissions since 1960, partially due to the large air traffic growth. Hydrogen, which combines high energy density with low carbon emissions, might be the solution the aerospace sector has been looking for, as long as it can overcome some of its shortfalls, like the volume needed for its storage in current commercial aircraft.

However, as specialized literature states, the repercussions on climate impact from hydrogen aviation are not clear, e.g. the radiative forcing from cryogenic contrails is uncertain (Marquart et al., 2005); the bounds for NO_x emissions are broad (Funke et al., 2019); and the impact of these emissions is highly dependent on the flight altitude (Grewe & Stenke, 2008), which by the way will increase for hydrogen aircraft. This study is not meant to solve these uncertainties, but to provide a methodology in which these uncertainties can be adapted and investigated. Therefore, the objective of this study is to create and use a methodology to determine the surface temperature increase caused by a fleet of both hydrogen and kerosene combustion aircraft.

Methodology

This research evaluates the impact on climate change of an aircraft using hydrogen combustion. Figure 1 displays an overview of the research methodology and how information flows through the different modules. Inputs required for the study include the aircraft information to be analyzed and a flight database to create a routing network. Data from two aircraft with a similar mission range and payload are used to understand the surface temperature increase caused by hydrogen and kerosene. The aircraft selected are the hydrogen FZM1G (standard tube-and-wing design) and the kerosene B767S (with improvements added in aerodynamics, weight and engines) from (Beddoes et al., 2022). A flight database (FlightRadar24[1]) is used to extract precise flight datapoints required to investigate non-CO2 effects, which are dependent on latitude and altitude.

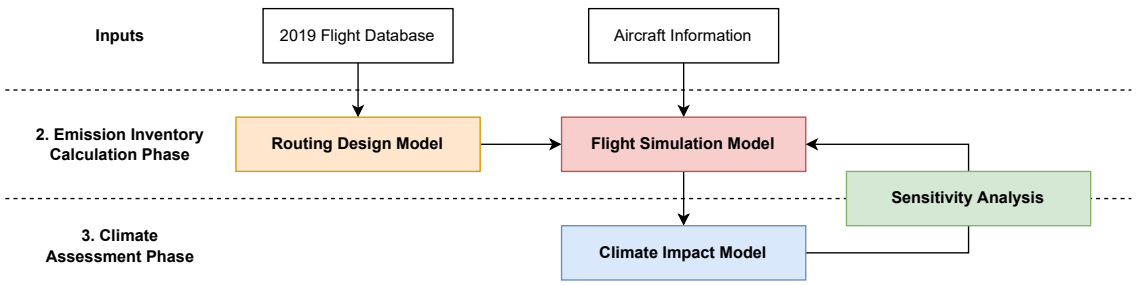

Figure 1: Overview methodology chain for climate assessment of hydrogen and kerosene aircraft composed of different modules differentiated by color.

The routing design then selects the routes to be flown based on flight range, frequency and global coverage. Moreover, it removes non-commercial flights from the database to standardize data. Then, the flight simulation module uses those routes and the aircraft parameters to simulate the flights; when a certain route is selected, total range is used to compute initial weight of the aircraft (Initial Weight Estimator). Next, aircraft speed and rate of climb and descent are used to compute the flight plan (Flight Planner). When the flight iteration begins, the state of the aircraft (angle of attack, speed, flight path angle, weight, etc.) is ran through a module which declares if the aircraft should climb,

[1]FlightRadar24 (2021, November) Live Air Traffic https://www.flightradar24.com

cruise or descend (Auto Pilot). Then the state of the aircraft is ran through the flight dynamics model which updates its status using the energy equations from Eurocontrol (2004). An interpolation over an engine model (created for each aircraft using Proesmans and Vos (2021)) is used to rapidly convert engine thrust in fuel flow. Fuel flow is used to compute NO_x Emission Index ($EINO_x$) at every step of the flight and to update the fuel weight of the aircraft. $EINO_x$ is calculated using the BFFM2 method (Turgut & Usanmaz, 2017). Next, aircraft weight and flown distance are updated. When flown distance equals the total range of the flight, the extra fuel weight is computed (contingency fuel). If fuel remaining is $\pm$ 10 % of required contingency fuel (5% of the consumed fuel), the simulation is finished, and the next route can be analyzed. Finally, when all flights have been simulated, an emission inventory with the following information is created: longitude and latitude, pressure altitude, fuel burn and NO_x emitted, flown distance and flight frequency. The emission inventory will serve as input for the climate assessment model.

The last module observed in Figure 1 is the climate impact module. AirClim is the tool selected to compute final surface temperature increase due to its availability, versatility and climate metric, which provided numerous advantages with respect to other tools as CAST (Planès et al., 2021), MAGICC (Meinshausen et al., 2011) or LinClim (Lim & Lee, 2006). Using any climate impact tool requires a well defined scenario as displayed in Table 1.

Table 1: Scenario assumptions for the hydrogen and kerosene aircraft climate change comparison.

Scenario Parameters	**Value**	**Scenario Parameters**	**Value**
Simulation Start Year	2030	Simulation End Year	2130
B767S (ker) Start Year	2030	FMZ1G (hyd) Start Year	2030
Market Growth BAU (2019-2025)	6.0%	Market Growth BAU (2025-2050)	1.2%
Market Growth BAU (2050-2075)	1.0%	Market Growth BAU (2075-2130)	0.8%

The scenario includes a simulation start and end year, in this case separated by 100 years, a technology start time, which corresponds with the beginning of the simulation, and the market growth over the course of the simulation (Grewe et al., 2021). Simulation cannot be fully realistic because, in order to compare fleets, all of them were introduced in the market simultaneously and instantaneously, with hydrogen technology being fully operational by 2030. It is also important to mention changes introduced in AirClim to account for hydrogen technology in the simulation: radiative forcing of hydrogen contrails is reduced by 69% with respect to kerosene contrails due to the reduction in soot particles; and emission indexes of CO_2 and H_2O become 0 and 9 as observed in Table 2.

Table 2: Hydrogen and kerosene species adaptations for AirClim.

Fuel	Contrail RF Change (Soot)	$EICO_2$	EIH_2O
Kerosene	-	3.155	1.25
Hydrogen	- 69%	0	9

Results & Discussion

From the routing design module, 1128 city-pairs that satisfied the route requirements are chosen, for a total of 2.24 million flights. These flights are unevenly distributed in latitude: 78% on temperate areas, 21 % on the Tropics and less than 1 % on frigid areas. Emissions of the two aircraft analyzed in the study are displayed in Table 3. It can be observed that the fuel consumption of the kerosnee B767S is 2.48 times larger than the hydrogen FZM1G due to the higher energy density of hydrogen fuel. $EINO_x$ is reduced from 13.1 to 10.8 because the engine is able to use the lower lean limit of hydrogen. CO_2 is completely removed for the hydrogen aircraft while H_2O emissions are almost tripled.

Table 3: Species emitted and fuel used by the FZM1G and B767S.

Aircraft	Fuel	NO_x	$EINO_x$		CO_2	$EICO_2$		H_2O	EIH_2O	
	Mt	kt	g/kg	g/MJ	Mt	kg/kg	kg/MJ	Mt	kg/kg	kg/MJ
FZM1G	16.7	179	10.8	0.0898	0	0	0	150	9	0.075
B767S	41.5	544	13.1	0.305	131	3.155	0.734	51.8	1.25	0.029

These emissions can be transformed into surface temperature change using AirClim, which also uses them to generate data on contrails and their effects. Figure 2 displays surface temperature increase by 2130 for emissions and contrails. As it can be observed, effects of hydrogen aviation on temperature rise are lower than those of kerosene aviation, with several considerations. Contrail effects are the largest individual contributor to climate change for both kerosene and hydrogen aircraft, followed by CO_2 in the case of the B767S and NO_x in the case of hydrogen aviation (FZM1G). H_2O effect on climate change from hydrogen aviation is 4.7 times higher than that from kerosene aviation, due to the higher emission index of H_2O of hydrogen combustion.

The lower effect of hydrogen contrails in surface temperature is caused by its lower contrail radiative forcing (69%); the difference between hydrogen and kerosene contrails effect on climate would be further enlarged if hydrogen aircraft flew at lower altitudes. NO_x influence is 67% lower in the case of Hydrogen because of the reduction in NO_x due to the higher energy density of hydrogen and the reduction in $EINO_x$ that takes advantage of the lower lean limit of hydrogen in the combustion chamber.

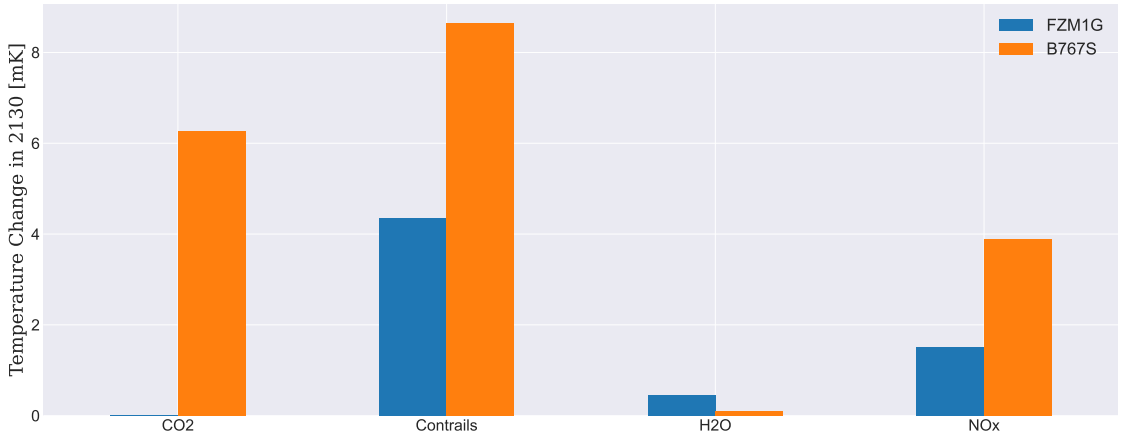

Figure 2: Contribution to surface temperature increase from each of the species per aircraft model.

Adding the individual contributions of the species, hydrogen aviation effect on temperature change is 12.6 mK lower than that of kerosene aviation (18.9 vs 6.3 mK, a 1/3 ratio). But analyzing trend over time is also important: in Figure 3 it can be observed how the hydrogen aircraft temperature change slope (FZM1G) is less steep over time, while the kerosene aircraft slope (B767S) remains steep. This difference is due to the cumulative nature of CO_2 emissions, which are non-existent for the hydrogen aircraft.

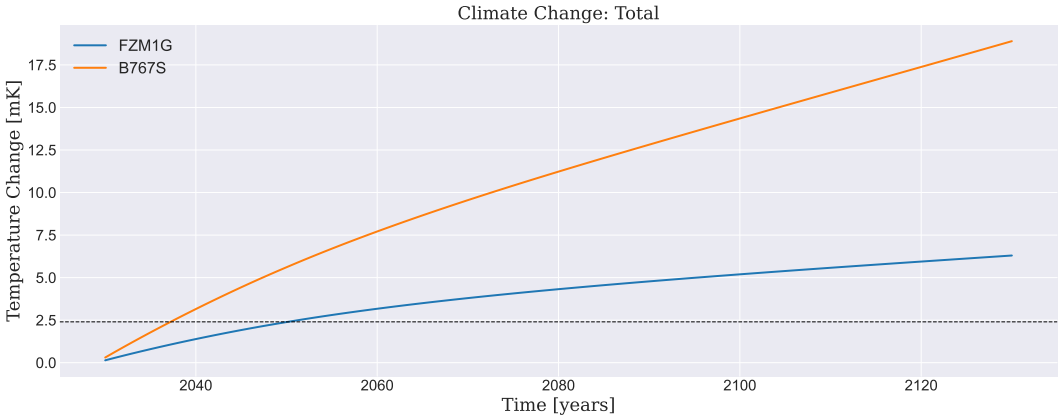

Figure 3: Change in average surface temperature for the FMZ1G and B767S aircraft. The dashed line corresponds to the maximum temperature increase the aircraft can cause to meet the Paris Agreement.

The non-CO_2 geographic effects were also investigated for each aircraft. Table 4 displays temperature change caused by aircraft flying over specific latitudes. It can be observed that temperature increase caused by hydrogen aircraft is larger than that of kerosene aircraft above the Tropics (14% vs. 12.7%). This is due to the higher cruise altitude of hydrogen aircraft, which translates in a higher contrail probability of formation. In frigid areas, this effect is the opposite, because of the lower limit of contrail formation probability, as observed in Figure 4.

Table 4: Temperature increases caused by the FZM1G and B767S at different latitudes.

	Frigid		**Temperate**		**Tropics**	
Parameter	**ATR**	**%**	**ATR**	**%**	**ATR**	**%**
Unit	**mK**	**-**	**mK**	**-**	**mK**	**-**
FZM1G	0.0820	1.3	5.34	84.7	0.883	14.0
B767S	0.309	1.63	16.2	85.6	2.41	12.7

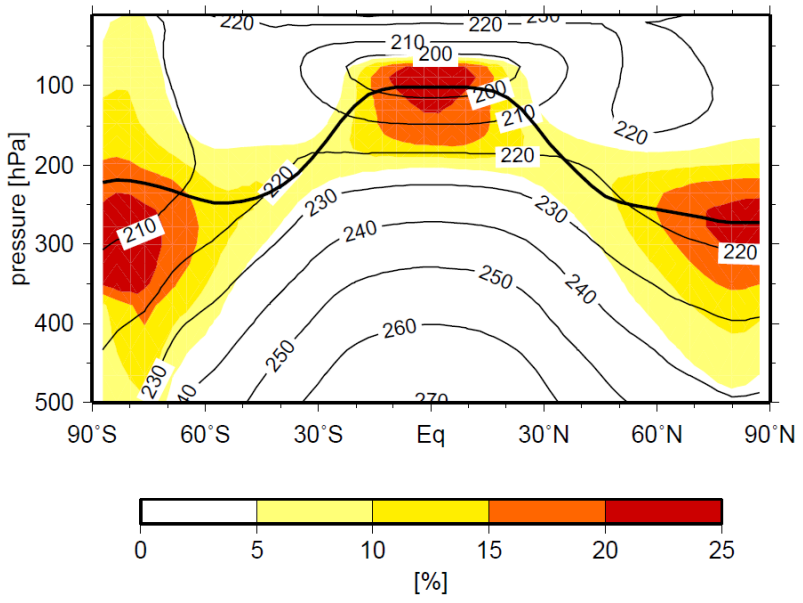

Figure 4: Probability of contrail formation when varying altitude and latitude (Grewe & Stenke, 2008).

Two study cases were proposed in this study: the first one considers an alternative aircraft, the Flying-V, either kerosene powered (named FV8) or hydrogen powered (named FVHY). The second proposes a more realistic scenario, where the kerosene B767S and the FZM1G previously mentioned, are introduced in the market in 2030 and 2050 respectively.

The results of the first study case show that both Flying-V aircraft are comparable in terms of fuel consumption to their respective competitors (FZM1G vs. FVHY and B767S vs. FV8) as observed in Table 5. However, the larger wing area of the Flying-V technology requires these alternative designs to fly at a higher altitude, which causes a detrimental effect on climate as observed in Figure 5.

Table 5: Species emitted and fuel used by the tube-and-wing and Flying-V aircraft.

Aircraft	Fuel	NO_x	$EINO_x$		CO_2	$EICO_2$		H_2O	EIH_2O	
	Mt	kt	g/kg	g/MJ	Mt	kg/kg	kg/MJ	Mt	kg/kg	kg/MJ
FZM1G	16.7	191	11.5	0.0958	0	0	0	150	9	0.075
B767S	41.5	544	13.1	0.305	131	3.155	0.734	51.8	1.25	0.029
FV8	42.9	669	15.6	0.363	135	3.155	0.734	53.6	1.25	0.029
FVHY	16.2	206	12.7	0.106	0	0	0	146	9	0.075

Figure 5 shows how the effects of NO_x, contrails and H_2O of the Flying-V aircraft are magnified due to the higher cruise altitude. Although the NO_x emitted by the FVHY is similar to the NO_x emitted by the FZM1G, the higher altitude of the FVHY increases the surface temperature change by 5 mK. Overall, the surface temperature increase for the kerosene Flying-V compared with the kerosene B767S is 95% (18.0 mK). For the hydrogen Flying-V, the total temperature increase with respect to the FZ1MG is 134% (8.45 mK).

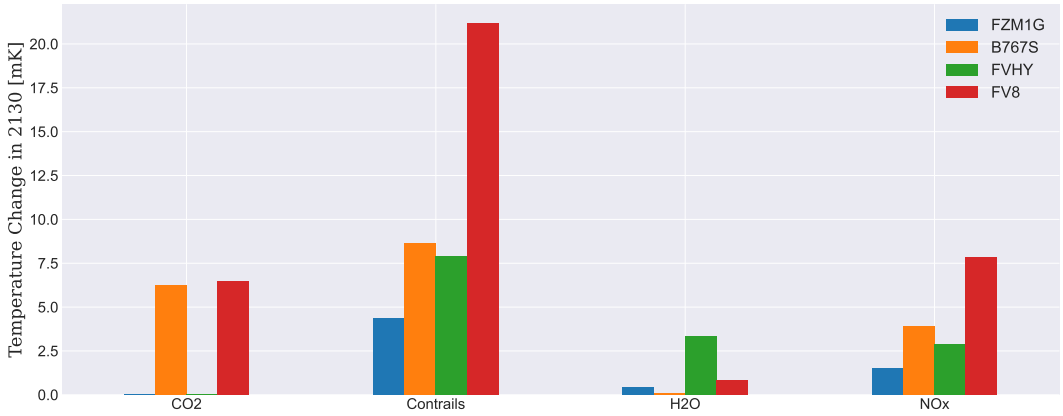

Figure 5: Contribution to average surface temperature from each of the species for the tube-and-wing aircraft and the Flying-Vs with the improved engine.

In the second study case a new baseline aircraft is introduced to represent current aviation (B767ER), also used by Beddoes et al. (2022). As observed in Figure 6, in 2130, 100 years after the introduction of the B767S, the surface temperature change with respect to the baseline aircraft is 33% lower. Moreover, the hydrogen aircraft (FZM1G) temperature change is 78% lower than the baseline aircraft after 100 years of flying (2050-2150).

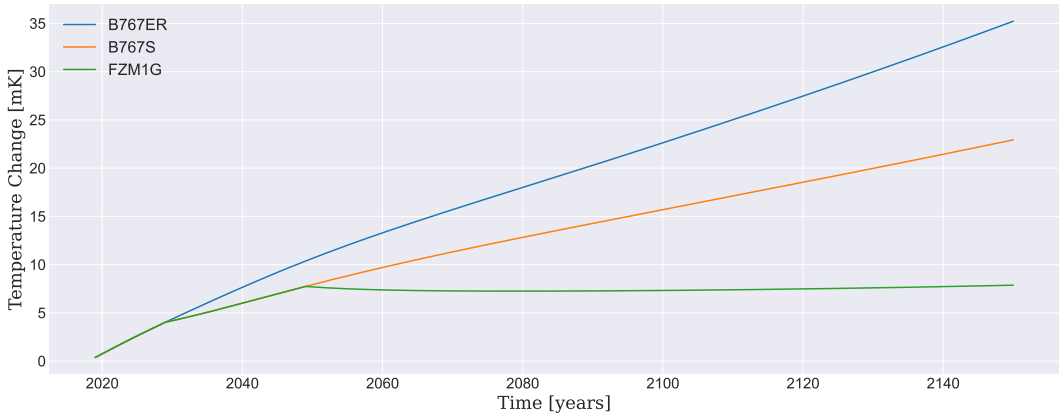

Figure 6: Surface temperature increase caused by the B767S, FZM1G and B767ER, where the B767S is introduced in 2030 and the FZM1G in 2050.

Many uncertainties and deviations in literature exist when measuring climate impact from hydrogen, which have to do with $EINO_x$ hydrogen reduction and hydrogen contrails radiative forcing. This study assumes a hydrogen contrail radiative forcing reduction with respect to kerosene of 69% (Burkhardt et al., 2018) due to soot reduction. However Marquart et al. (2005) considers percentages ranging from -30% to 30%. This study also assumes a 0.75 $EINO_x$ ratio of hydrogen to kerosene (Carter, 2021), even though Funke et al. (2019) says it can be reduced to 0.1 if using micromix combustion or even increased to 1.3 if the lower lean limit of hydrogen combustion is not used.

To account for all these uncertainties, a sensitive study has been carried out where worst (30% increase in hydrogen contrails radiating forcing and 1.3 $EINO_x$ hydrogen ratio) and best case scenarios (69% decrease in hydrogen contrails radiating forcing and 0.1 $EINO_x$ hydrogen ratio) have been analyzed for hydrogen aircraft (Figure 7). The green area unites these bounds for the hydrogen aircraft (FZM1G). It can be noted that the worst case scenario creates a slightly higher climate warming than the B767S kerosene aircraft until 2100, however, beyond that year, temperature change is lower than the kerosene aircraft. The difference is again due to the cumulative nature of the CO_2 emissions.

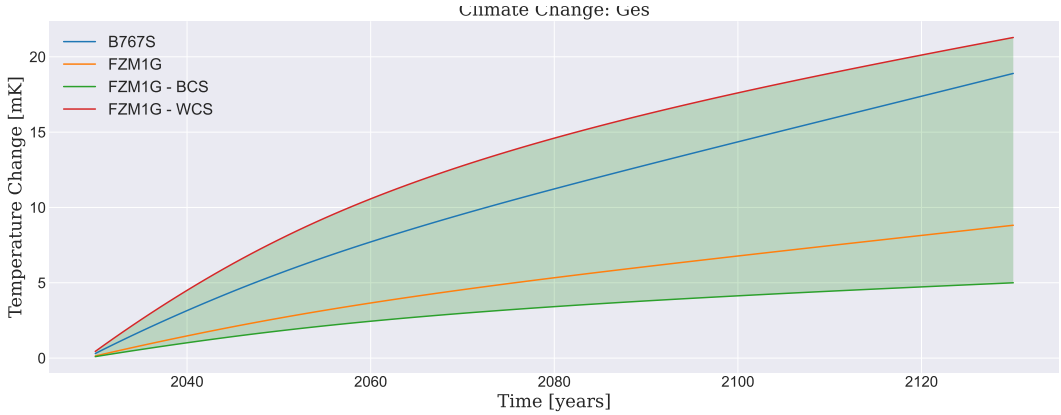

Figure 7: Surface temperature increase caused by the B767S and FZM1G. Including a best and worst case scenario (BCS, WCS) for the later.

The sensitivity study also includes the analysis of flight altitude variations. The higher the cruise altitude, the lower the fuel consumption, however, as it has been noted before, a higher altitude comes at a cost, which is a higher impact on surface temperature change. Results show that the increase in surface temperature with altitude was higher for the kerosene aircraft than for the hydrogen aircraft.

Conclusions

This study develops a methodology to model and compare emissions and surface temperature change (climate impact) of hydrogen and non-hydrogen aircraft flying defined flight plans. Results show benefits for hydrogen aviation when compared to kerosene aviation:

- Lower fuel consumption: 16.7 megatons of hydrogen compared to 41.5 megatons of kerosene.
- Lower surface temperature increase: 6.3 mK for hydrogen models compared to 18.9 mK for kerosene models.
- Lower climate susceptibility to cruise altitude: climate wise, hydrogen aircraft always perform better than kerosene aircraft when flying at the same altitude. Variation delta with altitude is also lower.
- Non-cumulative effects of hydrogen emissions: evolution with time shows better results than kerosene powered aircraft due to lack of CO_2 effects.

Disadvantages of hydrogen relate to altitude and geographical location. Lighter hydrogen powered aircraft must use higher altitudes, and even though they perform better compared to kerosene, it has an impact on surface temperature. This is more notable when flying in tropical regions due to higher contrail probability of formation at higher altitudes.

At the end of the study, I believe that hydrogen combustion has the potential to become a new milestone in the development of a much more sustainable aviation. We have demonstrated that even the worst case situation for hydrogen aircraft is advantageous with respect to kerosene aviation. However, aviation on its own will not cure all environmental problems, since humanity as a whole is still far from meeting the Paris Agreement Goals.

Contents

Nomenclature

Abbreviations

Abbreviation	Definition	Topic
ATR	Average Temperature Response	Emissions & Climate
BAU	Business As Usual	Emissions & Climate
BWB	Blended Wing Body	Aircraft & Performance
CAD	Computer Aided Design	Software
CASK	Cost of Available Seat Kilometer	Economics
ERF	Effective Radiative Forcing	Emissions & Climate
FPR	Fan Pressure Ratio	Aircraft & Performance
GHG	Green House Gases	Emissions & Climate
GTP	Global Temperature change Potential	Emissions & Climate
GWP	Global Warming Potential	Emissions & Climate
KBE	Knowledge-Based Engineering	Software
MPW	Maximum Payload Weight	Aircraft & Performance
MTOW	Maximum Take Off Weight	Aircraft & Performance
OEO	One Engine Operative	Aircraft & Performance
OEW	Operative Empty Weight	Aircraft & Performance
OPR	Overall Pressure Ratio	Aircraft & Performance
PAH	Polycyclic Aromatic Hydrocarbon	Emissions & Climate
RF	Radiative Forcing	Emissions & Climate
ROCD	Rate Of Climb and Descend	Aircraft & Performance
RPK	Revenue Passenger Kilometers	Economics
SLCP	Short-Lived Climate Pollutant	Emissions & Climate
STC	Surface Temperature Change & Climate	
TIT	Turbine Inlet Temperature	Aircraft & Performance
TSFC	Thrust Specific Fuel Consumption	Aircraft & Performance
UHC	Unburnt Hydrocarbons	Emissions & Climate
UV	Ultra Violet	Emissions & Climate

Symbols

Symbol	Definition	Unit
a	Stoichiometric Coefficient of the Oxidizer	$[-]$
b	Span	$[m]$

Symbol	Definition	Unit
C_D	Drag Coefficient	$[-]$
$C_{D,0}$	Zero-Lift Drag Coefficient	$[-]$
C_L	Lift Coefficient	$[-]$
c	Chord	$[m]$
c_j	Specific Fuel Consumption	$[kg/Ns]$
c_p	Constant Pressure Specific Heat	$[kJ/kgK]$
D	Drag	$[N]$
G	Mixing Gas Slope	$[Pa/°C]$
G_r	Green's Function for the Near Surface Temperature Response	$[-]$
g_0	Gravitational Acceleration of the Earth	$[m/s^2]$
H	Time Horizon	$[years]$
I	Humidity Factor	$[-]$
h	Altitude	$[m]$
k	Lift-Induced Drag Coefficient Factor	$[-]$
L	Lift	$[N]$
l	Length	$[m]$
M	Mach Speed	$[-]$
$\dot{m}$	Mass Flow	$[kg/s]$
N_{eng}	Number of Engines	$[-]$
P	Ambient Pressure	$[Pa]$
P_{t_3}	Pressure Combustion Chamber	$[Pa]$
p_3	Pressure Combustion Chamber	$[psia]$
Q	Fuel Specific Heat	$[kJ/kg]$
R	Range	$[km]$
S_{ref}	Wing Area	$[m^2]$
T	Thrust	$[N]$
t	time	$[s]$
W	Weight	$[N]$
$W_{\text{f,c}}$	Weight Fuel Contingency	$[N]$
$W_{\text{f,rec,c}}$	Weight Required Fuel Contingency	$[N]$
$W_{\text{f,used}}$	Weight Fuel Used	$[N]$
W_{pay}	Payload Weight	$[N]$
V	Flight Velocity	$[m/s]$
z	Chemical Composition of Air	$[-]$
γ	Flight Path Angle	$[°]$
Δ_{in}	Flying-V Fuselage Sweep	$[°]$
Δ_{out}	Flying-V Wing Sweep	$[°]$
Δ_{pm}	Change in Soot Particles	$[-]$
δ_{amb}	Pressure Dimensional Coefficient	$[-]$
η	Overall Propulsion Efficiency	$[-]$

Symbol	Definition	Unit
θ_{amb}	Temperature Dimensional Coefficient	$[-]$
ϵ	Ratio of the molar masses of water and air	$[-]$
ρ	Density	$[kg/m^3]$

List of Figures

List of Tables

1 Introduction

Concerned about rapidly rising temperatures, international institutions, nations and companies around the world are studying every day how to reduce emissions in all economic sectors. Aerospace is one of the only industries whose emissions are released both at the earth's surface and in the upper troposphere. Despite the small number of emissions compared to other transportation sectors, emissions at higher altitudes have a greater impact on the climate (Grewe et al., 2017b). The fragility of the climate with respect to higher altitude emissions drives the aerospace industry to mitigate emissions by seeking alternatives to the methods currently used. Some of the solutions used by the industry include aerodynamic and propulsion improvements and changes in fleet operations (Zheng & Rutherford, 2020), however it has been shown that these proposals are not sufficient to fight climate change and meet the 2.0°C maximum increase proposed by the Paris Agreement (Delbeke et al., 2019), as demand for air transport is expected to increase exponentially in the coming decades[1]. Consequently, the aerospace sector needs revolutionary ideas and technological combinations to reduce greenhouse gas emissions (Clean Sky, 2020). This is where the use of alternative fuels such as hydrogen could intervene.

Hydrogen combustion completely removes carbon emissions, however, it leads to a seven times higher emission of water vapor (H_2O), an element with a large greenhouse effect and highly related to contrail formation (Kärcher, 2018), as well as a possible increase in the formation of nitrogen oxide (NO_x) (Funke et al., 2019). Therefore, the objective of this study is to create and use a methodology to determine the surface temperature increase caused by a fleet of both hydrogen and kerosene combustion aircraft. In addition to the main objective, the local effects of the emissions will be investigated; how each kerosene and hydrogen emissions affect climate at different latitudes and altitudes. Moreover, two study cases are proposed to increase the relevance of the study. The first includes the climate analysis of the Flying-V as a innovative aircraft design where the kerosene and hydrogen Flying-V versions will be analyzed. This will allow us to understand the influence of new aircraft designs on climate impact. The second study case evaluates a scenario including different technology introduction years for the hydrogen and kerosene aircraft.

Before solving the questions described above, it is necessary to understand what compounds are produced when burning kerosene and how they change when burning hydrogen. It is also necessary to explain the relationship between these compounds and climate impact, since not all emissions have the same effect and are highly dependent on the latitudes and altitudes at which they are released. This background knowledge as well as the improvements in aviation to date, the history of hydrogen aviation and a brief description of the aircraft used in the study, will be detailed in Chapter 2. The methodology employed to solve the objective of the study will be explained in Chapter 3, this includes the methodology to choose the routes to be flown, the simulation of the flights with their respective emissions, and the calculation of the climate impact for each of the aircraft. Chapter 4 will discuss the results of the study, the design details of the fleets involved, the routes selected, the total calculated emissions and finally the change of temperature on the surface of the earth with the use of the different fleets, to ultimately assess whether the hydrogen aircraft is a superior option to fight climate change. Finally, a short conclusion in Chapter 5 will dictate the most important findings of this study.

[1] International Civil Aviation Organization (2021, November 25). Future of Aviation https://www.icao.int/Meetings/FutureOfAviation/Pages/default.aspx

2

Theoretical Background

This chapter summarizes some valuable information to understand the topics discussed in the next chapters of the study. In-depth detail varies depending on the previous understanding of the problem at hand. Moreover, the chapter highlights the relevance of the thesis project and identifies the existing knowledge gap. The topic of the study includes aviation emissions, climate impact, hydrogen emissions, hydrogen aviation performance, and hydrogen aircraft designs. Climate impact from current aviation emissions is studied in Section 2.1, and improvements to solve climate change through hydrogen aircraft are investigated in Section 2.2, accompanied by the historical trends that improved climate change in conventional aviation.

2.1. Climate Impact from Aviation Emissions

The hydrogen aircraft emissions are released in the atmosphere, and to understand how they interact, it is helpful to first study the atmosphere through both the chemistry cycle and transportation (Section 2.1.1). Furthermore, it is also relevant to explore the aviation emissions and their relation to climate change (Section 2.1.2). Finally, to investigate the climate impact of the hydrogen aircraft, it is crucial to compare it to a baseline scenario. Therefore, the trends and future aviation scenarios will be studied (Section 2.1.3).

2.1.1. Atmospheric Chemistry and Physics

To understand the atmosphere's behavior, it is crucial to understand the atmospheric composition and the chemistry cycle of the species. How long do species last in the atmosphere? Where do those species accumulate, and how do they move? Which species have a higher climate effect, and how can we safely measure those effects? These questions will be answered in Section 2.1.1.

Atmospheric Composition

The majority of the atmosphere (99.9%) is composed of nitrogen (N_2, 78%), oxygen (O_2, 21 %), and argon (Ar, 0.9%), but many other gases compose that extra 0.1% (Mason, 2013; Catling, 2015). These other species are usually the main drivers of the atmospheric chemistry. In Figure 2.1 the different gasses present in the atmosphere are depicted. The temporal scale of these gases[1] depends on their size, reactivity, and solubility. Long-lived species (characterized by a lower solubility, size, and reactivity) tend to become uniform in the atmosphere through transportation (Cadle, 2015).

Aerosols play a key role in Earth's climate and human health and can be formed either naturally or anthropologically. Furthermore, anthropological aerosols can form physically, like soot, or by chemical reactions in the atmosphere, like ammonium sulfate and ammonium nitrate. These last two from aviation created from NO_x, ammonia (NH_3), and SO_2. The aerosol thermodynamic process from ammonia can be observed in Figure 2.2.

[1] The higher the species size, reactivity, and solubility, the higher the removal rates and the lower the temporal scale.

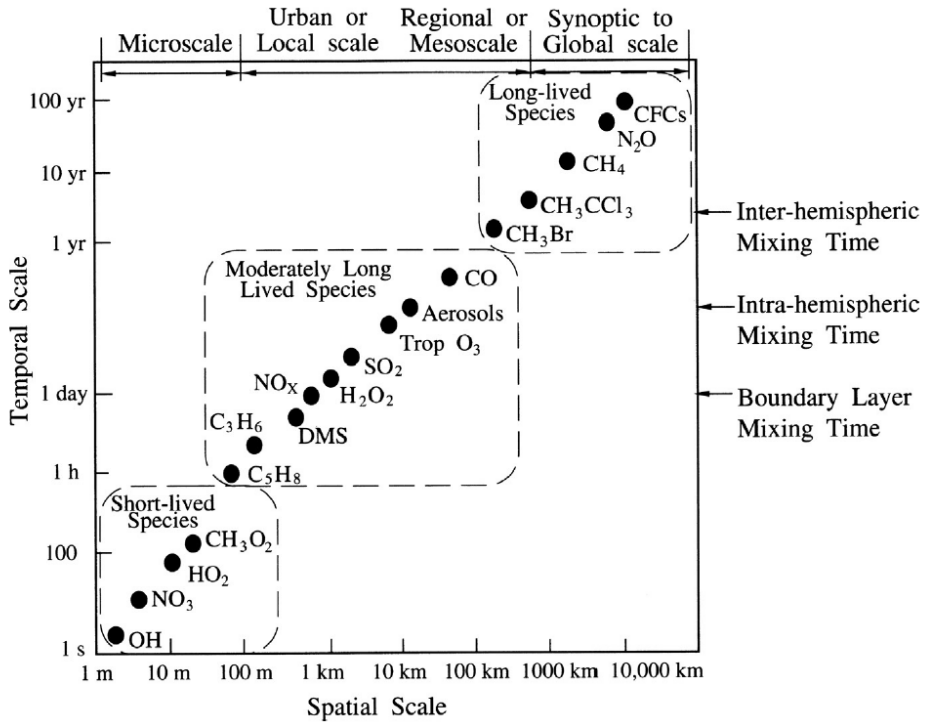

Figure 2.1: Atmospheric gases variability with respect to time, the space scale is dependent of the time scale, due to transportation distance (Cadle, 2015).

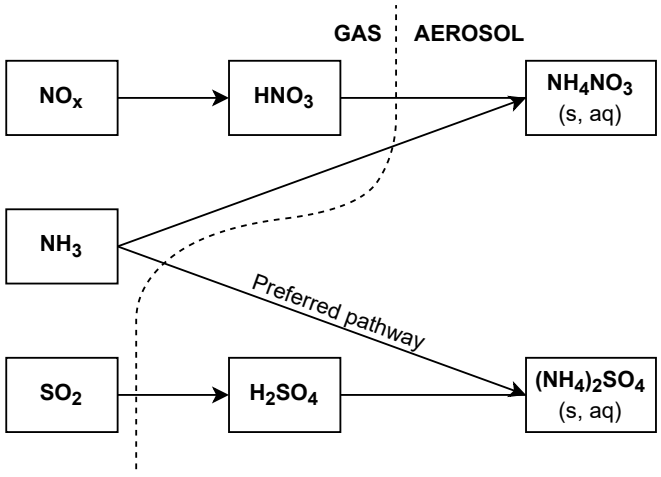

Figure 2.2: Aerosol thermodynamics from aviation (Dedoussi, 2021a).

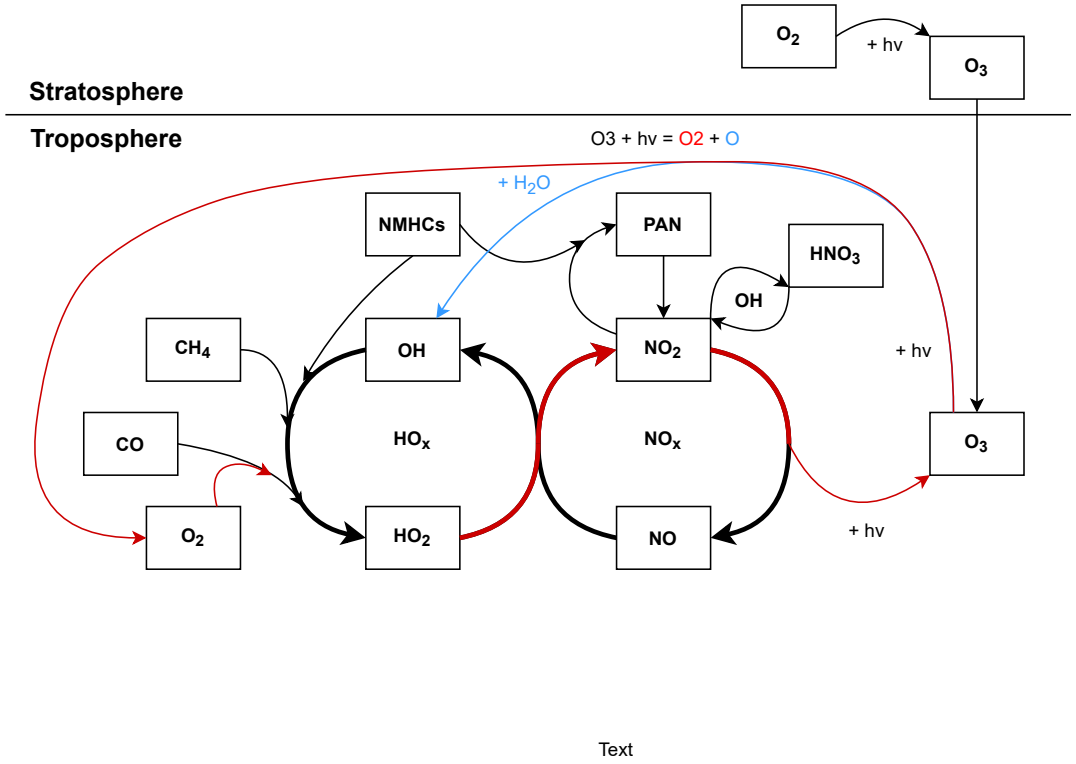

Figure 2.3: Atmospheric Ozone Chemistry including the ozone cycle in red and the OH formation cycle from Grewe (2021a) and Jacob (2000).

In the upper link, NO_x is oxidized with OH to form gaseous nitric acid (HNO_3). In the lower link, SO_2 is oxidized with OH (described in the next section) and H_2O to form aqueous sulfuric acid (H_2SO_4). The ammonia then is mixed with HNO_3 and H_2SO_4 to form ammonium sulfate ($(NH_4)_2SO_4$) and ammonium nitrate (NH_4NO_3). The preferred path for NH_3 is to form $(NH_4)_2SO_4$ because it is a faster reaction. The ammonia left reacts to form NH_4NO_3.

Suspended particles are not only differentiated by chemical composition but also by their size. $PM_{2.5}$ are fine particles with an aerodynamic diameter of 2.5 μm or smaller, and PM_{10} are particles with an aerodynamic diameter between 2.5 μm and 10 μm. Please note that the aerosols discussed above are considered as $PM_{2.5}$ aerosols. While PM_{10} particles last only a few hours before settling or being washed out, $PM_{2.5}$ particles can remain suspended for weeks (Dedoussi, 2021a).

Atmospheric Chemistry Cycle

The species OH and O_3 are formed through photolysis. Hydroxyl radical (OH), is one of the most important reactants in the atmosphere and it is also called atmospheric detergent because it reacts with many different species creating soluble components which can be deposited (Grewe, 2021a).

NO_x, CO, non-methane hydrocarbons (NMHC) and CH_4 are species relevant for ozone production, and their lifetime varies between hours to weeks in the case of NO_x and NMHC, from one to three months in the case of CO, and to approximately twelve years in the case of CH_4. O_3 is relevant for OH production and its lifetime can vary from weeks to months. The relations between these compounds can be observed in Figure 2.3 and the lifetimes in Figure 2.1.

In Figure 2.3 it can be observed that the group species HO_x and NO_x are continuously interacting. HO_x group is composed by OH and HO_2 while the NO_x group is composed by NO_2 and NO. OH was described as the atmospheric detergent and thus, its life cycle is worth being investigated. OH formation (depicted in Figure 2.3 as the blue arrow) starts with ozone photolysis, when ozone is decomposed into O_2 and an excited oxygen atom. The atom then reacts with water to form two molecules of OH as seen in Equation 2.1.

$$O_3 + hv \rightarrow O_2 + O(^1D) \quad H_2O + O(^1D) \rightarrow 2OH \tag{2.1}$$

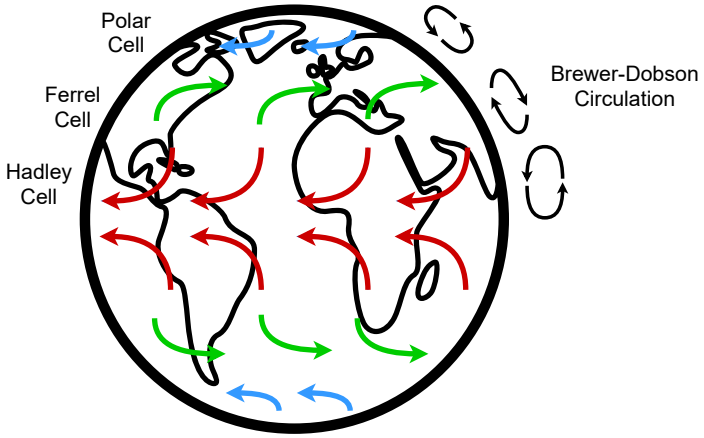

Figure 2.4: Earth winds on the Hadley cell, the Ferrell cell and the Polar cell, including Brewer-Dobson circulation.

The ozone cycle is depicted by the red arrows in Figure 2.3. Ozone is broken into O_2 due to photolysis, and then is combined with OH to form HO_2. HO_2 is then combined with NO to form NO_2 which is photolysed to O_3 (Jacob, 2000). There are two very important cycles which will be very valuable when investigating the climate effects of NO_x emissions. In Figure 2.3 it can be observed that NO_x species lead to two important interactions with green house gases. NO_x emissions increase O_3 production while decreasing the lifetime of CH_4 (Fuglestvedt et al., 1997).

In Figure 2.3 it can be observed that the species are not stationary. The ozone is transported from the stratosphere to the troposphere, and similarly, other species are transported longitudinally and latitudinally. These transportations will be described in the following section.

Atmospheric Transportation

To understand the transportation of the species along the atmosphere, the planetary winds must be understood. The winds tangent to the earth's surface can be explained with the use of the Hadley cell, the Ferrel cell, and the Polar cell, as observed in Figure 2.4.

The vertical transportation of the species is driven by the winds perpendicular to the Earth's surface between the stratosphere and the troposphere. The troposphere is the atmospheric region between 0 and 10 kilometers altitude, although these vary depending on the latitude, from 7 at the poles to 18 kilometers in the equator. The stratosphere is the atmospheric layer from the tropopause[2] to an altitude of 50 kilometers. The Brewer-Dobson circulation theory explains that air rises at the equator and descends at the poles but also rises at the equator and descends at mid-latitudes; these winds perpendicular to the Earth's surface are represented in Figure 2.4.

Is important to study the water and ozone concentrations across the globe and at different altitudes. Ozone concentrations are small in the tropopause and the troposphere but vast in the stratosphere, with a small peak close to the surface (Grewe, 2021a)[3]. Water concentrations are small in the stratosphere and tropopause but high in the troposphere. OH concentrations are high at the stratosphere and troposphere but low at the tropopause. This small concentration is due to the low content of water vapor and ozone at the tropopause Equation 2.1, which are the main products of OH (Grewe, 2021a). Figure 2.5 depicts the humidity percentage at different altitudes[4]. The right of the image shows the humidity at 10 kilometers altitude; the left at the surface of the Earth. The red areas depict zones where the humidity is low, while the blue areas show zones where the humidity is high. As observed, the atmospheric humidity reduces as increasing the altitude.

The concentrations of the species around the globe and their interactions with the atmosphere have been studied. However, not all species contribute to climate change. The following section will describe the greenhouse effect and analyze the atmospheric species that play a part.

[2]The tropopause is the top of the troposphere.

[3]Copernicus (2021, November 09). Ozone layer and ultra-violet radiation, https://atmosphere.copernicus.eu/ozone-layer-and-ultra-violet-radiation

[4]Windy, Compernicus and NASA (2021, November 6). Windy, https://www.windy.com

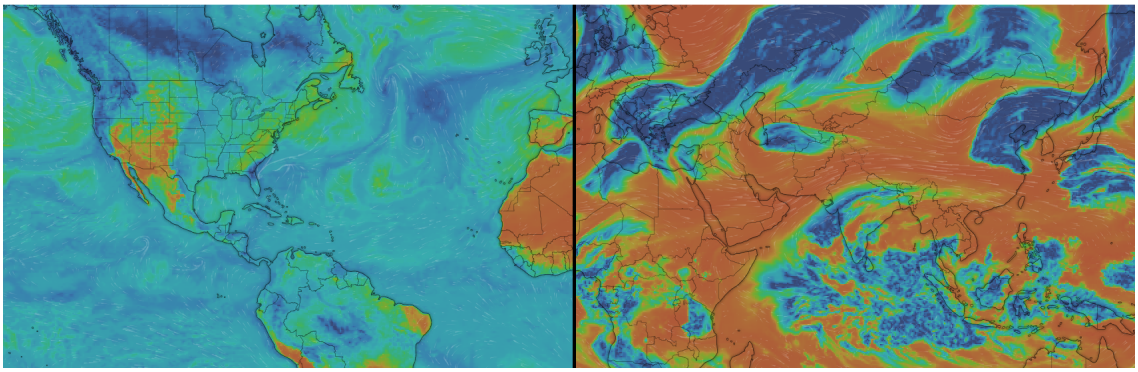

Figure 2.5: Humidity percentage (red low, blue high) at the Earth's surface on the left and at 10 kilometer altitude on the right.

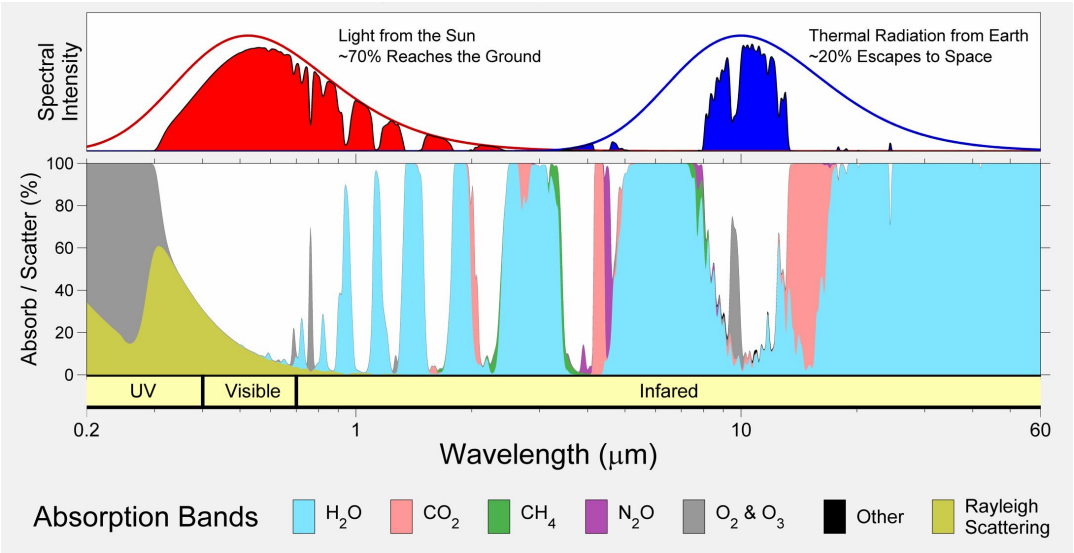

Figure 2.6: Solar energy absorbance of different atmospheric species.

Greenhouse Effect

Earth temperature is regulated by the amount of energy that is contained within the atmosphere and the Earth itself. The sun is the source of most of the energy on the Earth and it should not be a surprise that global warming is related to the sun. When the radiation of the Sun arrives on Earth, it interacts with the different species which form the atmosphere. This interaction is mainly based on the radiation wavelength and the absorption (Figure 2.6[5]). Jain (1993) and Wei et al. (2019) corroborate the information displayed in Figure 2.6.

In Figure 2.6 different wavelength groups are displayed. Ultra Violet (UV) light is mostly absorbed by the Ozone and scattered due to Rayleigh effects. UV light has the potential to harm living cells and cause cancer but is not a primary contributor to climate change. The visible light is altered by the Rayleigh Scattering which gives the sky the blue color during the day and the reddish color during the sunset. Climate change, or warming, is mostly attributed to infrared wavelengths, which, by definition, is a type of radiant energy that is invisible to human eyes but that can be felt as heat. It can be observed that most of the infrared is absorbed by the water vapor, the second-largest contributor is carbon dioxide, and methane and ozone also have some contribution to the energy absorbance. The complete list of greenhouse gases includes: H_2O, CO_2, CO, N_2O, CFCs, O_3, and CH_4 [6].

[5]Rohde, R. (2021, November 08) Clear-Sky Atmospheric Transmission, https://twitter.com/RARohde/status/1196761516051238912/photo/1

[6]National Oceanic and Atmospheric Administration (2021, November 10) Carbon Monoxide (CO) and other reactive gases, https://www.ncdc.noaa.gov/monitoring-references/faq/greenhouse-gases.php#co

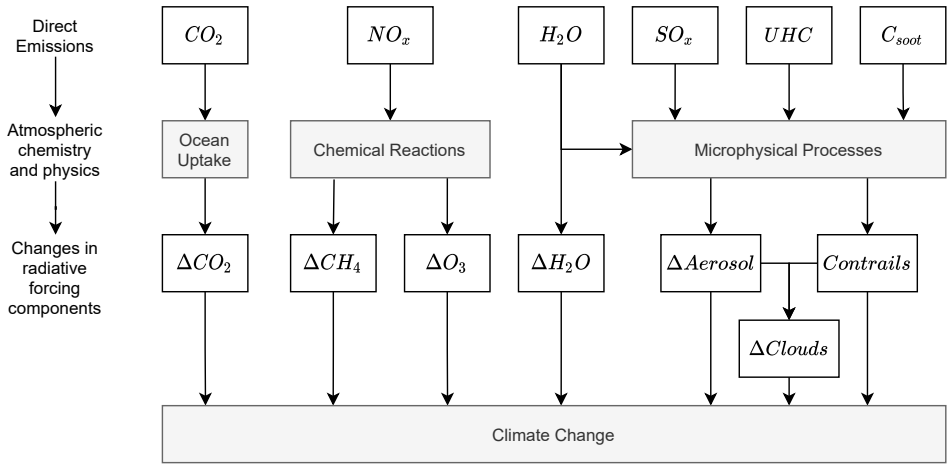

Figure 2.7: Climate impact from aviation emitted species (Fahey & Lee, 2016).

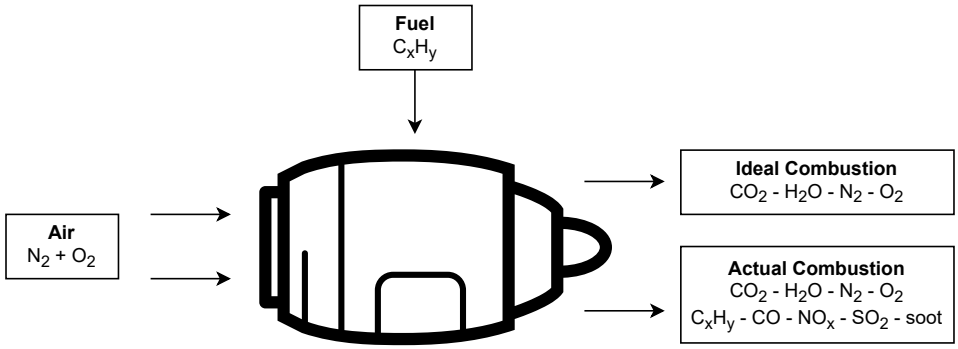

Figure 2.8: Aircraft Emissions for ideal and actual combustion of hydrocarbon fuel (Dedoussi, 2021b).

This section has studied the interactions between the species in the atmosphere and their transportation. Furthermore, with the greenhouse effect, the contribution from certain species was examined. The following section will relate aviation emissions to climate change.

2.1.2. Aviation Climate Impact

This section will describe aviation emissions and how they affect climate change depending on the region and type of emission. Finally, it will also propose a metric to measure the impact of these emissions. Figure 2.7 depicts the direct emissions from aviation and through which mechanisms affect climate change. It is important to keep in mind these relations when understanding the effects of each emission species.

Emissions from Aviation

The use of fossil fuels in the aviation industry is a convention. While alternative fuels are being researched and tested (Prussi et al., 2019), most of the commercial flights are operated with petroleum-based fuels. These petroleum-based fuels are mixed with air and burnt inside the engine, to produce thrust.

The emissions of an aircraft engine are the result of fossil fuel combustion (Equation 2.2). CO_2 and H_2O are the products of complete combustion. CO, UHC and soot are the products of incomplete combustion. NO_x, is a by-product of combustion and SO_x and NO_x are products of fuel impurities (Dedoussi, 2021b), mainly sulfur and aromatics (Chevron, 2007). The production of these emission species will be described below.

Carbon Dioxide (CO_2): CO_2 is a product of complete combustion. Equation 2.2 represents the balanced chemical equation for the ideal [7] combustion of hydrocarbon fuels. a is the stoichiometric coefficient of the oxidizer and z is the chemical composition of air (Dedoussi, 2021b).

$$C_xH_y + a\,(O_2 + zN_2) \rightarrow xCO_2 + \frac{y}{2}H_2O + a \cdot zN_2 \tag{2.2}$$

CO_2 is directly proportional to the fuel burn, and using Equation 2.2 it can be calculated that roughly about 3.14 kilograms of CO_2 are emitted per kilogram of kerosene. Similar to ozone, methane and water vapor, CO_2 has a direct effect on climate due to the absorbance of infrared waves. When sunlight reaches the Earth, some of the energy is emitted back as infrared waves, also felt as heat. CO_2 then absorbs and radiates half of the energy into space and half of the energy back to the surface of the Earth, increasing the temperatures on the Earth system. CO_2 is one of the most emitted aviation species and its effects are long-lasting. From 1940 to 2018, CO_2 emissions alone accounted for 32 % of the total radiative forcing impact from aviation species (Lee et al., 2021).

Water Vapor (H_2O): H_2O is a product of complete combustion. Equation 2.2 can be used to calculate the amount of vapor emitted per kilogram of fuel burnt, typically emitted at a rate of 1.23 kg of water vapor per kilogram of fuel (Whiteley, 2018). The reduction of H_2O is attributed to a reduction in fuel burn.

H_2O is the most important greenhouse gas, but the radiative forcing of H_2O is small (Wilcox et al., 2012; Gauss et al., 2003). Although the contribution is small, it has a positive radiative forcing and thus a warming effect. In the case of H_2O emissions in the stratosphere, the effective radiative forcing is 2 mW/m^2 which corresponds to 2% of the total emissions. The emission of H_2O does not have a high direct consequence on the climate, but it does affect the contrail formation as shown in Equation 2.3.

Carbon Monoxide (CO) & Unburnt Hydrocarbons (UHC): CO is a very weak greenhouse gas[6] and it is a product of incomplete combustion. CO depends greatly on the engine combustion type, the thrust setting, the flight altitude, and the speed. CO formation is the greatest at engine idle condition. Although it is a weak greenhouse gas, CO reacts with O_2 in the troposphere to form CO_2.

UHC are a product of incomplete combustion. The combustor is not homogeneous and some drops of the fuel do not get ignited by the flame. Its production can also be caused by an excess of fuel for the amount of air going into the engine, which causes unburnt remnants of the fuel to be ejected from the nozzle. Similar to CO, UHC formation is the greatest at engine idle conditions (Dedoussi, 2021b).

CO and UHC are formed as a result of incomplete combustion. Both are the greatest at idle conditions and thus most of the experiments from literature have been conducted at ground level (Sorokin et al., 2006). The emission rates of CO and UHC are very low, and very dependable on ambient temperature conditions. Although they are known to be involved in aerosol formation, CO and UHC have a very low climate impact (Fahey & Lee, 2016) and thus they will not be further investigated in this assignment.

Soot: Soot is difficult to model. Although there are many unknowns related to soot formation, there is evidence that it is related to polycyclic aromatic hydrocarbon (PAH) species (Johansson et al., 2018; Di Domenico et al., 2010). Soot formation occurs through chemical and physical processes and builds up from mostly hydrogen content to a higher carbon content (Omidvarborna et al., 2015). Soot emissions are maximized at maximum thrust conditions (Dedoussi, 2021b).

The total soot radiative forcing from absorption and scattering of sunlight was calculated to be 0.71 W/m^2 with a 90% uncertainty range (Baklacioglu, 2015). This result includes all the anthropogenic soot emissions, aviation is responsible for 0.44% of those emissions. From these numbers, the total aviation soot radiative forcing should circle 0.0031 W/m^2. This result is in line with the results from Lee et al. (2010) and between the bounds dictated by Lee et al. (2021). Although the climate impact from soot is marginal compared with the radiative forcing of other species it is important to understand their contribution to contrail formation.

[7] The ideal combustion does not include incomplete combustion products, by-products of combustion, or products of fuel impurities, meaning that only CO_2, H_2O and N_2 are formed.

Sulfur Oxides (SO_x): Sulfur oxides (SO_x) form during combustion when the sulfur fuel impurities mix with oxygen (Federal Aviation Administration (FAA), 2005). The fuel sulfur content is usually around 600 ppm and it is 98% SO_2 and 2 % SO_4. As for Soot, sulfur emissions are the highest at full thrust conditions (Dedoussi, 2021b).

Most of the sulfates are emitted as SO_2 with roughly 3% is emitted as sulfuric acid (H_2SO_4) (Petzold et al., 2005). The uncertainty of the predicted radiative forcing is big and by unifying different models a value of -7.4 mW/m^2 was found (Lee et al., 2021). SO_x, like soot, also contributes to contrail formation as observed in Figure 2.7, Although sulfur compounds have a cooling effect, when deposited by the rain it creates a harmful phenomenon called acid rain (Lanza et al., 2014).

Nitrogen Oxides (NO_x): Although, NO_x can be a product derived from fuel impurities it is mostly treated as a by-product of combustion. NO_x is formed in the combustion chamber of the aircraft engine, and it is largely dependent on the combustion temperature, pressure, and mass flow (Chandrasekaran & Guha, 2012). NO_x is formed by four mechanisms: the Zeldovich mechanism, which is the dominant pathway; the prompt NO, where it is generated at the flame front; the N_2O pathway under high pressures; and the fuel bond nitrogen, where nitrogen fuels react to form NO_x (Dedoussi, 2021b).

The reduction in NO_x emission is not as straightforward as the reduction in CO_2. Current engine design trends make efforts to increase fuel efficiency, thus decreasing CO_2 emissions. The counter effect is that, by increasing fuel efficiency [8] there is also an increase in NO_x emissions. Techniques are being investigated to reduce NO_x formation, which focus mainly on reducing combustion temperatures and combustion residence times (Ommi & Azimi, 2012). Other methods to further reduce NO_x include multi-fuels as the primary source of energy (Rao et al., 2014; Grewe et al., 2017a) and low NO_x combustion technique (Abbot et al., 2021).

Many different models have tried to predict the emission of NO_x. Deidewig et al. (1996) proposes the fuel flow method, which was also the approach followed by Turgut and Usanmaz (2017). The fuel flow method (BFFM2), consists on correlating the fuel flow to a certain NO_x emission and then correct these emissions for temperature and pressure at an altitude. This method relies heavily on the fuel flow at sea level conditions. The DLR method is explained by Turgut and Usanmaz (2017) and similarly to the BFFM2 method it correlates the emissions to the temperature, pressure but adding the influence of mach. Chandrasekaran and Guha (2012) explains other methods that can be used to calculate the emitted NO_x, including the correlation-based models, the P_3-T_3 Method, the simplified physics-based model and high fidelity simulations. The P_3-T_3 method is simple yet the most dependable. P_3 and T_3 correspond to the temperature and pressure before the combustion chamber of the engine.

When discussing atmospheric chemistry and physics, it was noted that NO_x contributed to both the production of O_3 (short-term effect) and the depletion of CH_4 (long-term effect). The depletion of methane involves two long-term effects, the decrease in ozone and the decrease in stratospheric water vapor (Lee et al., 2021). The emission of NO_x due to the short-term ozone increase yields a radiative forcing of 36 mW/m^2. The methane decrease yields a negative ERF, thus a cooling effect of -21.2 mW/m^2. The long-term ozone decrease yields a negative ERF of -10.6 mW/m^2 and the stratospheric water vapor decreases yields a negative ERF of -3.2 mW/m^2 (Reekers, 2021). NO_x emissions have a high climate impact; therefore, it is necessary to model them accurately. Different methods exist to calculate the amount of NO_x emitted, which depend on the amount of information known about the engine and the flight conditions (Chandrasekaran & Guha, 2012).

Contrails: Contrails are trails of condensed water formed behind the aircraft. There are two different types of contrails, aerodynamic and exhaust contrails. The aerodynamic contrails occur at surfaces due to a change in pressure (Gierens et al., 2009). Exhaust contrails occur at the engine exhaust. These contrails form under certain atmospheric and engine exhaust conditions (Whelan et al., 2017). These conditions can be observed in Figure 2.9 where the Schmidt-Appleman criterion (SAC) (Schumann, 1996) is used to understand (1) if a contrail will form and (2) if a contrail will persist.

It can be observed that, if the atmospheric and exhaust conditions satisfy the Schmidt-Appleman criterion, persistent contrails will be formed. If the contrail maintains the linear shape it is defined as a persistent contrail, else it is defined as a cirrus contrail (Kärcher, 2018). The slope of the temporal evolution of the exhaust line can be calculated with Equation 2.3. c_p is the specific heat of air at

[8] Fuel efficiency is usually increased by increasing the combustion temperature (Chandrasekaran & Guha, 2012).

constant pressure, P is the ambient pressure, ϵ is the ratio of the molar mass of water and air, EI_{H_2O} is the emission of water vapor per kilogram fuel burnt, Q is the fuel-specific heat and η the overall propulsion efficiency. Given the right atmospheric conditions, the higher the slope of the temporal evolution of the exhaust conditions line (G), the more probable persistent contrails are formed.

$$G = \frac{c_p P}{\epsilon} \frac{EI_{H_2O}}{Q(1-\eta)} \tag{2.3}$$

The contrail is generated behind the jet, where warm exhaust gases are mixed with the cold ambient air, resulting in liquid saturation and the nucleation of ice crystals (Iwabuchi et al., 2012). To nucleate, the ice crystals involve aerosol particles. The number of ice crystals formed depends greatly on the aerosol radius (Gorbunov et al., 2001) and the concentration of aerosols on the jet exhaust and air (Ström & Gierens, 2002; Kärcher, 2018). The aerosol particle characteristics will also determine the climate impact of the contrails. Global warming from contrails occurs when radiation from the earth is scattered back to the surface. Similarly, clouds can reflect the sun's radiation to space. The ability to reflect or to absorb radiation is measured by the optical depth of the cirrus, which is defined as the degree to which it modifies the light passing through it. The optical depth of the contrails depends on the ice crystal number density, effective ice crystal radius, and ice mass content (Gierens et al., 2009), therefore, the composition of the contrail cirrus is very important to understand its climate effect.

Grewe et al. (2017a) mentioned that, simulations with a reduction of 80% in soot particles showed a 60% reduction in the radiative forcing of the contrails. Further improvements (from 50 to 70 %) could be achieved by reducing the aromatic content in fuel (Voigt et al., 2021). The effective crystal radius depends on the ice mass and the ice mass content depends on the emitted amount of water vapor and atmospheric humidity (Ström & Gierens, 2002). The radiative forcing from contrail cirrus is mainly proportional to the optical depth and cloud coverage (Kärcher, 2018). For the period from 1940 to 2018, the RF of contrails was estimated to be around 111.4 mW/m^2. From those, 20 % of the radiative forcing is calculated to be caused by persistent contrails while the 80% by cirrus contrails[9]

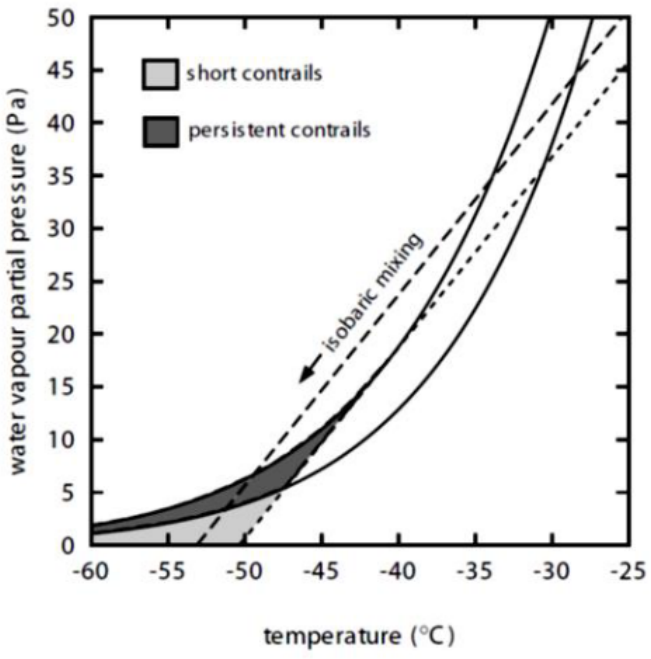

Figure 2.9: Schmidt-Appleman Criterion where the x-axis is the temperature and the y axis is the water vapor partial pressure. The solid upper line represents the saturation line with respect to water and the blue dashed line represents the saturation line with respect to ice. The straight dashed line represents the temporal evolution of the exhaust conditions. The dotted line indicates the warmest temperatures for contrail formation. The initial point on the left of these lines represents the atmospheric conditions (Djojodihardjo, 2015).

[9]The difference between persistent and cirrus contrail is based on the linearity of the contrail.

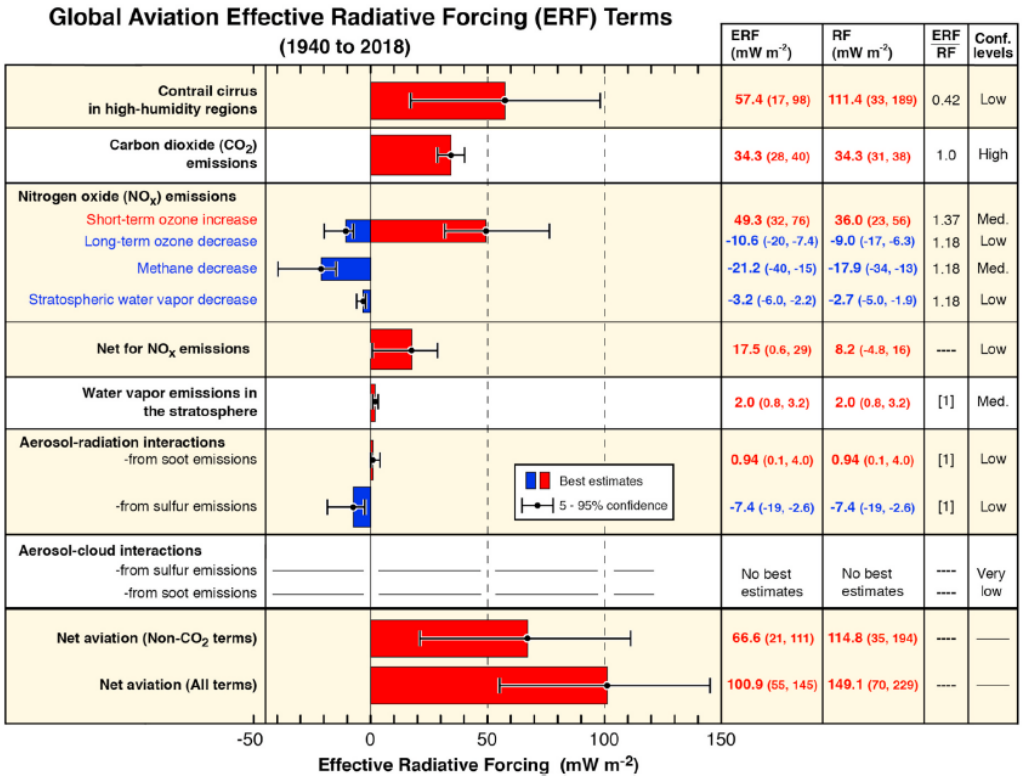

Figure 2.10: Estimates for climate forcing terms from global aviation from 1940 to 2018 (Lee et al., 2021).

(Intergovernmental Panel on Climate Change (IPCC), 2013). Contrail radiative forcing is the largest contributor of all emitted species. It is important to note as well that contrail radiative forcing has an uncertainty of 70 %. This is due to the difficulty of differentiating contrail-induced clouds from natural clouds and the variability of the physical and optical properties of the contrails depending on region and time of measurement (Kärcher, 2018).

Radiative Forcing from Emissions Summary: Table 2.1 depicts the emission rates for the different emission species from burning kerosene. Please note that there is large uncertainties due to their variability depending on the flight conditions.

Table 2.1: Emission rates extracted from (Whiteley, 2018; Cecere et al., 2014; Intergovernmental Panel on Climate Change (IPCC), 1999; Herndon et al., 2006). Please note that the emission rates vary depending on the power settings, and the type of combustion techniques.

Emission species	**CO_2**	**H_2O**	**CO**	**UHC**	**Soot**	**SO_x**	**NO_x**
Approximate emission index	3.15	1.23	1-2.5	3.8-5.1[10]	0.01-0.1	0.084	19 ± 9[11]
Units	$\frac{kgCO_2}{kg\text{Fuel}}$	$\frac{kgH_2O}{kg\text{Fuel}}$	$\frac{gCO}{kg\text{Fuel}}$	$\frac{gCH_4}{kg\text{Fuel}}$	$\frac{gSoot}{kg\text{Fuel}}$	$\frac{kgSO_x}{kg\text{Fuel}}$	$\frac{gNO_x}{kg\text{Fuel}}$

In Figure 2.10 both the radiative forcing and the effective radiative forcing of each of the aviation emission species listed before is displayed. While the bars are the best estimates, the whiskers are the confidence intervals. It can be observed that non-CO_2 terms account for 66 % of the total radiative forcing but at the same time, it accounts for the largest uncertainties (mainly due to contrail cirrus). *Special attention should be paid to non-CO_2 effects.*

It can also be observed that Aerosol-cloud interactions have not been estimated. This is because different studies yielded very different results based on cirrus formation from sulfur and soot with large uncertainties (Lee et al., 2021).

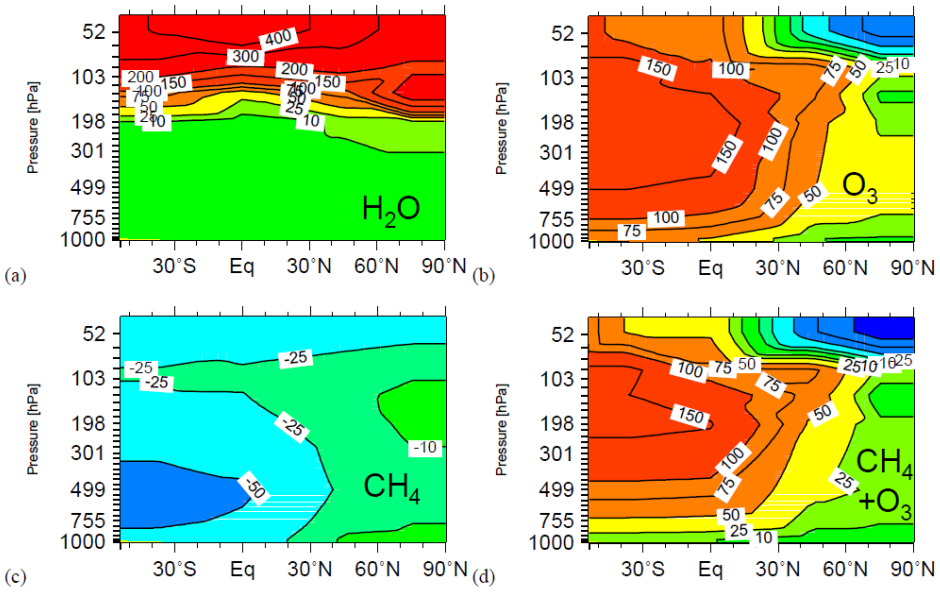

Figure 2.11: Altitude impact on the temperature change of emissions in the year 2100 for (a) water vapour, (b) ozone, (c) methane and (d) ozone and methane. Ozone and methane being the atmospheric response to NO_x emissions. (Grewe & Stenke, 2008)

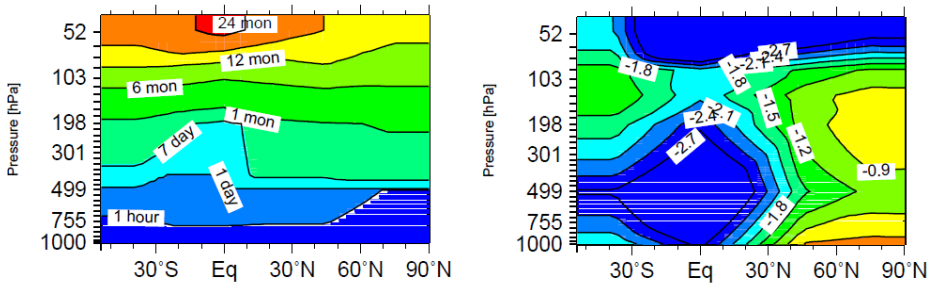

Figure 2.12: H_2O lifetime (a) and methane lifetime change in percentage (b) (Grewe & Stenke, 2008).

Climate impact of non-CO_2 effects, such as NO_x, H_2O and contrails, depends greatly on the time and location of the emissions. Special attention should be given to the latitudes and altitudes, while the variation in terms of longitude is not so relevant, highlighting *the importance of investigating a wide variety of locations and altitudes around the globe.*

Climate Impact vs. Region of Emission

Figure 2.11 includes the temperature perturbations in 2100 for the equal emission quantities at different altitudes.

The climate impact of H_2O depends mostly on the altitude, the higher the altitude the higher the temperature change due to the same emission fraction, as observed in Figure 2.11. The same observations were made in Intergovernmental Panel on Climate Change (IPCC), 1999, where the emissions of a subsonic fleet flying between 9 and 13 km altitude were compared with a supersonic fleet cruising at 18 km altitude. The climate impact of a similar hydrogen emission index of a supersonic fleet was found to be an order of magnitude higher(0.003 Wm^2 for the subsonic fleet to 0.05 Wm^2 for the supersonic fleet). Furthermore, climate warming is slightly accentuated at latitudes close to the poles. The lifetime of H_2O also varies per region of the emission, the higher in the atmosphere the longer the residence times. The lifetime effects can be observed in Figure 2.12.

NO_x emissions have a higher impact at 10-12 km altitude. NO_x emitted at 11 km leads to a 200% greater ozone increase and 40% stronger methane depletion per emitted mas of NO_x than at 5 km (Köhler et al., 2013; Köhler et al., 2008). These effects are also observed in Figure 2.11, where

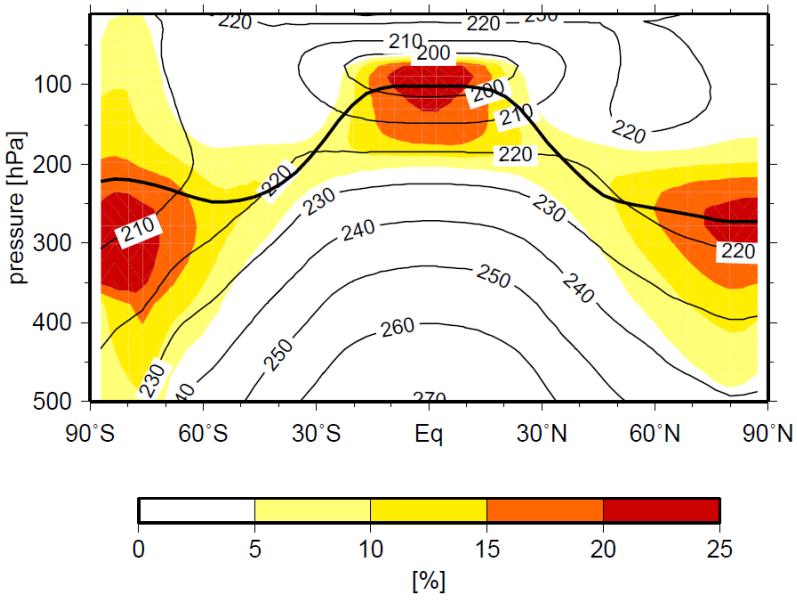

Figure 2.13: Probability of contrail formation with varying altitude and latitude.(Grewe & Stenke, 2008)

the methane cooling effect is outbalanced by the ozone warming effect. For reference, the altitude corresponding to 103 hPa is 14.5 km and the altitude corresponding to 301 hPa is 9 km.

Probability of contrail formation is dependant on the altitude and latitude as well. The largest being at around 9 kilometers altitude close to the poles, and at 14.5 kilometers at the equator (Figure 2.13). It can be observed that these areas correspond to the atmospheric areas of higher relative humidity calculated in Thatcher and Jablonowski (2016). These are the areas that should be avoided during the flight routes. For reference, Amsterdam is situated at a latitude of 52.37.

Contrails also have different climate impacts depending on the time of the day. During the daytime, contrails generate both a cooling and a warming effect, but during the night, contrails only reflect the infrared radiation from the earth to the surface generating a warming effect (Reekers, 2021).

Until now, emissions have been treated independently, but it is possible to group them into long and short time climate pollutants.

Long vs Short Time Climate Pollutants

Two main emission groups were observed when burning petroleum-based fuels: short-lived climate pollutants (SLCP), such as soot, tropospheric ozone, and contrails; and cumulative pollutants, such as CO_2 and CH_4.

It is important to understand the necessity of reducing both emission groups. This is reflected by Allen et al. (2016). While both the short-lived and the cumulative emissions have a comparable impact on global temperatures, CO_2 emissions persist for centuries, and non-CO_2 (except for CH_4 such as the contrails decay rapidly. *Therefore, reducing the emission of SLCP will lower global temperatures and reducing cumulative pollutant emissions will stabilize temperatures.* This information was also corroborated with the lectures from Grewe (2021b) which explain the difference in climate impact longevity on pulse emissions.

Aviation emissions have been described, and efforts were made to calculate the impact on climate using radiative forcing. However, in literature, many other indicators have been used to define the climate impact of certain species. These metrics will be analyzed in the following section.

Climate Indicator Assessment

One of the most common ways in literature to refer to climate change is by using the Radiative Forcing (RF) caused by an emitted species. However, in the news, it is commonly understood as near-surface temperature change. Climate change does not have only one definition because multiple metrics can predict and calculate the effect of emitted species on the earth's climate.

RF is the radiation change caused by a concentration change in the atmosphere, and past emissions are used to calculate it. This already assumes an emission scenario or a reference time. Another relevant climate metric is the Global Warming Potential (GWP). GWP is an integration of the radiative forcing over a period of time. GWP was created to compare the climate impact of different gases and thus is expressed in relation to the absolute climate indicator of generally CO_2 (Grewe, 2021b). In Equation 2.4, it can be observed that the climate impact of a kilogram of NO_x is relativized to the climate impact of a kilogram of CO_2, H being the time horizon.

$$GWP^{NO_x}(H) = \frac{\int_{t_0}^{t_0+H} RF^{NO_x}(t)dt}{\int_{t_0}^{t_0+H} RF^{CO_2}(t)dt} \tag{2.4}$$

RF and GWP allow for comparison between emissions but they certainly do not give relevant climate information. Climate metrics that include relevant information are mostly related to temperature, which is the common way to measure climate change. Global Temperature Change Potential (GTP) is the direct alternative to GWP. GTP goes a step further than GWP and includes the temperature change of the emissions on a time horizon. The problem with GTP is its dependence on time. The output of GTP is just a snapshot of the temperature increase due to a certain emission and while the steady-state is accurate, the transient state is not. The Average Temperature Response (ATR) metric reduces the time dependency because evaluates the change in temperature for each year, as observed in Equation 2.5(Grewe, 2021b). This equation uses NO_x as an example.

$$ATR^{NO_x}(H) = \frac{1}{H}\int_{t_0}^{t_0+H} \Delta T^{NO_x}(t)dt \tag{2.5}$$

Many metrics have been presented, but how should the used metric be chosen? Grewe and Dahlmann (2015) states that the metric selection depends on the baseline, the emission scenario, and the research question of a project. The example used by Grewe and Dahlmann (2015) is regarding the EU-project AHEAD with the hydrogen engine mounted on the blended wing body (Rao et al., 2014). The question: "Is the AHEAD technology better in reducing the long-term climate impact, when introduced in 2050, than conventional technology?". The baseline should be conventional technology improvements, and the emission scenario would include a fleet of AHEAD aircraft starting in 2050. Grewe and Dahlmann (2015) suggest using the average temperature response change over 100 years (ATR_{100}). However, when investigating the climate impact of the AHEAD technology, Grewe et al. (2017a) calculated near surface temperature change and radiative forcing using AirClim (Grewe & Stenke, 2008) with Equation 2.6.

$$\Delta T = \int_{t_0}^{T} G(t-t')RF^*(t')dt' \tag{2.6}$$

Where ΔT is the perturbation temperature compared to the baseline, G is the Green's function for the near surface temperature response, and RF^* is the normalized radiative forcing. The equations for G and RF^* can be found in Grewe and Stenke (2008).

Section 2.1 has analyzed the emissions from aviation and has related those emissions to climate change. Furthermore, it also has shown the differences in metrics and locations of emissions. The following section will treat the trends and future scenarios in the aviation sector concerning climate impact.

2.1.3. Trends and Future Scenarios of Aviation Climate Impact

To investigate the effects of aviation on climate, it is important to analyze the past but also to look into the future. Therefore, both the history and trends of aircraft designs will be described.

History and Trends

Although affected by some disturbing world crises, like the recent one caused by COVID 19, aviation is a growing business. The aviation transportation sector relies heavily on kerosene and although the improvements in fuel efficiency are notable (Zheng & Rutherford, 2020), the growth rate of the sector outgrows the fuel efficiency improvements. This situation creates an environmentally unsustainable

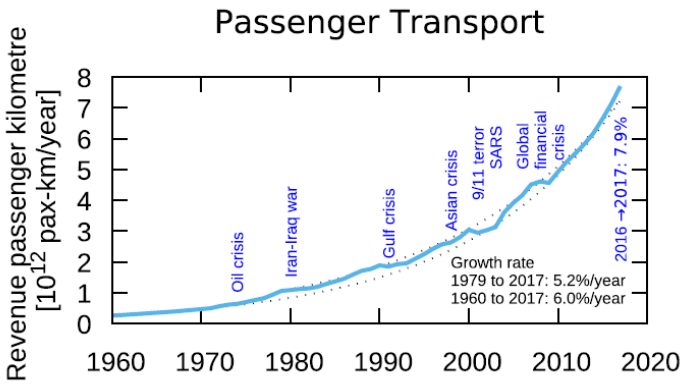

Figure 2.14: Passenger transportation revenue growth from 1960 to 2020 (Grewe et al., 2021).

business. Figure 2.14 shows this only increasing revenue, and for those who count in the current COVID situation to solve major problems, it will soon just be another historical drop in the aviation revenue, probably with no notable effect on climate in the long run[12].

This growth rate trend is widely accepted, Clean Sky (2020) states that assuming the current growth rate of 3 to 4 percent per year and an efficiency improvement of 2 percent, aviation emissions will more than double by 2050. To put into perspective, the total CO_2 emissions from commercial aviation in 2018 were calculated to be 812 Mt (Seymour et al., 2020). This is roughly 100 times more weight than the amount of plastic that ends up in the ocean every year[13]. The past has been studied, and now, we can observe the future.

Scenario Predictions and Policies

Future scenarios can be predicted depending on the policies and technology advancements. These future scenarios were presented by Grewe et al. (2021). In Figure 2.15 the different predictions and how they affect the Revenue Passenger Kilometers (RPK)[14], CO_2 and NO_x are displayed. CurTec is the first of the proposed scenarios which assumes that the current technology is frozen. Business as Usual (BAU) assumes that the technology improves at the same rate as it is improving now. The Carbon Offsetting and Reduction Scheme for International Aviation (CORSIA) stipulates that the growth in the sector must be such that the carbon emissions do not grow. Finally, the FP2050 and the FP2050-cont assume a reduction of 75% of CO_2 and 90 % of NO_x, the first one assumes late technology advancements and the second one continuous.

Grewe et al. (2021) compare these scenarios with the ultimate goal of keeping temperature change below 2.0°C, now updated to be 1.5°C (The Group of Twenty (G20), 2021). It was found that CurTec and BAU scenarios are not sustainable, and around 2040 they cross the 2.0°C target. The CORSIA scenario starts stabilizing around the year 2080 but well past the 2.0°C target, at around 2.7°C. FP2050 and FP2050-cont both stabilize below the 2.0°C target at around 2080, although the FP2050 scenario overshoots the 2.0°C target before stabilizing. Grewe (2021b) suggests that it is important to understand the scenario where the emissions are released, since this will dictate the importance of each emission. For example, in an increasing emission scenario, the radiative forcing from short-term forcers is more important, while for a decreasing emission scenario, the same forcers get less important, and more attention should be paid to long-term forcers like CO_2.

The scenarios listed above already contain some of the current policies, but it is important to list the agreements and policies which limit climate change (Larsson et al., 2019).

- Paris Agreement on 2.0°C target in 2015.

[12]The World Bank and ICAO (2021, November 09) Air transport, passengers carried, https://data.worldbank.org/indicator/IS.AIR.PSGR

[13]Parker, L. (2021, November 09) The world's plastic pollution crisis explained, https://www.nationalgeographic.com/environment/article/plastic-pollution

[14]RPK is a performance indicator commonly used in the aviation sector to monitor the number of kilometers travelled by paying passengers.

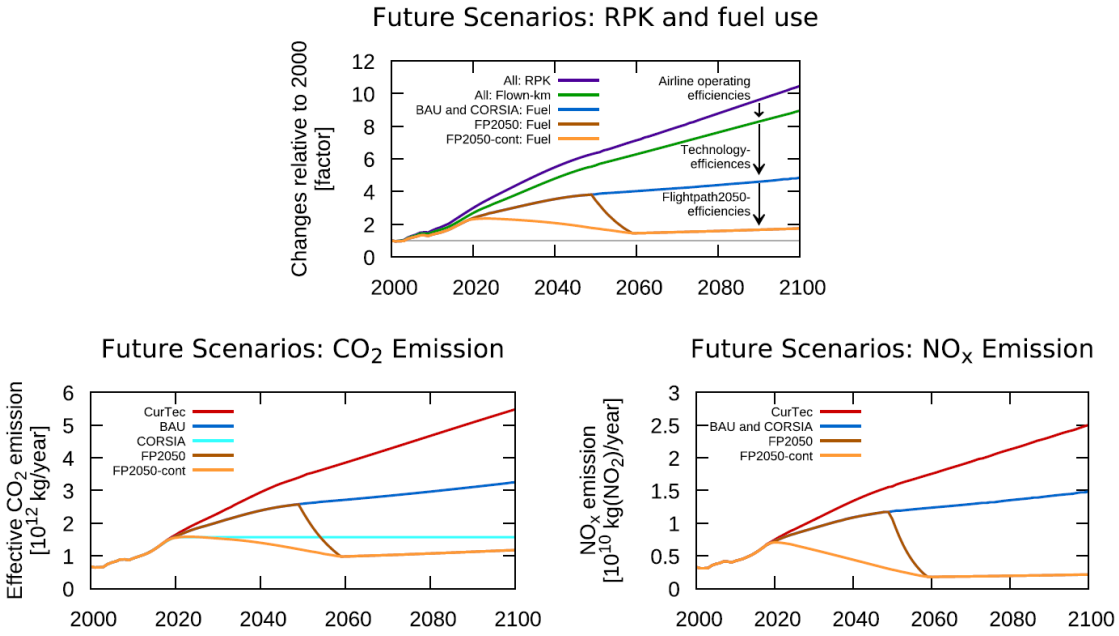

Figure 2.15: Possible future scenarios from 2021 to 2100 (Grewe et al., 2021).

- G20 Agrees on 1.5°C target in Rome 2021.
- ICAO implements CORSIA to reduce emissions in 2016.
- The European Union implements ETS to further reduce emissions in 2017.

Future policies that could be implemented in addition to EU ETS include:

- Distance-based air passenger tax.
- Tax on jet fuel.
- A quota obligation for alternative fuels.
- A charge on aircraft NO_x emissions or the inclusion in the EU ETS (European Union Aviation Safety Agency (EASA), 2020).
- Reduction in aromatics within fuel specifications.
- Avoidance of flying on ice-supersaturated areas.
- A charge on climate impact.

These possible future policies would tip the balance towards alternative fuels, so special attention should be paid to the future cost of alternative fuels when including the taxes included above.

In Section 2.1 it was clear that the location of the emissions influences the climate impact of the species. Therefore, an investigation on the current airspace distribution is crucial for the future analysis of hydrogen aircraft.

Airspace Flight Distribution

Current aviation trends on global quantities have been described but the localized trajectories of those flights are equally important. Figure 2.16 depicts the summed flight routes around the globe in 2019[15].

From Figure 2.16 it can be observed that three main markets exist. These are the United States market, the European market, and the Asian market. The national and international market segments are supposed to increase. China's regional air traffic, for example, is expected to grow by more than

[15]International Civil Aviation Organization (2021, November 13) ICAO traffic flow 2019. https://gis.icao.int/gallery/TRAFFICFLOW2019zoomsimpOP.pdf

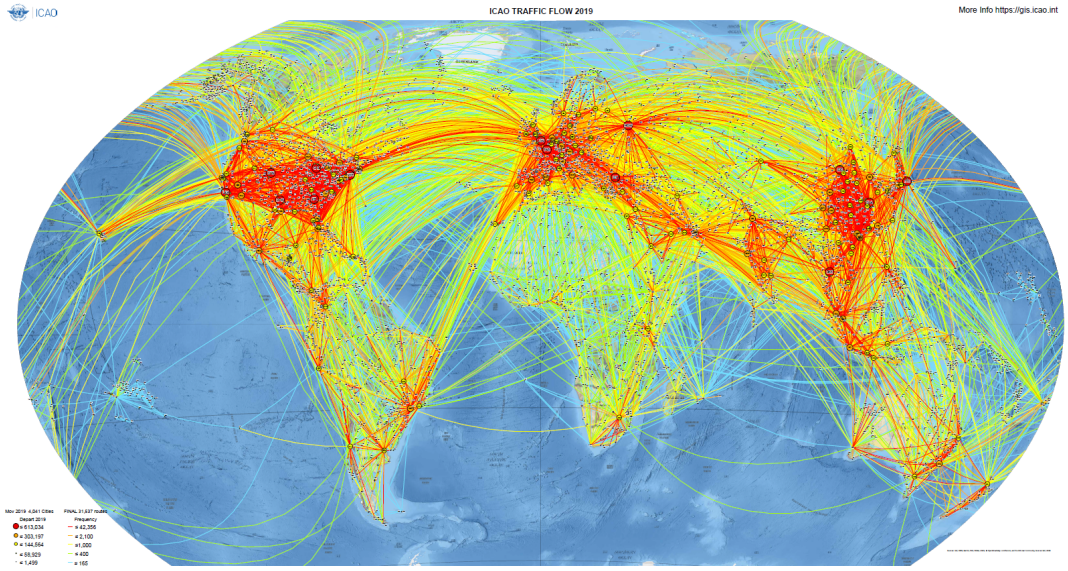

Figure 2.16: Aviation routes based on frequency.

200% in the next 20 years and flights between Europe and North America and Europe and the middle east are also increasing[16]. Special attention should be paid to flights that cross regions of high climate impact defined where NO_x and H_2O will be released and contrails will be formed.

Section 2.1 has analyzed the atmospheric chemistry and transportation and how the different emissions from aviation affect climate. Furthermore, it has developed a vision into the past and future of aviation climate impact. Section 2.2 will define the current solutions followed by the aviation sector to make it sustainable.

2.2. Solutions for Aviation Climate Change

This section will have a look at the solutions proposed by the aviation sector to fight global warming (Section 2.2.1). Furthermore, it will analyze the possibility of using hydrogen in exchange for kerosene Section 2.2.2.

2.2.1. Improvements in Aircraft Technology

A way to examine the historical improvements of aviation technology is to look back at the fuel efficiency of the airliners. Figure 2.17 shows the average block fuel burn of airliners per year. The block fuel is the fuel burn per flight.

In Figure 2.17 a decrease of 41 % from 1970 to 2019 in aircraft block fuel burn is observed. This decrease has multiple jumps and imbalances that can be explained due to advancements in technology. For example, the dotted lines represent the introduction of the widebody 747 families with a high bypass turbofan that, when fielded, accounted for a major reduction of block fuel reaching -2.8%.

The aircraft sector is a slow market. Aircraft are in service for an average of 30 years and the process from designing to flying new aircraft can take several years. For example, the 7E7 program was announced in 2003, and the first commercial flight took place in 2011 [17]. Fuel burn decreases when there is competition, and competition and new improvements can take several years to arrive. That is why in Figure 2.17 fuel efficiency improvements stagnate for a few years. This is the case from the 70s to the 80s.

During the 80s the average fuel block decreased again by 2.8 %. This was the result of introducing in the market the fuel-efficient narrowbody and smaller widebody aircraft, covering more flights more

[16] Treat, J. and Conant, E. and Nowakowsky, K. (2021, November 13) Take a look inside the Flying-V feature, https://www.nationalgeographic.com/magazine/graphics/take-a-look-inside-the-flying-v-feature

[17] Aircraft variations among families should take less time to develop.

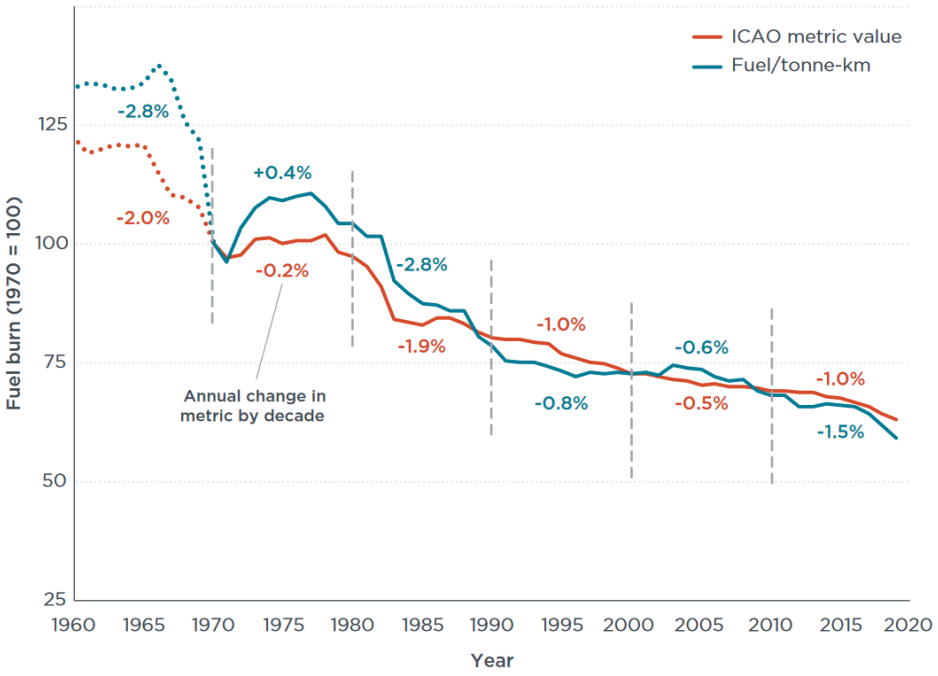

Figure 2.17: Average block fuel burn of airliners from 1960 to 2019, including freighters (Zheng & Rutherford, 2020).

efficiently. The market again stagnated from the 90s to 2005 due to the use and delivery of similar aircraft and engines. Cost-effective technologies improved the reduction in fuel block used until 2015 and could potentially improve it further (Elliott, 2015). The drop of fuel burn in 2015 is due to the introduction of widebody aircraft like the 787 and A350 and the re-engineered narrow-bodies like the A320neo and the 737 MAX (Graver et al., 2020).

It might look like policies also play an important role in fuel block reduction. As mentioned before, ICAO included the CORSIA measures in 2015, these measures are targeted for aircraft sold in 2028 but current aircraft already comply with these requirements (Zheng & Rutherford, 2020). This reinforces the idea that stronger policies are needed. These improvements will be described independently in the following sections.

Engine Improvements

The Boeing 747 introduced the high bypass turbofan. In a turbofan, the air initially passes through the fan, and it is divided into the cold flow and the core flow. The core flow initially gets compressed by the low and high-pressure compressor, and it is then mixed with fuel in the combustion chamber. Finally, the core flow passes through the high and low-pressure turbines and is exhausted from the nozzle. The energy obtained in the turbine is used to drive the compressor and the fan. The cold flow is accelerated by the fan and is later mixed with the hot air from the nozzle (Rao, 2019a). The whole process can be observed in Figure 2.18[18].

The high bypass turbofan concept compared to the turbojet[19] concept compromises power for a higher fuel efficiency (Rao, 2019b). The thrust is a function of the amount of air mass and the change in speed of that mass. The higher the air mass ($\dot{m}$) and the exhaust velocity (V_e), the larger the thrust (T). At the same time, propulsive efficiency is a measure of exhaust velocity. The higher the exhaust velocity, the lower the propulsive efficiency and thus the fuel efficiency. Equation 2.7 depicts the mentioned problem, V being the flight speed.

$$T = \dot{m}V\left(\frac{V_e}{V} - 1\right) \quad \text{conflict} \quad \eta_{prop} = \frac{2}{1 + \frac{V_e}{V}} \tag{2.7}$$

[18] Duesentrieb, B. (2021, November 11) Turbofan operation, https://commons.wikimedia.org/w/index.php?curid=460106

[19] A turbojet engine can be described as a turbofan with zero bypass ratio.

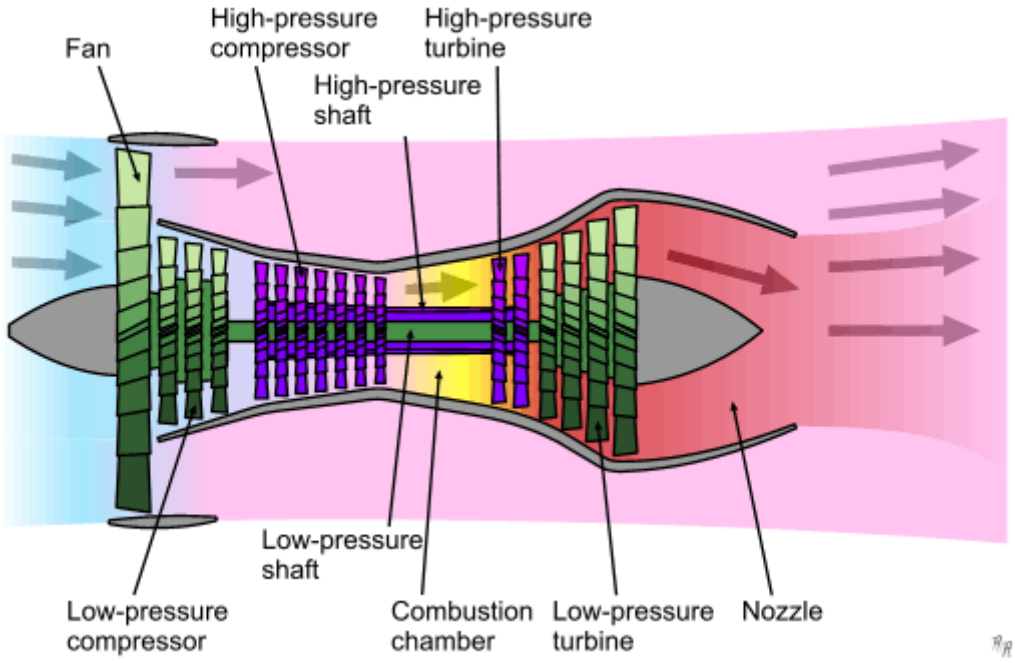

Figure 2.18: Turbofan representation.

Other aircraft also improved the efficiency of the engine. The 757 included improvements on the high bypass turbofan engines (Norris & Wagner, 1998). Boeing suggested that 787 would reduce fuel consumption by 20% concerning the 767. For which, 8% of the improvement would come from the new engine (Slayton & Spinardi, 2016). The A320neo and the Boeing 737 MAX focused on the reduction of fuel consumption by using better engines[20][21].

Operative Empty Weight Reduction

The fuel used in a flight depends on the aircraft's weight, composed of the Operative Empty Weight (OEW) and the payload weight. The payload weight (passengers and cargo) depends on the aircraft's mission, but the OEW can be reduced during the design phase. The A320 was the first aircraft using solely fly-by-wire systems[22]. Furthermore, only two crew members were needed to pilot it[23]. Finally, it was the first narrow-body airliner to have a considerable part of the structure made of composite materials. These three improvements had a substantial impact on the OEW; this reduction had a positive effect on fuel performance (Gilani, 2019). The Boeing 787 was the first airliner built mainly on composite materials to be produced in series (Slayton & Spinardi, 2016). The A350 OEW was reduced by using composites and aluminum. For future designs, Airbus seems to be focusing on reducing the structural weight by employing more composites[24].

Aerodynamic Improvements

The fuel used in flight is not only a function of the weight but also of the drag. Therefore, reducing aerodynamic drag improves fuel efficiency. The Boeing 767 mainly improved the aerodynamic design process by using computers and a total of 26000 hours in the wind tunnel (Norris & Wagner, 1998). The wing of the 767 was designed with a supercritical airfoil, allowing it to fly at higher altitudes reducing

[20] Airbus (2021, November 12) A320 Family, https://web.archive.org/web/20110704055351/http://www.airbus.com/aircraftfamilies/passengeraircraft/a320family/

[21] Boeing, (2021, November 12) Boeing launches 737 new engine family with commitments for 496 airplanes from five airlines, https://web.archive.org/web/20130515172539/http://boeing.mediaroom.com/index.php?item=1907

[22] The fly-by-wire system replaced heavy hydraulic and mechanical systems that connected the pilot controls directly to the control surfaces

[23] The previous aircraft required a flight engineer to be on board for the flights.

[24] Airbus (2021, November 17) Aircraft: Setting the standard for the modern aviation industry, https://aircraft.airbus.com/en/aircraft/

Table 2.2: Characteristics of liquid hydrogen and kerosene.

Characteristics	H_2	Kerosene / Jet A	Source
Heating Value $[kJ/g]$	120	42.8	(Janić, 2014)
Density at 283 K $[kg/m^3]$	71	811	(Janić, 2014)
Flame Temperature $[K]$	1486	1380	(Derakhshandeh et al., 2021)
Ignition Energy $[mJ]$	0.02	0.65	(Reider & Edeskuty, 1979)
Flame Speed $[m/s]$	2.7	0.42	(Reider & Edeskuty, 1979)
Fuel Cost 2040/2050 $[\$/kg]$	2.0-2.86	1.37	(Demir & Dincer, 2018)

the fuel consumption in terms of flight performance. Supercritical airfoils delay wave drag (Vos, 2019), which increases exponentially at high speeds when the airfoil experiences pockets of supersonic air. Delaying wave drag allows the aircraft to fly faster/higher without experiencing large drag Harris, 1990. The A320neo design changed the wingtips for sharklets, assumed to improve fuel efficiency by 3.5%[20]. Now, Boeing is focusing on aerodynamic design to reduce fuel use. The next-generation 737 will increase the fuel efficiency utilizing advanced wing design, which will decrease the drag and increase the speed, and thus less fuel will be burnt[25].

Operational Improvements

It was explained before that the Boeing 747 family included the high bypass turbofan. This aircraft also introduced a second floor and a widebody to carry 529 passengers. The widebody design allowed it to accommodate eight passengers per row. The increased number of passengers reduced the fuel used per passenger on board. It saved 1.2 billion gallons of jet fuel in 1980 relative to 1973 (Greene, 1992). The Boeing 757 improved operationally by finding a niche as a US transcontinental. It also was designed to land and take off from short runaways. The new A350 allows for the aircraft to stay more time in the skies, Airbus claims that it can be on the air for 40 more days than the competitor B777[24]. Furthermore, the A350 accommodates 325 passengers in a two-seat class configuration, therefore carrying more payload to a longer distance than the respective competitors.

Not all aircraft are being developed for the same missions; the company Boom Supersonic is developing the Boom Overture, a sustainable supersonic airliner that is supposed to roll out by 2025 and take passengers by 2029[26]. Moreover, Blended Wing Body (BWB) aircraft are also being investigated, but none have entered the market officially.

Summary

To summarize, fuel consumption has been reduced through improved operations, weight reductions, aerodynamic improvements, flight performance improvements, and engine improvements mainly driven by competition. All these improvements have indeed reduced the block fuel used, but to stop climate impact, it is necessary to go a step further. It is necessary to change the fuel of the aircraft. In the following section, Hydrogen will be analyzed as an alternative to further reduce emissions.

2.2.2. Alternative Fuel: Hydrogen

Hydrogen (H_2) has been proposed for commercial aviation by several projects due to its high specific energy density (Hoffmann, 1981, 2001). Furthermore, hydrogen is one of the most abundant gases on earth, and unlike hydrocarbons, it does not contain any form of carbon. One of the conclusions from Section 2.2.1 is that aircraft weight and volume are always kept to a minimum to increase fuel efficiency. Therefore, the fuel type should not be an exception. Table 2.2 displays some characteristics of liquid hydrogen compared to kerosene; these will serve to explain some of the key advantages and disadvantages of using hydrogen as aviation fuel. The following section will describe the hydrogen aviation performance.

[25] Boeing (2021, November 17) Boeing: The Boeing Company, https://www.boeing.com/commercial/737ng/
[26] Boom Supersonic (2021, November 18) Overture, https://boomsupersonic.com/overture

Table 2.3: Hydrogen density vs temperature and pressure.

Hydrogen Analysis Resource Center: ***Hydrogen Density (kg/m^3) at Different Temperatures (°C) and Pressures (MPa)***

	Pressure (MPa)						
Temperature (°C)	0,1	1	5	10	30	50	100
-255	73,284	74,252					
-250	1,1212	68,747	73,672				
-225	0,5081	5,5430	36,621	54,812	75,287		
-200	0,3321	3,3817	17,662	33,380	62,118	74,261	
-175	0,2471	2,4760	12,298	23,483	51,204	65,036	
-150	0,1968	1,9617	9,5952	18,355	43,079	57,343	
-125	0,1636	1,6271	7,9181	15,179	37,109	51,090	71,606
-100	0,1399	1,3911	6,7608	12,992	32,614	46,013	66,660
-75	0,1223	1,2154	5,9085	11,382	29,124	41,848	62,322
-50	0,1086	1,0793	5,2521	10,141	26,336	38,384	58,503
-25	0,0976	0,9708	4,7297	9,1526	24,055	35,464	55,123
0	0,0887	0,8822	4,3036	8,3447	22,151	32,968	52,115
25	0,0813	0,8085	3,9490	7,6711	20,537	30,811	49,424
50	0,0750	0,7461	3,6490	7,1003	19,149	28,928	47,001
75	0,0696	0,6928	3,3918	6,6100	17,943	27,268	44,810
100	0,0649	0,6465	3,1688	6,1840	16,883	25,793	42,819
125	0,0609	0,6061	2,9736	5,8104	15,944	24,474	41,001

Hydrogen Performance

Hydrogen has a heating value of 120 kJ/g while the kerosene heating value is almost three times smaller (42.8 kJ/g). Meaning that the same flight distance could be covered using one-third of the fuel. This advantage comes at a cost; the density of hydrogen in gaseous form at 283 K is 0.08988 kg/m^3, while the density of kerosene is around 811 kg/m^3. Hydrogen in the gaseous form at 283 K occupies around 3000 times more volume than kerosene.

However, hydrogen can be liquefied under certain combinations of pressure and temperature. The benefit of liquefying hydrogen is that the density is increased significantly. Table 2.3[27] displays the relation between temperature, pressure, and density for hydrogen. The observed jump in density corresponds to the liquefaction of the hydrogen.

In Table 2.3, it can be observed that it is not possible to achieve a similar density to that of kerosene (811 kg/m^3). Studies suggested that cryogenic hydrogen should be stored around temperatures of 20 K and between pressures of 0.125 to 0.175 MPa (Onorato, 2021; van Woensel, 2021). This corresponds to densities close to 70.8 kg/m^3. Liquid hydrogen then occupies around four times more volume than kerosene.

This section has investigated the main properties of hydrogen, and the feasibility concerning aircraft performance was proven. However, hydrogen was suggested as a sustainable solution. The following section will analyze the hydrogen climate implications.

Hydrogen Emissions

The potential weight improvement in aircraft operations by using hydrogen has been proven. The compound burned in the combustion chamber of the engine is different. Therefore the emissions would be different. As commented before, the main difference is that now carbon species are not expected in the exhaust, which eliminates CO_2, CO, UHC, Soot. The lack of aromatics in the fuel also eliminates SO_x formation. The new chemical equation for ideal combustion is represented in Equation 2.8 (Kahraman et al., 2018).

$$H_2 + a\frac{1}{2}(O_2 + zN_2) \rightarrow H_2O + (a-1)\frac{1}{2}O_2 + a \cdot \frac{z}{2}N_2 \tag{2.8}$$

Four different emission species are expected: H_2O, O_2 and N_2 and contrails[28] (Gauss et al., 2003).

[27] National Institute of Standards and Technology (2021, November 13) Reference Fluid Thermodynamic and Transport Properties Database (REFPROP), https://www.nist.gov/srd/refprop

[28] Please note that contrails is not a direct emission but is still treated as one.

The products of the actual combustion differ from those of ideal combustion. Nitrogen and Oxygen can react to form NO_x through thermal mechanisms. The following chemical formulae represent these mechanisms (Kahraman et al., 2018):

$$O + N_2 \leftrightarrow N + NO \tag{2.9}$$

$$N + O_2 \leftrightarrow O + NO \tag{2.10}$$

$$N + OH \leftrightarrow H + NO \tag{2.11}$$

Larger quantities of H_2O and NO_x are emitted when burning a kilogram of hydrogen compared to a kilogram of kerosene. Therefore, it is crucial to investigate the effects that a more substantial emission index of H_2O and NO_x have for the climate; and due to the higher water vapor content, revise the contrail formation probability. From simulations in Gauss et al. (2003), the cryoplanes emit 2.55 times more water vapor. The radiative forcing increase due to a higher water vapor emission rate depending on the region of emission and season. For cryoplanes flying in northern mid-latitudes, the radiative forcing was calculated to be 0.0027 W/m^2 in October and 0.0135 W/m^2 in April. Lower values were observed for the kerosene aircraft (0.0026 W/m^2). Increasing the cruise altitude by one km almost doubles the accumulated water vapor in the atmosphere; flying higher on hydrogen combustion will be detrimental for the climate .

NO_x emitted per kilogram of fuel is also supposed to increase when burning hydrogen due to the higher flame temperature of the hydrogen. A higher flame temperature indicates also a higher burn temperature in the combustor, which favors NO_x formation. However, it is important to remember that hydrogen has almost 3 times more energy per kilogram of fuel, and therefore the total NO_x emissions will also be reduced by 3. Some studies compared the NO_x emissions on turbofans by burning hydrogen and kerosene. Derakhshandeh et al. (2021) calculated that, even with an increase in $EINO_x$[29], the total emission of NO_x was to be reduced by 68.25% at the cruise phase, with further improvements if the engine was optimized. Moreover, Yahya et al. (2019) indicates an increase in $EINO_x$ of 2.38% but a total NO_x decrease of 57.94 %.

The formation of **contrails** depends on atmospheric, aircraft, and fuel characteristics and the number of aerosol particles present in the exhaust. The use of cryoplanes will alter the fuel characteristics and the number of aerosol particles. As mentioned before, hydrogen includes a higher water vapor emission index, increasing the probability of contrail formation. But at the same time, hydrogen combustion does not produce aerosol particles where the ice crystals from the contrail can nucleate(Gauss et al., 2003). Some studies suggest that even if there are no particles from direct hydrogen combustion, aerosol particles present in the air might serve as nuclei (Ström & Gierens, 2002). Marquart et al. (2005) suggests that the radiative forcing of hydrogen contrails in 2050 will be 30 % lower globally than that of conventional contrails, mainly due to the decrease in optical depth. Boretti (2021) also suggests a lower contribution to global warming from hydrogen contrails.

Hydrogen should not only be sustainable and economically viable but it should propose no harm to humans in the first place. Hydrogen safety must be considered due to the novelty of the gas in the transportation sector. The following hydrogen specifications contribute to hydrogen safety (Najjar, 2013; Reider & Edeskuty, 1979) (specifications beneficial for safety are marked with + and detrimental are marked with −):

Hydrogen Safety

The following hydrogen specifications contribute to hydrogen safety (Najjar, 2013; Reider & Edeskuty, 1979):

+ High buoyancy: Hydrogen is 14 times lighter than air; therefore, it can dissipate fast in an open-air issue.
+ Low flame emissivity in the air: reduces heat transferred, delaying undesired ignitions.
+ Non toxic spillage.
– Mechanical damage might result from the solidification of impurities.

[29] $EINO_x$ is the emission index of nitrogen oxide, defined as the amount of NO_x emitted per unit of energy value.

- Low ignition energy (0.02 mJ) and fast flame velocity (2.7 m/s) makes combustion in confined volumes dangerous.
- Hydrogen flames are nearly invisible in daylight.
- Hydrogen is very light, which might lead to leakage.
- Hydrogen is odor-free, tasteless and, colorless; a hydrogen leakage is dangerous and might pass unnoticed.
- Liquefied hydrogen low temperatures might cause ice formation and frostbite to touch.
- Liquefied hydrogen needs to be stored in pressurized vessels.

The most delicate safety link in the hydrogen logistics chain is aircraft refueling, where all these risks become more vibrant. Using hydrogen might be dangerous, but previous studies show that both hydrogen and kerosene can be equally safe (Airbus Deutschland GmbH, 2003) when precise measures and policies are applied (Clean Sky, 2020). Using hydrogen as the new aviation fuel might be desirable for the climate. But further research has to be made for hydrogen production and logistics.

Hydrogen Production & Logistics

The production of hydrogen is a very delicate matter. Hydrogen production should not paint black the green color drawn by the lower climate impact from hydrogen emissions. Hydrogen can be produced from renewable and non-renewable sources. Non-renewable sources include coal and natural gas, and next to hydrogen also carbon dioxide and carbon monoxide are produced. Renewable sources include biomass and water. While hydrogen production emissions from biomass also include CO and CO_2, creating hydrogen through water electrolysis does not generate any warming emissions (Janić, 2014). International Energy Agency (IEA) (2019) states that 76% of the hydrogen is produced using steam reforming of natural gas, 23% is produced from coal, and only about 2% is produced using electrolysis.

Next to the hydrogen logistics chain is transportation. Studies suggest that dedicated H_2 plants should be located close to the airports to satisfy the needs of the aviation sector and reduce the transportation costs (Janić, 2014; Grouset & Ridart, 2018). The advantage of hydrogen is that the resources are not localized, and hydrogen production plants could be located anywhere with access to water and electricity.

Finally, hydrogen supply or refueling at the airport could be done through dedicated pipelines and roads, which distribute the liquid hydrogen to the aircraft gates. Janić (2014) suggests placing adapters at the gate stands to fuel the aircraft and highlights the importance of removing all impurities from the tanks and venting the tanks to prevent liquid hydrogen boiling-off. These suggestions must be economically viable or else they will never be adopted.

Economics

Hydrogen production is not cheap. Svensson (2005) predicted that about 12% of the energy used by Sweden would be required to create through photolysis the hydrogen to fuel the Swedish aviation sector in 2050. Therefore, the cost from the production to the distribution of hydrogen must be analyzed.

Demir and Dincer (2018) studied different scenarios. One of the scenarios treated is Scenario 3, which is the hydrogen pathway that adapts best for hydrogen production and distribution in airports[30]. For the scenarios, Demir and Dincer (2018) assume a starting point in 2017 lasting 20 years to serve for a total of 80 refueling stations. The cost per kilogram of hydrogen would be 2.73 $\$/kg$, and if tube trailers want to be used, the cost would be 2.86 $\$/kg$. These results are in line with the costs displayed in Janić (2014) which determines that the long-term cost (2040/2050) of liquid hydrogen could be 2.0 $\$/kg$. For comparison, the price of Jet A1 aviation fuel is now 0.73 $\$/kg$ [31]. The role of future policies and how they might increase the price of carbon-based fuels due to taxes on emissions was investigated by Janić (2014) expects an increase to 1.37 $\$/kg$ by 2040/2050. Clean Sky (2020) identifies the use of hydrogen as an economically viable solution. However, it also notes a 5 to 30 % increase in the Cost of Available Seat Kilometer (CASK), depending on the range of the aircraft.

[30] Scenario 3 is designed for a city supply, where the hydrogen is transported to nearby cities and is distributed using pipelines. Therefore, due to the shorter distances on an airport, the price of hydrogen could be even lower.

[31] International Air Transport Association (2021, November 14) Jet Fuel Price Monitor, https://www.iata.org/en/publications/economics/fuel-monitor/

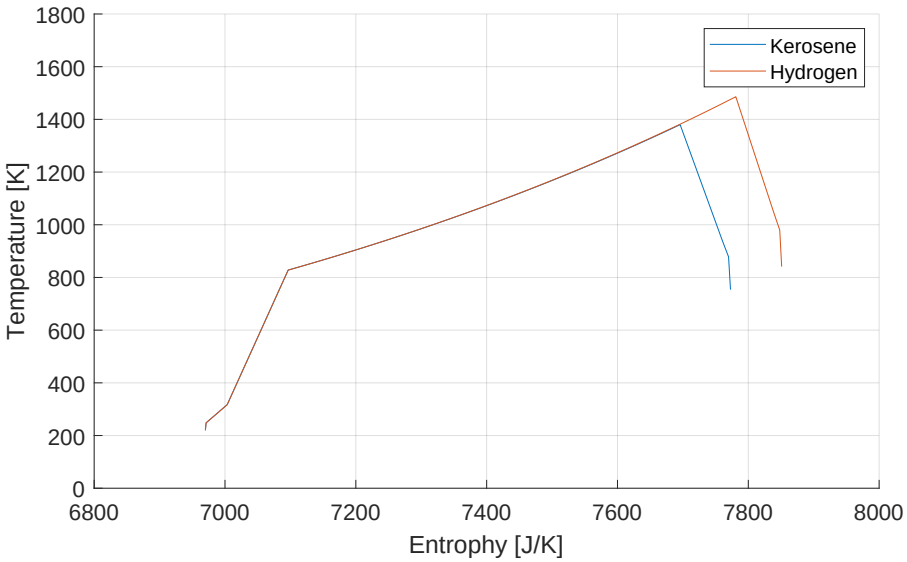

Figure 2.19: Temperature-enthalpy diagram comparing hydrogen and kerosene burning turbofan.

Hydrogen Feasibility Summary

The current cost and the risks that it carries make it impossible for short-term market implementation of hydrogen as aviation fuel. Policies, measures, and reductions in production costs are required and expected for long-term use in the aviation sector. Environmentally speaking, hydrogen has a clear advantage over kerosene, free of carbon emissions which contribute greatly to climate impact mitigation, but further analysis on water vapor and contrail emissions is required. Furthermore, hydrogen has different properties than kerosene. Therefore, when introduced in the combustion chamber of a turbofan engine, the thermodynamics might differ. This is analyzed in the following section.

Hydrogen Engine

An analysis must be done to understand how the introduction of hydrogen might affect the efficiencies of a turbofan engine. The working principles of a turbofan engine were explained in Section 2.2.1, but, how does the thermodynamic cycle change when burning hydrogen? Moreover, how does an optimized version of a turbofan engine differ from the kerosene variant?

Following the thermodynamic equations explained by Derakhshandeh et al. (2021) and Osigwe et al. (2021) it can be observed that the differences start when calculating the values related to the combustion chamber due to the different fuel mass flow and the different Turbine Inlet Temperature (TIT). This can be observed better in Figure 2.19 where the differences in temperature and enthalpy between the two engines can be visualized[32] (Rao et al., 2014).

For a turbofan with no limit on the combustion chamber temperature, the temperature at which hydrogen is burnt might be higher and thus, following the thermodynamic equations, a higher thrust would be obtained. However, engines are usually designed to give a specific amount of thrust and assuming higher temperatures in the combustion chamber might not be realistic, since the materials composing the engine might melt or expand. Both engine design approaches have been investigated, while Derakhshandeh et al. (2021) assumed a higher TIT, Osigwe et al. (2021) assumed a constant thrust. The characteristics of the two engine designs are presented in Table 2.4.

Although these engines might look comparable at first (due to similar thrust), the engine geometry is very different, as the bypass ratio is larger for (Derakhshandeh et al., 2021). From Table 2.4, the main information that can be obtained is that the Thrust Specific Fuel Consumption (TSFC) is improved by 282 % in the first case and by 283 % in the second case. Values for efficiencies were not found in Osigwe et al. (2021), but Derakhshandeh et al. (2021) calculated a slight decrease in engine efficiency when introducing hydrogen on the turbofan engine, as observed in Table 2.5.

[32]Please note that the example taken does not include kerosene but another form of cleaner combustion, liquefied natural gas (LNG), which is closer to kerosene than hydrogen.

Table 2.4: Engine characteristics for different hydrogen design options.

Engine Characteristics	Constant Thrust (Osigwe et al., 2021)		Increased TIT (Derakhshandeh et al., 2021)	
	Hydrogen (LH_2)	**Kerosene**	**Hydrogen (LH_2)**	**Kerosene**
Net thrust $[kN]$	89.54	89.54	80.59	72.45
Mass flow $[kg/s]$	269	269	63.79	64.55
Altitude $[m]$	10000	10000	10668	10668
Cruise Mach [-]	0.7	0.7	0.83	0.83
Bypass ratio [-]	4.8	4.8	8.1	8.1
OPR [-]	28.5	28.5	40.44	40.44
Fuel flow rate [kg/s]	0.45	1.27	0.49	1.25
TSFC [g/kNs]	5.02	14.18	6.08	17.25
TIT [K]	1164.15	1173.15	1487.52	1380.7

Table 2.5: Engine characteristics for optimized hydrogen engine (Derakhshandeh et al., 2021).

Engine Characteristics	Original Engine		Optimized Engine
	Hydrogen (LH_2)	**Kerosene**	**Hydrogen (LH_2)**
Net thrust $[kN]$	80.59	72.45	84.24
Mass flow $[kg/s]$	63.79	64.55	63.80
Bypass ratio [-]	8.1	8.1	10.3
OPR [-]	40.44	40.44	39.49
FPR [-]	1.65	1.65	1.61
Fuel flow rate [kg/s]	0.49	1.25	0.50
TSFC [g/kNs]	6.08	17.25	5.9
TIT [K]	1487.52	1380.7	1487.52
Propulsive efficiency [%]	87.21	87.94	87.79
Thermal efficiency [%]	38.31	38.50	39.52
Overall efficiency [%]	33.41	33.86	34.70

Derakhshandeh et al. (2021) went a step further and improved the design of the engine by adapting the bypass ratio and the Fan Pressure Ratio (FPR) to optimize the thrust specific fuel consumption and the specific thrust. The overall efficiency was improved by 1 % to the kerosene original version and by 1.3 % to the hydrogen original version. The observations of these reports were contrasted with (Kahraman et al., 2018), whose conclusions seem to be in line with the results presented here.

A way that kerosene turbofan engines are trying to cope with the high emissions is through lean combustion. As explained before, NO_x formation is increased with flame temperature. Lean combustion increases the amount of air and thus increasing the air to fuel ratio. This reduces the temperature of the flame, but if too much air is introduced, the flame can be extinguished. Kerosene and hydrogen have different equivalence ratios[33] for which the engine can operate without extinguishing the flame (Figure 2.20).

In the case of kerosene, the control range for equivalence ratios is quite high. Hydrogen on the other hand is very flammable, and it can still operate at lower equivalence ratios. The hydrogen then allows for lean combustion at higher air to fuel ratios, reducing temperature and thus reducing further NO_x emissions. Funke et al. (2019) and Sorokin et al. (2006) assume that a larger reduction in $EINO_x$ can

[33]Equivalence ratio is defined as the ratio of the fuel to air ratio to the stoichiometric fuel to air ratio. Stoichiometric is the perfect balance to generate the optimal amount of heat.

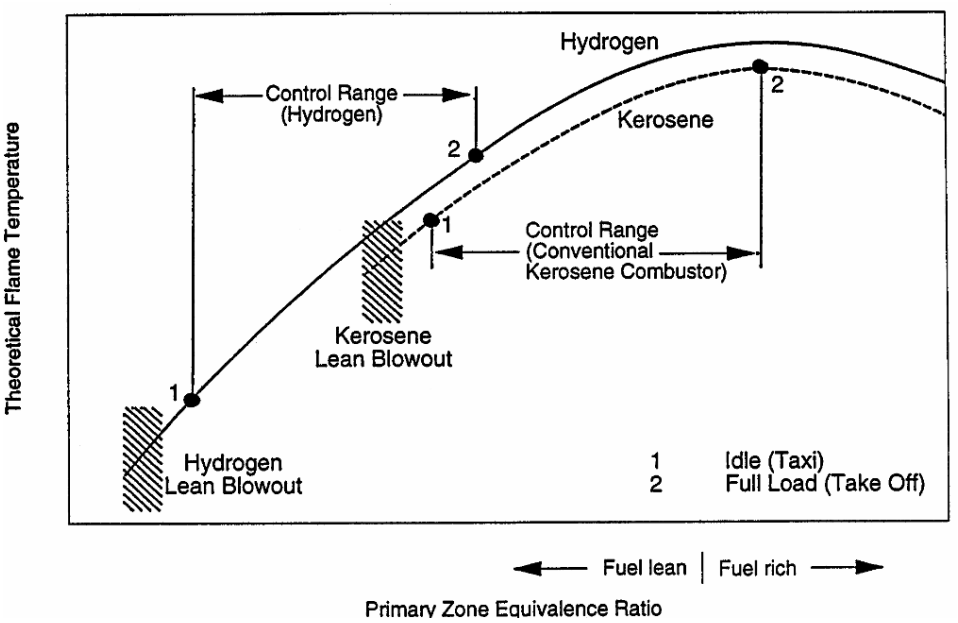

Figure 2.20: Combustion ranges for hydrogen and kerosene (Svensson, 2005).

be achieved if micromix combustion is used. Funke et al. (2019) assumes a 90% reduction while Sorokin et al. (2006) assumes 80%. However Funke et al. (2019) also mentions that, if micromix combustion is not used, it is possible that $EINO_x$ emissions increase by 30%. Due to the large discrepancies in the possible outcome of $EINO_x$ when using hydrogen, it will be subject to sensitivity analysis.

History of Hydrogen Aviation

Hydrogen combustion is not only a good method to reduce emissions but it was also proven to be a good method to improve engine efficiency and specific fuel consumption. Current aviation is still far from using hydrogen-powered engines, but, what have been the technology advancements in this sector?

After the Graf Zeppelin[34], NACA, with the help of Abe Silverstein, founded the project Bee in 1955 to determine the feasibility of flying an aircraft with liquid hydrogen. Only two years after, NACA flew one of his Martin B-57B for 20 minutes powering with hydrogen on one of the two engines [35]. At the end of the 1950s, hydrogen-powered military aircraft designs were being investigated. Lockheed Skunk Works director and chief aircraft design proposed the Lockheed CL-400 Suntan. However, this program was canceled due to the range and cost specifications [36]. The Tupolev Tu-154 airliner was heavily modified to fly with hydrogen on one engine, resulting in the Tu-155, which flew for 21 minutes (Brewer, 1991). Figure 2.21 depicts the first models that used hydrogen. It is important to note that the drawing is not to scale.

For hydrogen use on unmanned vehicles, the Aerovironment Helios program from NASA developed the Helios prototype in 1999. Helios used a combination of solar cells and hydrogen fuel cell technology to power the aircraft during the day and night. This program was continued with the AeroVironment Global Observer, which had the first flight in 2010 and was fully powered by a hydrogen fuel cell system footnoteBrelje, B. (2021, November 15) Hydrogen-powered aviation part 1: a history, https://brelje.net/blog/hydrogen-powered-aviation-part-one-history/.

Due to climate change and the need to reduce the climate impact from aviation, more recent studies have been carried out to investigate the use of hydrogen in airliners. In 2003 Europe launched the cryoplane project to study the transition from kerosene to hydrogen in aviation (Airbus Deutschland GmbH, 2003). The cryoplane was expected to have a larger wetted area due to the placement of the

[34]The Graf Zeppelin was an airship made of aluminum and cotton silk, filled with hydrogen, with a positive buoyancy on air.

[35]National Advisory Committee for Aeronautics (2021, November 15) NACA Research on Hydrogen for High-Altitude Aircraft, https://history.nasa.gov/SP-4404/ch6-4.htm

[36]National Advisory Committee for Aeronautics (2021, November 15) Suntan, https://history.nasa.gov/SP-4404/ch8-1.htm

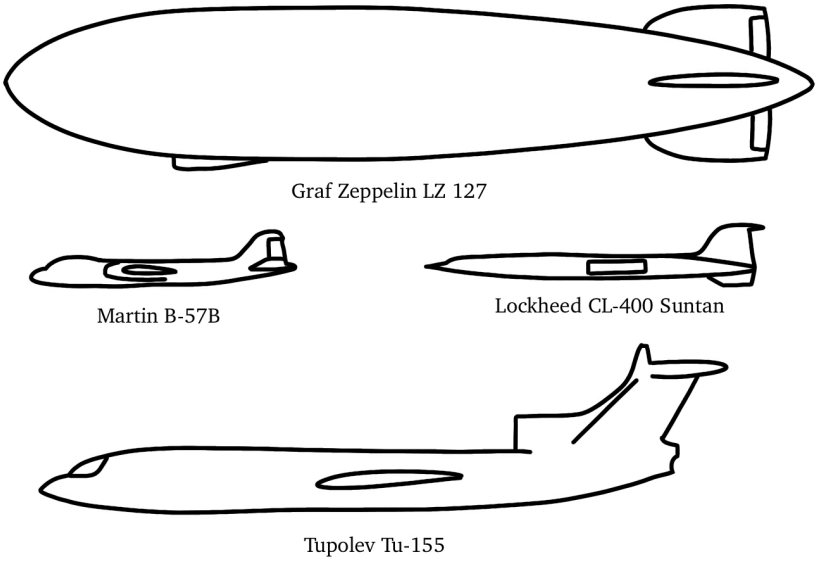

Figure 2.21: Hydrogen-powered aircraft history, aircraft drawings not to scale.

hydrogen storage; and the increase in the operative empty weight. Note that these results are detrimental for the aircraft performance and fuel consumption as explained in Section 2.2.1 and make it almost impossible for long-range aircraft. The cryoplane project already confirmed that hydrogen combustion on turbofan engines would not decrease efficiency. Airbus Deutschland GmbH (2003) admitted that *although hydrogen aviation could be a suitable alternative, it was unattractive under today's conditions and that the earliest implementation could be expected in 15 to 20 years.* After almost 19 years, the first official projects from leading civil transportation firms have only arrived.

Ultimately, aircraft producers will have the strong hand to decide whether hydrogen implementation is efficient and viable. While some producers like Airbus or Embraer have revealed hydrogen concepts[37][38], other producers like Boeing remain cautious about hydrogen and prefer to focus on sustainable fuels[39]. In September 2020, Airbus revealed the ZEROe concepts for hydrogen aviation. The turbofan and turboprop concepts relied on extending the fuselage to increase the volume available for tank storage. This idea poses the same problem that the cryoplane faced (Airbus Deutschland GmbH, 2003), which is the increase in wetted area and operative empty weight. Airbus introduced a new option, the Blended-Wing Body (BWB) for wide body concept. However, the BWB design faced many challenges and forced the aircraft design sector to look into other aircraft designs. In 2015, the Flying-V was revealed. The Flying-V is a concept similar to the blended wing body developed by Benad (2015) and has shown the possibility to be powered by liquid hydrogen (van Woensel, 2021).

2.2.3. Aircraft Analyzed

This section will introduce the aircraft used in the study to analyze the climate impact of hydrogen combustion compared to kerosene. Initially the analysis was entirely proposed for the Flying-V, however the Flying-V design has been proposed as a study case to suggest an alternative to the common tube-and-wing design.

[37] Embraer (2021, November 15) Embraer presents the Energia Family – Four New Aircraft Concepts Using Renewable Energy Propulsion Technologies, https://embraer.com/global/en/news?slug=1206950-embraer-presents-the-energia-family-four-new-aircraft-concepts-using-renewable-energy-propulsion-technologies

[38] Airbus (2021, November 15) Towards the world's first zero-emission commercial aircraft, https://www.airbus.com/en/innovation/zero-emission/hydrogen/zeroe

[39] Boeing (2021, November 15) Boeing Commits to Deliver Commercial Airplanes Ready to Fly on 100% Sustainable Fuels, https://boeing.mediaroom.com/2021-01-22-Boeing-Commits-to-Deliver-Commercial-Airplanes-Ready-to-Fly-on-100-Sustainable-Fuels

Tube-and-Wing Aircraft: FlyZero

The Aerospace Technology Institute[40] is promoting transformative technology in air transport, their project FlyZero includes the road-map aiming to realise zero-carbon emission of commercial aviation by 2030. Beddoes et al. (2022) proposed three different aircraft designs for the regional, narrowbody and widebody market segments. The widebody market segment is the second largest source of aviation emissions after the narrowbody segment. The stronger motivation to introduce hydrogen technology in the widebody sector is induced by the fact that the route network in this sector includes a small number of major airports, which will benefit the initial hydrogen infrastructure costs and will ease the entry into service. Therefore, this study will focus its attention on the widebody midsize hydrogen aircraft displayed in Figure 2.22.

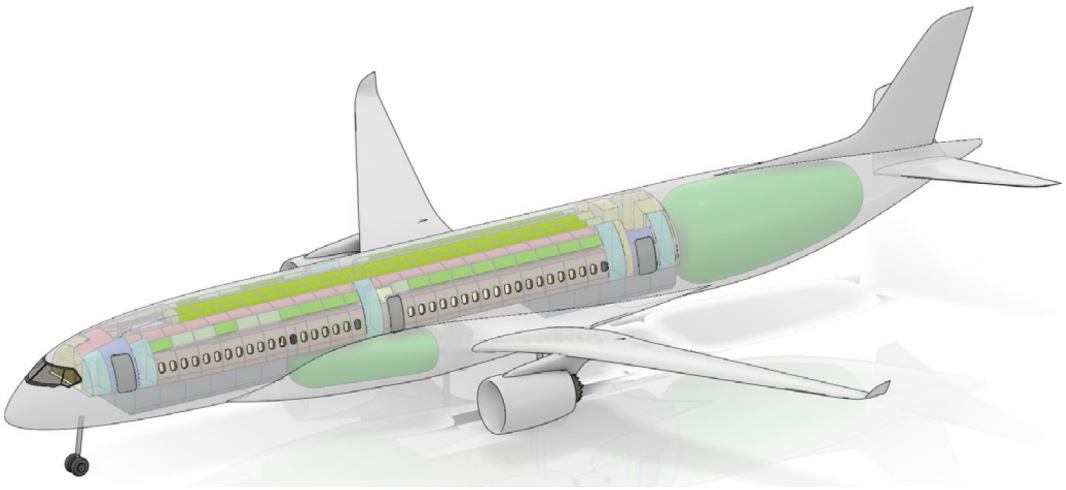

Figure 2.22: Midsize widebody aircraft designed by the Aerospace Technology Institute (Beddoes et al., 2022).

Figure 2.22 displays in green the hydrogen tanks, these have to be located outside the engine rotor failure zones, zones where bird strikes might affect the airplane and general crashworthiness. The tank position has also been designed to allow for sufficient longitudinal stability during the flight phases. To increase tank space the fuselage diameter has been increased, which will cause slightly higher zero-lift drag compared with kerosene aircraft. The most relevant information for the study has been listed in Table 2.6.

Alternative Aircraft: Flying-V

The Flying-V is a V-shaped aircraft, which combines the fuselage and the wings in a single component as observed in Figure 2.23. The design from Benad (2015) was born at the technical university of Berlin in collaboration with Airbus. It was designed as a competitor to the Airbus A350-900, with similar characteristics in passengers (315), cargo (36 LD3), and cruise speed (0.85 Mach). While the aircraft had the same span of 64.75 meters, the length was considerably reduced compared to the A350. After several improvements and studies, the new Flying-V-900 achieved a reduction in fuel consumption of 20% concerning the A350-900 (Faggiano et al., 2017; Oosterom, 2021). The climate impact of the kerosene Flying-V design was tested by Reekers (2021) and the results proved that when flying at the same altitude of 11 km the Flying-V resulted in 11% less surface temperature increase than its competitor, the A350-900. This reduction, although beneficial, seems to waste the opportunities of the Flying-V. The high volume of the Flying-V makes it special for the use of hydrogen. van Woensel (2021) investigated the hydrogen Flying-V design which can be observed in Figure 2.24, where the yellow containers represent the hydrogen tanks, the black container the space for luggage and the main grey area the cabin for the passengers. The two Flying-V's which are going to be used in this study are, the Hydrogen Flying-V from (van Woensel, 2021) and the kerosene FV-800 from (Oosterom, 2021) as both are designed for a similar payload capacity and range as the widebody tube-and-wing aircraft hydrogen aircraft selected above. The parameters for both versions of the Flying-V's are listed in Table 2.6.

[40] Aerospace Technology Institute (2022, June 06) https://www.ati.org.uk/

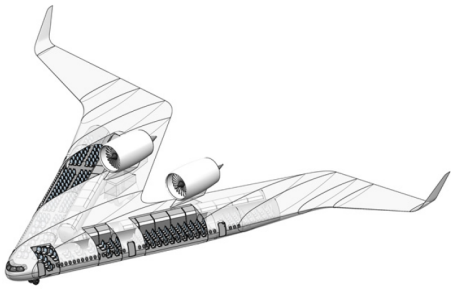

Figure 2.23: Original Flying-V design from (Benad, 2015).

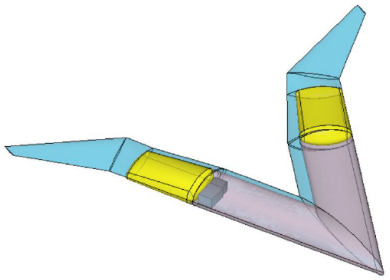

Figure 2.24: Hydrogen Flying-V 1000 final configuration (van Woensel, 2021).

Aircraft Parameters

The aircraft parameters used during the study are listed in Table 2.6, namely, the hydrogen widebody aircraft designed by the Aerospace Technology Institute (FZM-1G), the baseline aircraft with similar mission requirements that will serve as the kerosene version in this study (B767S), the hydrogen version of the Flying-V based on the FV-900 (FVHY) designed by van Woensel (2021), and FV-800 kerosene version designed by Oosterom (2021).

Table 2.6: Characteristics of the aircraft investigated in the study.

Characteristics	**FZM1G**	**B767S**	**FV8**	**FVHY**
Fuel Type	hydrogen	kerosene	kerosene	hydrogen
Cruise Altitude $[km]$	10.7	10.0	12.6	13.0
MTOW $[kg]$	150 800	170 000	164 000	159 000
OEW $[kg]$	104 800	96 500	89 000	110 200
Design Range $[km]$	10 650	10 650	11 160	10 650
Design Payload $[kg]$	29 250	29 250	27 600	29 250
Design Fuel $[kg]$	16 750	44 250	47 040	19 550
S_{ref} $[m^2]$	245	255	684	793
Span [m]	52.0	52.0	57.1	60.7
Wing Loading $[kg/m^2]$	616	667	239	201
CL/CD [-]	19.9	22.1	22.1	21.6
$C_{D,0}$ [-]	0.01	0.012	0.00595	0.0056
k [-]	0.052	0.050	0.086	0.095

From Table 2.6 several observations can be made. The MTOW for the hydrogen aircraft is lower than for the kerosene aircraft. The lower MTOW is caused by the lighter fuel weight, which has to do with the energy density of hydrogen, as explained in Section 2.2.2. However, the hydrogen aircraft have a heavier OEW, caused by the heavier tank required to store liquefied hydrogen, as the tank needs to stand high pressures and provide enough insulation for the cold temperatures of the fuel (van Woensel, 2021). If we compare the MTOW of the tube-and-wing aircraft and the Flying-V, it can be noticed that while the FV8 has a lower weight than the B767S, the FVHY has a higher MTOW than the FZM1G. This deviation is mainly due to the amount of hydrogen carried on board and therefore the heavier tank weight. It can be observed that for the hydrogen Flying-V to perform the same mission than the FZM1G, it requires 16% more hydrogen fuel. The increase in fuel consumption is caused mainly by the engine assumptions, being considerably more optimistic for the FZM1G as it will be observed in Chapter 3. The kerosene Flying-V should have a lower fuel consumption than the B767S due to the higher cruise altitude and similar CL/CD, however, the fuel consumption for the B767S is reduced due to the optimistic engine performance assumption of (Beddoes et al., 2022). The coefficients k and $C_{D,0}$ will be used to compute the thrust force required to keep a certain flight profile, it can be observed that

$C_{D,0}$ is higher for the regular tube-and-wing aircraft due to the less efficient aerodynamic design and lower for the Flying-V designs. The mission parameters will be used to calculate the payload weight on board given the range of the mission and the engine perforamance parameters. These interactions will be better discussed in Chapter 3.

Figure 2.25 displays the payload-range diagram for the aircraft aforementioned. The values for the tube-and-wing aircraft were taken from Beddoes et al. (2022), for the kerosene Flying-V from Oosterom (2021) and for the hydrogen Flying-V from (van Woensel, 2021). It must be noted that the ferry range (maximum range) will not be used, as the maximum mission range will be set to the design range to prevent a shortage of passengers.

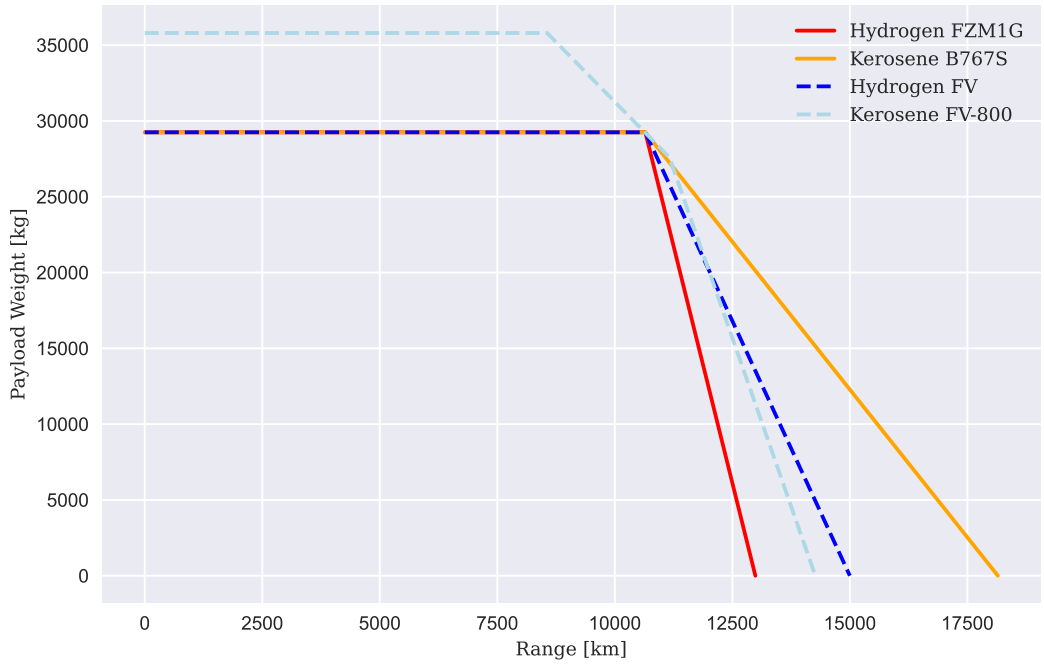

Figure 2.25: Payload-range diagram displaying the mission capabilities of the different aircraft.

From Figure 2.25 it can also be noted that the Kerosene Flying-V is able to fly more payload weight (specifically cargo weight as the number of passengers for the three aircraft is the same). In case a comparison with the rest of the fleets is required, the climate impact will be divided by the payload flown. It is important to note that all aircraft coincide on a single point (29000 kg of payload at a range of 10650 km), which will ease the comparison of the aircraft.

3

Methodology

The methodology can be divided in two main phases, the emission inventory calculation phase (Section 3.1 & Section 3.2), and the climate assessment evaluation phase (Section 3.3). A sensitivity study is carried out to understand the implications of uncertainties in the methodology related to flight performance of and the climate impact model. The relations between the different modules are displayed in Figure 3.1. The routing design model (orange) selects the city-pairs to be flown by the aircraft on the flight simulation model (red), which generates an emission inventory with location data, amount of fuel burnt, NO_x emitted and flight frequency. The emission inventory is passed to the climate impact model (blue), which computes the change in surface temperature for the two aircraft.

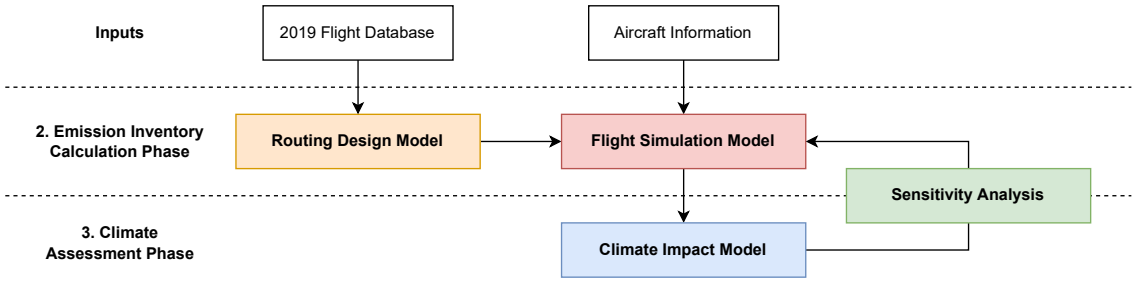

Figure 3.1: Overview methodology chain for climate assessment of hydrogen and kerosene aircraft composed of different modules differentiated by color.

The objective of this study is to create and use a methodology to determine the surface temperature increase caused by a fleet of both hydrogen and kerosene combustion aircraft. To understand the implications of hydrogen on climate change, we have to select at least two aircraft able to perform a similar mission, meaning that they should have a similar payload range diagram. This allows us to choose the FZM-1G (FZM1G) and the B767-2030 (B767S) proposed by (Beddoes et al., 2022), the B767S design is suggested as a sustainable aircraft with 2030 technology. The study will analyze the climate impact of the Flying-V as a study case, which is why the Flying-V was introduced in Table 2.6. The hydrogen Flying-V (FVHY) and the kerosene Flying-V (FV8) will help us understand the implications of alternative aircraft designs on climate impact. Figure 3.2 displays the four aircraft, the color of the arrows indicates the relevance of the comparison to the study. The most important comparison to meet the objective of the research is between the FZM-1G and the B767-2030. Then, we can compare each of the models to their competitors, the Flying-V designs, and finally we can compare the two Flying-Vs.

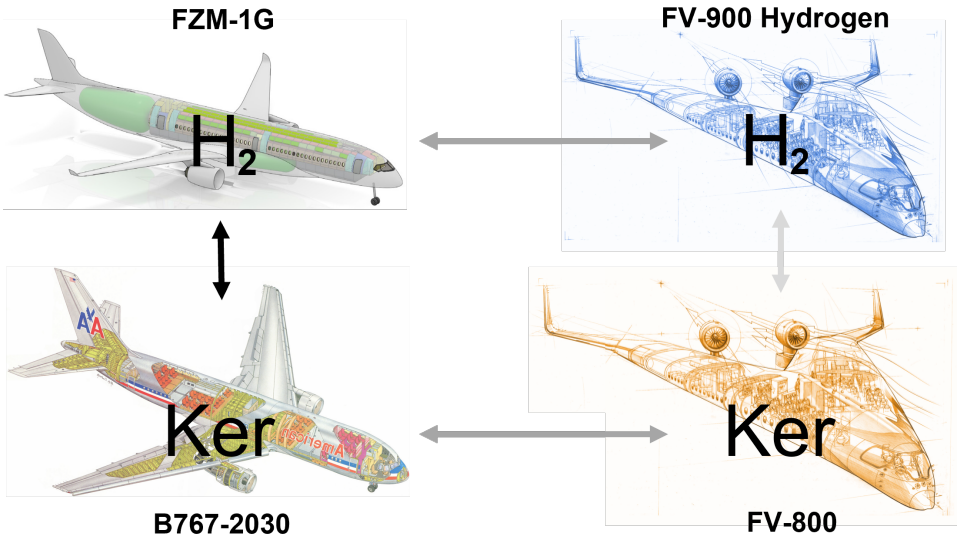

Figure 3.2: Selected aircraft designs. The intensity of the arrows displays the comparison´s importance for the study.

3.1. Routing Design

In Section 2.1 it was explained that both CO_2 and non-CO_2 climate effects must be analyzed. Non-CO_2 effects depend greatly on location of the emission. Therefore, the different aircraft used in the study (FZM1G, B767S) and in the case study (FVHY, FV8) will have to fly climate significant routes to properly model the surface temperature change.

3.1.1. Route Requirements

When selecting routes it is important to establish certain requirements: the routes selected must be flown by conventional aircraft with similar capabilities to the ones in Figure 3.2 in terms of range and payload. The minimum range was set to 3000 km and was selected following the market demand for widebody aircraft. The maximum range was selected as the design range of the FZM1G aircraft, 10650 km. The design range for all the aircraft is very similar which allows for a fair comparison. Routes will also be selected based on flight frequency. One flight a day will ensure that selected routes can be meaningful for climate and will eliminate flights which are not commercially scheduled. Finally, it is important to guarantee a global coverage to consider the local non-CO_2 effects on climate.

3.1.2. Data Processing

FlightRadar24[1] provided flight information from all around the globe for 2019 and 2020. Initially, the data comprised more than 50 million flights (10.2 GB of data) which has to be processed before it can be useful. The following subsections will detail the data processing steps.

Data Filtering

The flight file contains scheduled commercial air transport services, non-scheduled services[2] and general aviation[3] (International Civil Aviation Organization (ICAO), 2009). Only flights from scheduled commercial air transport were selected [4]. The complete list of aircraft codes kept for the routing analysis can be found in Appendix A. Further filtering was applied to keep only information related to the flight

[1] FlightRadar24 (2021, November) Live Air Traffic https://www.flightradar24.com
[2] Non-scheduled services include charter flights and on demand flights.
[3] General aviation includes non-commercial business aviation, aerial working, instructional flying and pleasure flying.
[4] International Civil Aviation Organization (2022, January 17) Aircraft Type Designators https://www.icao.int/publications/DOC8643/Pages/Search.aspx

origin and destination, time and type of aircraft. When the required information was unknown or the origin and destination airports were the same, the flight was removed.

Airport Information

The IATA codes for origin and destination airports were used to obtain the longitudinal, latitudinal and altitudinal coordinates for the flight take-off and landing. Extra airport information[5][6][7] was combined with the filtered flight data. It must be mentioned that flights for which no airport information was found were eliminated.

From Flights to City Pairs

Theoretically, this study does not consider the climate effects of emissions depending on the time of the year. Therefore, the flights could be grouped by routes. This means that, instead of having one row for each flight (300 rows for the flights from Amsterdam to Madrid), now there is a row per route (1 row for the flight from Amsterdam to Madrid with a frequency of 300). Moreover, the route from airport A to airport B was combined with the route from airport B to airport A, assuming that there is no difference on flight orientation. The file created after this initial data filtering weights 24.7 MB and it is more manageable.

Flight Distance and Location

The flight range is one of the most important route parameters which will be used in the flight simulation module. The python package geographiclib was used to calculate the geodesic from origin to destination airport[8]. In order to track transoceanic and transcontinental flights, the origin and arrival country was substituted by the continent. After all data processing is done, the final data file includes 253445 different routes for a total of 30 MB of data.

Waypoint Calculation

The data processing includes one extra step. The climate impact model (AirClim) will require an emission inventory. The emission inventory is composed by the flight route of the aircraft given in waypoints. These waypoints must include the altitude, the longitude and the latitude along the flight. The routing design includes the calculation of these waypoints using the python package geographiclib[8].

3.1.3. Flight Finder (FF)

The data processing was useful to organize and reduce the working size of the data, however a route selection tool was developed to organize faster the data and select the most relevant flights depending on the application. The tool is displayed in Figure 3.3.

[5] OurAirports (2021, November 14). Open data downloads https://ourairports.com/data/

[6] Partow, A. (2021, November 14) The Global Airport Database https://www.partow.net/miscellaneous/airportdatabase/

[7] OpenFlights.org (2021, November 14) Airport, airline and route data https://openflights.org/data.html

[8] Karney, C. (2021, November 23). Geographiclib 2.0 Documentation https://geographiclib.sourceforge.io/html/python/

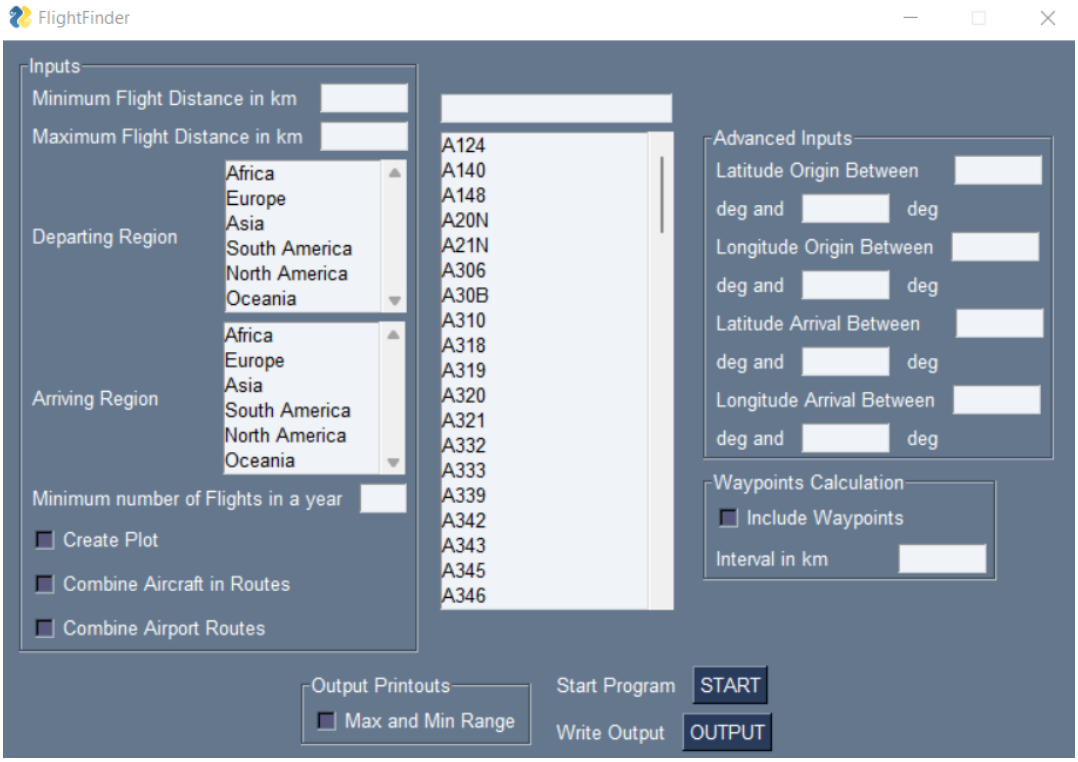

Figure 3.3: Flight finder tool GUI displaying the different options to run the code.

The tool includes a filter for flights with a minimum and maximum flight distance and for the continent where it is arriving or departing. The aircraft ICAO codes can be chosen to filter based on aircraft types. The option "Create Plot" can be selected to include an image of the selected flights. The "Advanced Inputs" can be used to include a better filtering of the airport location. To reduce further the dataset, the boxes "Combine Aircraft in Routes" and "Combine Airport Routes" are included. If the first option is selected, all the flight routes will be combined regardless of the aircraft used to fly the route. If the second option is selected, flights will be combined in city pairs, independent of flight direction (AMS-MAD = MAD-AMS). The "Waypoints Calculation" box includes the option to create three extra columns in the output file. These columns represent the flight distance, latitude, longitude for each flight route with a chosen distance interval between the waypoints in kilometers. The "start" button saves the inputs and the "output" button saves the files in the program folder. The complete methodology for the routing design module can be observed in Figure 3.4

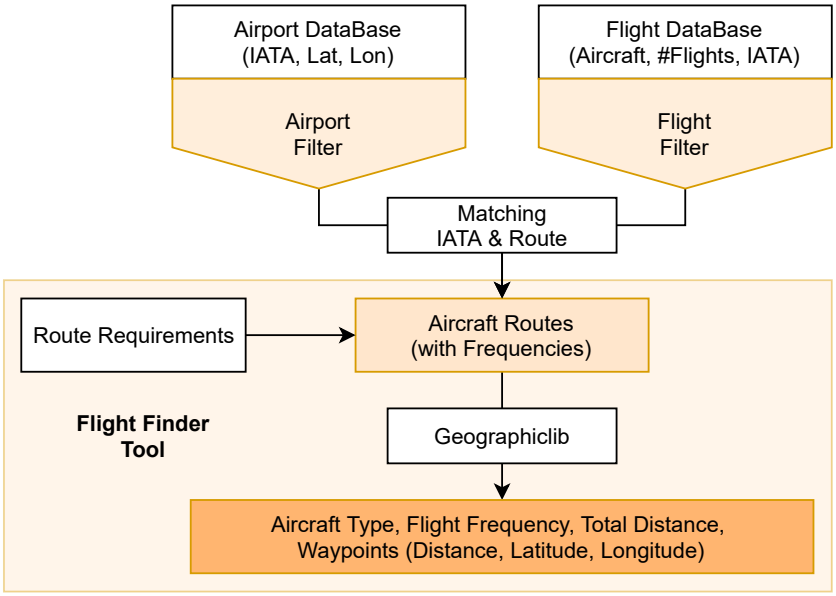

Figure 3.4: Detailed methodology of the routing design module. The methodology starts with a data filtering applied to the airport and flights database. Then the information from both is merged in a single file containing the routes, flight frequency, aircraft type, and airport information. Finally the flight finder tool was designed to filter flights.

3.2. Flight Simulation

The flight simulation methodology can be observed in Figure 3.5. The information used by the flight simulation model is composed by the aircraft characteristics and the routing design. The model evaluates all the routes selected in the routing design model. When a certain route is selected, total range is used to compute initial weight of the aircraft (Initial Weight Estimator). Next, aircraft speed and rate of climb and descent are used to compute the flight plan (Flight Planner). When the flight iteration begins, the state of the aircraft (angle of attack, speed, flight path angle, weight, etc.) is ran through a module which declares if the aircraft should climb, cruise or descend (Auto Pilot). Then the state of the aircraft is ran through the flight dynamics model which updates its status using the energy equations from Eurocontrol (2004). An interpolation over an engine model (created for each aircraft using Proesmans and Vos (2021)) is used to rapidly convert engine thrust in fuel flow. Fuel flow is used to compute NO_x Emission Index ($EINO_x$) at every step of the flight and to update the fuel weight of the aircraft. $EINO_x$ is calculated using the BFFM2 method (Turgut & Usanmaz, 2017). Next, aircraft weight and flown distance are updated. When flown distance equals the total range of the flight, the extra fuel weight is computed (contingency fuel). If fuel remaining is $\pm$ 10 % of required contingency fuel (5% of the consumed fuel), the simulation is finished, and the next route can be analyzed.

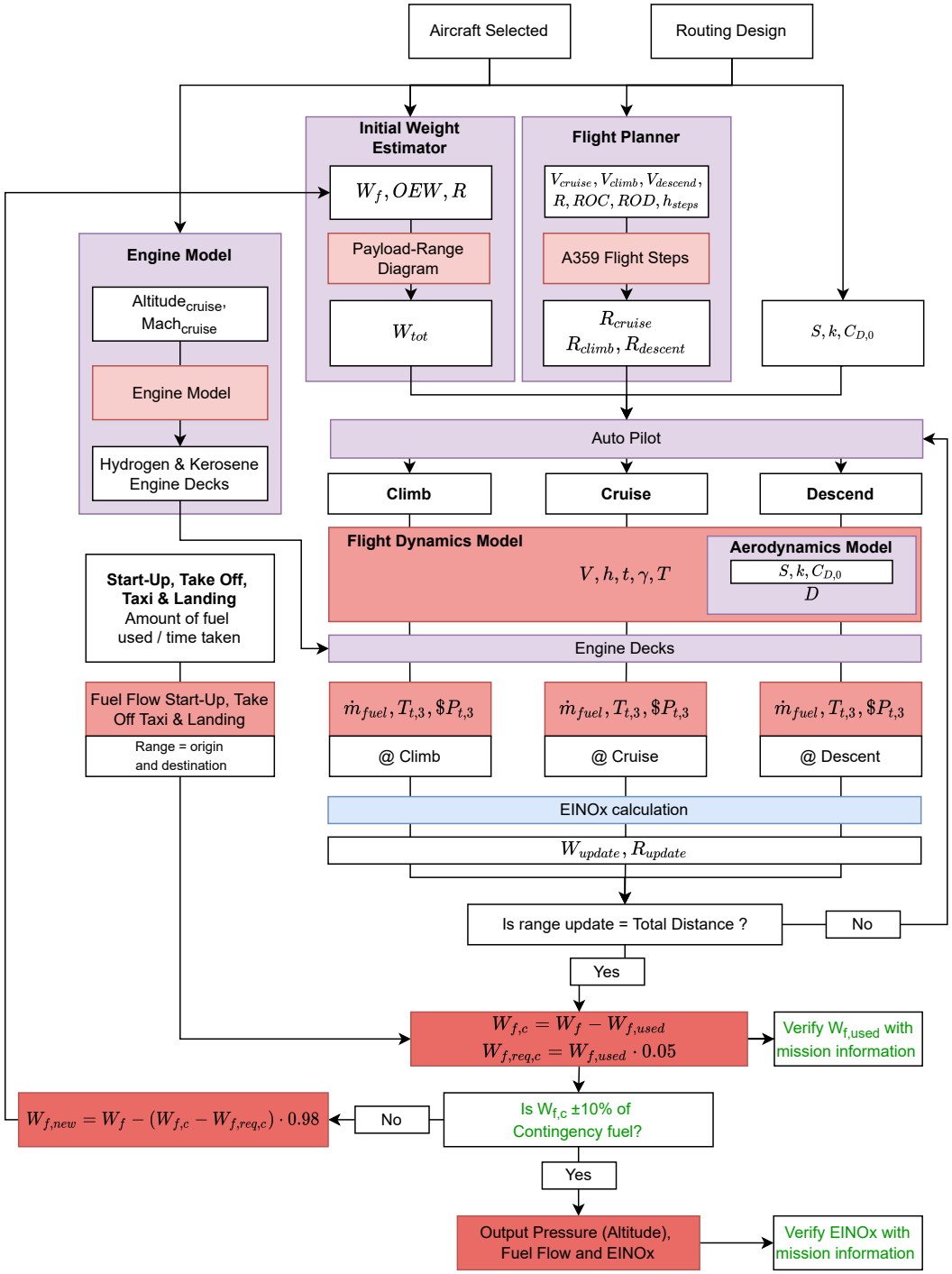

Figure 3.5: Flight simulation methodology.

Several modules were mentioned briefly during the explanation of figure Figure 3.5. These modules will be now explained in detail.

3.2.1. Initial Weight Estimator

The initial weight estimator outputs the initial aircraft weight composed by fuel weight, operative empty weight and payload weight. Operative empty weight and maximum take off weight are obtained from the aircraft characteristics, while payload weight is calculated with the payload-range diagram. It is assumed that the aircraft is carrying as much payload as it can for the specified range, although a

payload load factor could easily be applied when the payload range is maximum. If the mission range is longer than the design range maximum fuel weight is assumed, else, fuel weight is calculated using the maximum take off weight, the payload weight and the operative empty weight as in Equation 3.1. The initial weight of the aircraft is then passed to the flight simulation loop.

$$W_{\text{fuel}} = MTOW - OEW - W_{\text{pay}} \tag{3.1}$$

3.2.2. Flight Planner

The Flight Planner contains the information to plan the climb, cruise and descent of the aircraft. The climb and descend flight plan will imitate the one of the B767-200ER displayed in Figure 3.6[9]. The Flight Planner will provide the Auto Pilot with the altitude bounds to calculate if the aircraft should cruise, climb or descent. Aircraft velocity during initial climb, approach, climb to FL240 and cruise is considered constant. In the rest of flight phases, speed changes linearly to match the speed at the beginning of the next flight phase. Similarly, rate of climb and descend also varies linearly to match the rate of climb and descend at the beginning of the next flight phase.

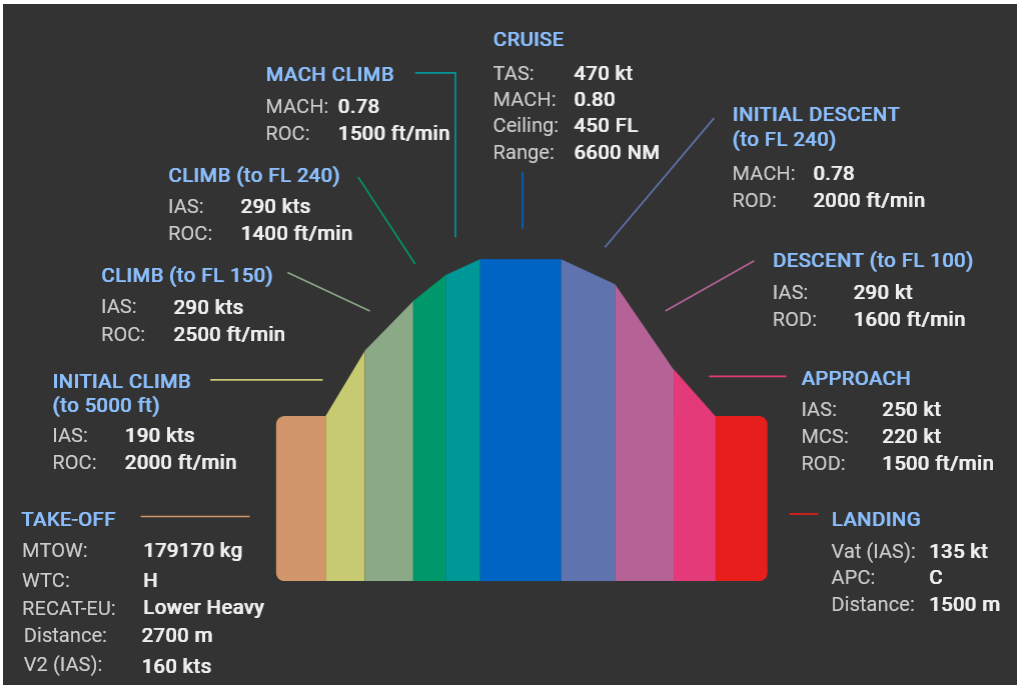

Figure 3.6: Climb and descend performance of the B767-200ER.

3.2.3. Auto Pilot

The auto pilot module is programmed to give commands to the aircraft to climb, cruise or descent. The Auto Pilot commands the aircraft to climb until the altitude is equal to the cruise altitude. In cruise, when the distance to the arrival airport is equal to the distance required to descend the Auto Pilot commands the aircraft to descend. For short range flights, the Auto Pilot is programmed to calculate the distance to descent at every point during the climb, and commands the aircraft to descend even if the cruise altitude has not been met.

3.2.4. Flight Dynamics Model

The Flight Dynamics Model initially updates the speed (V) of the aircraft at every step of the flight, following the guidelines of the Flight Planner and Auto Pilot. The aircraft altitude (h) and flight path

[9]Eurocontrol (2022, January 17) Aircraft Performance database, https://contentzone.eurocontrol.int/aircraftperformance/details.aspx?ICAO=B762&

angle (γ) is updated with the speed, rate of climb or descend ($ROCD$) and time (t) using Equation 3.2 and Equation 3.3.

$$h_i = h_{i-1} + ROCD\ t \tag{3.2}$$

$$\gamma = atan\left(\frac{ROCD}{V}\right) \tag{3.3}$$

To calculate the fuel flow it is necessary to calculate the thrust required per engine. The total energy model from Eurocontrol (2004) (Equation 3.4) will be used to calculate the thrust.

$$T = D + \frac{m\ g}{V}\ \frac{dh}{dt} + m\frac{dV_{TAS}}{dt} \tag{3.4}$$

The speed of the aircraft (V) is given in true airspeed. The drag (D) is calculated using the aerodynamics module. Which uses the parameters k, $C_{D,0}$ and C_L to obtain the drag coefficient as shown in Equation 3.5 and Equation 3.6.

$$C_D = C_{D,0} + k\ C_L^2 \tag{3.5}$$

$$D = \frac{1}{2}C_D\rho V^2 S \tag{3.6}$$

C_L is calculated using the weight of the aircraft ($m\ g$), the wing surface area (S), the air density (ρ) and the aircraft speed as displayed in Equation 3.7

$$C_L = \frac{m\ g\ cos(\gamma)}{\frac{1}{2}\rho V^2 S} \tag{3.7}$$

.

3.2.5. Engine Model

The engine model was obtained from Proesmans and Vos (2021). As explained in Section 2.2.3 the aircraft used in the study have different flight performances due to the different engine assumptions. Therefore, the engine parameters have to be chosen accordingly. To calculate the OPR for the tube-and-wing aircraft the different pressure ratios were varied until the aircraft consumed exactly the design fuel for the design mission range and payload (the BPR was given in Beddoes et al. (2022)). A similar procedure was followed for the Flying-Vs, where the BPR was also included in the design. Four different engines are generated, two hydrogen turbofan engines for the FZM1G and FVHY and two kerosene turbofan engines for the B767S and the FV8. The engine characteristics are listed in Table 3.1. It can be observed that the BPR of both engines is quite large, this is because Beddoes et al. (2022) assumes technology improvements from 2030. The Specific Energy Consumption (SEC) was also included to ease the comparison between the kerosene and hydrogen engine versions.

Table 3.1: Characteristics of the engines used to model the aircraft emissions.

Characteristics	**FZM1G**	**B767S**	**FV8**	**FVHY**
Fuel Type	Hydrogen	Kerosene	Kerosene	Hydrogen
BPR [-]	13	15	9.6	9.6
Fan Pressure Ratio [-]	1.4	1.3	1.35	1.32
Low Pressure Compressor Ratio [-]	1.51	1.5	1.4	1.4
High Pressure Compressor Ratio [-]	24	24	26	25
Overall Pressure Ratio [-]	51	47	49	46
SFC at Cruise [$kg/s/N$E-6]	4.94	13.5	14.9	6.13
SEC at Cruise [$MJ/s/N$E-6]	593	581	641	736

It can be observed that the SEC of the hydrogen aircraft is slightly higher than the SEC of the kerosene engine, this means that the hydrogen engine can generate less thrust with the same amount of energy. The lower efficiency of the hydrogen aircraft is due to the lower bypass ratio as explained in Section 2.2.1 (13 vs. 15). In the Flying-V case, this difference is mainly based on the OPR. After the engine is designed, the fuel flow required can be computed at off-design conditions. To reduce computational time and avoid running the engine model for every flight step an engine deck is created. The engine deck is designed with three different inputs, mach speed, altitude and thrust required. The engine deck allows for the flight simulation module to search through the deck and interpolate the output rapidly. The discretization of the engine model is verified in Appendix B.

3.2.6. EINO$_x$

Three different calculation methods were investigated to compute EINO$_x$ namely, BFFM2, P$_3$-T$_3$, correlation-based and ICAO. BFFM2 was selected for the computation of EINO$_x$ and Equation 3.8 is used to calculate the final emitted NO$_x$. The equation includes the fuel flow of the engine ($\dot{m}_{eng}$, time (t) and the number of engines (N_{eng}).

$$NO_x = EINO_{x,Alt}\, \dot{m}_{eng}\, t\, N_{eng} \tag{3.8}$$

EINO$_{x,Alt}$ at the flight altitude can be calculated using Equation 3.9, where EINO$_{x,SL}$ (at sea level) and the dimensionless coefficients θ_{amb} and δ_{amb} are used.

$$EINO_{x,Alt} = EINO_{x,SL} \left(\frac{\delta_{amb}^{1.02}}{\theta_{amb}^{3.3}} \right)^{0.5} e^{I} \tag{3.9}$$

The dimensionless coefficients represent the relative temperature and pressure with respect to sea level conditions.

$$\theta_{amb} = \frac{T_{amb}}{288.15} \tag{3.10}$$

$$\delta_{amb} = \frac{P_{amb}}{1013} \tag{3.11}$$

Moreover, EINO$_{x,SL}$ can be calculated using the relation proposed by Turgut and Usanmaz (2017), please note that Equation 3.12 is exclusively used for kerosene fuel, as it is extracted from kerosene combustion engines. $\dot{m}_{SL}$ can be calculated using Equation 3.13.

$$EINO_{x,SL} = 18.924 \dot{m}_{SL} + 0.763 \tag{3.12}$$

$$\dot{m}_{SL} = \dot{m}_{Alt} \frac{\theta_{amb}^{3.8}}{\delta_{amb}} e^{0.2M^2} \tag{3.13}$$

In Equation 3.13, M is the mach speed, and $\dot{m}_{Alt}$ is the calculated fuel flow at the flight altitude given by the engine model. Please note that the different cruise speeds of the aircraft to be analyzed in the study will cause a deviation on the NO$_x$ emitted. e^I represents the humidity factor correction. For that, Equation 3.14 with altitude h was used.

$$I = 19 \left(0.00634 - 10^{-3}\, e^{-0.0001426\,(h-12900)} \right) \tag{3.14}$$

The model fails to predict hydrogen emissions accurately. To calculate hydrogen EINO$_x$ emissions, the same engine model used for the hydrogen fuel is designed for kerosene fuel for the FZM1G and FVHY. On Equation 3.13 the kerosene fuel flow of the hydrogen engine is introduced. However, this method does not really represent the opportunities of hydrogen combustion to reduce the EINO$_x$ emissions. The percentage reduction on EINO$_x$ from Carter (2021) depends lightly on the thrust settings of the engine. Equation 3.15 was used to calculate the ratio of EINO$_x$ due to hydrogen to kerosene combustion for the different thrust settings (T, kN).

$$\frac{EINO_{X,H_2}}{EINO_{X,KER}} = 1\text{E}{-}10T^3 - 9\text{E}{-}08T^2 + 2\text{E}{-}05T + 0.7579 \tag{3.15}$$

3.2.7. Emission Inventory Output

Once the simulation for all the flights has been carried out, the emission inventory has to be generated. The emission inventory is created with the following information on each of the flight points:

- Longitude in degrees.
- Latitude in degrees.
- Atmospheric pressure in hPa.
- Fuel burn between flight points in kg.
- NO_x emitted between flight points in kg.
- Distance covered between flight points in km.
- Flight point yearly frequency in times per year.

The emission inventory will serve as input for the climate impact assessment module to calculate the temperature change caused by the aircraft. It can also be used to compute the total emissions and fuel consumed in flight. However, it is challenging to compare the fuel consumed in this study (using the so called tool) with reality due to a number of reasons:

- The same aircraft is being used for all the flights, FZM1G and B767S have been designed with futuristic technology and consume less fuel than the average airplane.
- The flights are assumed to be perfect great circle trajectories. In reality, flights suffer deviations and do not flight the shortest path. Less fuel should be consumed by the tool.
- In relation to flight trajectories, the analysis does not see a difference between flying east vs flying west, when in reality the wind speed will create disparities on fuel consumption. The fuel consumption calculated by the tool could be higher or lower.
- The tool assumes that all the flights arrive at cruise conditions of 11 km. In reality, the cruise altitude depends on the type of aircraft and the flight distance. More fuel should be consumed by the tool because of not following the optimal altitude flight path.
- This model does not assume engine deterioration, which has been proven to be a cause of higher fuel consumption (Naeem et al., 1998). Less fuel should be consumed by the tool.
- This model assumes the aircraft is always flying with maximum payload weight, in reality the passenger load factor in 2019 was close to 82 %[10] and the cargo load factor close to 75 %[11].

The methodology proposed has to be used carefully and understanding the assumptions made above. The aforementioned limitations affect equally all aircraft in this study and thus the methodology is seem as valid. The points described above can also be seen as possible tool improvements in case comparisons with real flights and more accurate climate predictions are required. Due to lack of time, this study will not investigate the consequences of these limitations, however it would make an interesting research.

3.3. Climate Impact Assessment

The Climate Impact Model takes as input the emission inventory generated by the flight simulation model and converts it into surface temperature change to describe climate impact. Several tools were investigated, namely: Climate and Aviation Sustainable Trajectories (CAST) developed by Planès et al. (2021); Model for the Assessment of Greenhouse Gas Induced Climate Change (MAGICC) developed by Meinshausen et al. (2011); LinClim developed by Lim and Lee (2006); and AirClim developed by Grewe and Stenke (2008). The potential models were listed by ICAO[12].

The tool selection narrowed down to availability, versatility, and relevance of the output climate metric. From Section 2.1 it was concluded that the metric should be related to temperature to provide

[10] Mazareanu, E. (2022, March 29) Passenger load factor of commercial airlines worldwide from 2005 to 2022, https://www.statista.com/statistics/658830/passenger-load-factor-of-commercial-airlines-worldwide/

[11] Mazareanu, E. (2022, March 29) Freight load factor of commercial airlines in Europe from 2015 to 2022, https://www.statista.com/statistics/1118141/freight-load-factor-commercial-airlines-europe/

[12] International Civil Aviation Organization (2021, November 24). Models and Databases https://www.icao.int/environmental-protection/pages/modelling-and-databases.aspx

direct climate relevance. CAST is an online tool and therefore is easily available, but it uses radiative forcing as the climate metric. Furthermore, CAST is not very versatile and it does not allow for an emission inventory implementation. MAGICC is also publicly available, and while it is a bit more versatile than CAST it still does not use an emission inventory. Furthermore, MAGICC does calculate the near-surface temperature change. LinClim includes the effects of multiple emission species and it splits the temperature effects of each species. LinClim is versatile but it does not include the ability to input an emission inventory, however LinClim is not easily available. AirClim's final output can be both radiative forcing and near-surface temperature change. It is also very versatile and has been used to measure the direct effect of emission inventories (Reekers, 2021). Regarding availability, AirClim can be provided directly by Prof. dr. V. Grewe.

The characteristics of each model are summarized in Table 3.2, it can be observed that, from the presented climate assessment tools, AirClim is the most complete tool. Furthermore, it was the one recommended by Dr. F. Yin and has been used in many different papers to evaluate the climate impact of certain aircraft designs (Linke et al., 2020; Grewe & Dahlmann, 2015; Reekers, 2021).

Table 3.2: Trade-off for different existing climate assessment models.

Climate Assessment Tool	Availability	Versatility	Climate Metric
CAST	+	-	-
MAGICC	+	-	+
LinClim	-	+	+
AirClim	+	+	+

3.3.1. AirClim

AirClim has been selected, but a deeper understanding of the working principles is required. AirClim evaluates the climate impact of CO_2, NO_x, H_2O and contrails. AirClim is divided into three different modules, as shown in Figure 3.7. The main model is displayed in blue, for which the input is the pre-calculated chemistry input data in red and the emission from the aircraft trajectory in yellow. The precalculated input data (red) consists of three steps: the first one defines the emission regions with a normalized emission strength; the second step performs a climate chemistry simulation with the chemistry model E39/C; finally, the third step calculates the radiative forcing of each perturbation scenario. The perturbation scenarios are calculated from the emission input data (yellow). AirClim allows for an emission inventory with distributed emissions along a 3D path (a flight route).

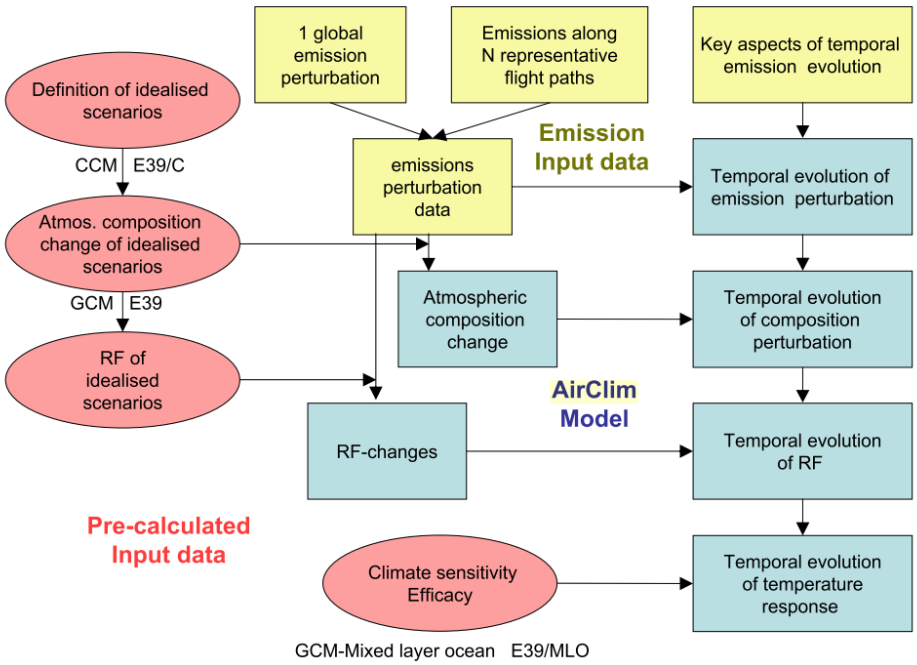

Figure 3.7: AirClim model architecture with dependencies between the three different modules.

The linear response model AirClim (blue) combines the precalculated input data (red) with the emission data (yellow) to calculate the changes in near-surface temperature. AirClim also uses a background aircraft scenario to isolate the change in temperature from the new technology. The CO_2 emissions are calculated differently from the rest of the emissions to allow for different time representations (each species has different lifetimes). A more insightful explanation of the model is presented in Grewe and Stenke (2008) and Dahlmann et al. (2016). The final output from AirClim is a temporal evolution of the near-surface temperature change. However, AirClim also includes the radiative forcing metric to be comparable to other publications.

Hydrogen Emissions

AirClim assumes that the fuel burn specified in the emission inventory is kerosene and thus it has to be adapted to recognize hydrogen. As explained in Section 2.2.2, the emissions of hydrogen combustion differ from the emissions of kerosene combustion. AirClim states different emission indexes for these species. Equation 3.16 and Equation 3.17 represent the chemical balance equations for kerosene and hydrogen combustion respectively. Information about the equations can be found in Section 2.1.2 and Section 2.2.2 respectively. Using the molar masses of each element the emission index of each of the species can be calculated.

$$C_{12}H_{24} + 18\,(O_2 + 3.762N_2) \rightarrow 12CO_2 + 12H_2O + 67.716N_2 \tag{3.16}$$

$$H_2 + \frac{3}{2}\,(O_2 + 3.762N_2) \rightarrow H_2O + O_2 + 5.643N_2 \tag{3.17}$$

The $EICO_2$ for kerosene is 3.155 kg per kg of fuel and for hydrogen is 0. The EIH_2O for kerosene is 1.29 kg per kg of fuel and for hydrogen is 9 kg/kg. The change in $EINO_x$ has already been discussed in Section 3.2.6. The increase in H_2O has both direct and indirect effects. H_2O is a greenhouse gas, but also increases the contrail formation probability. Hydrogen does not create soot particles which reduces both contrail formation probability and radiative forcing. Grewe et al. (2017a) assumes a 40 % reduction on formation and radiative forcing of contrails with a reduction of 80% in soot particles following Equation 3.18. Total reduction on soot particles is not possible because there is soot in the atmosphere that goes through the engine, however the number of soot particles in the plume of an aircraft is 4 orders of magnitude larger than the concentration of soot particles in the atmosphere

(Samset et al., 2013). Marquart et al. (2005) also assumes a reduction on the radiative forcing of contrails of 30%. Moreover, Burkhardt et al. (2018) states that with a low soot number scenario where crystal formation is reduced by 90 % a total of 69 % reduction in radiative forcing can be achieved. These parameters will be included in the sensitivity analysis due to the large variability observed in literature. Table 3.3 displays the deviations between hydrogen and kerosene climate factors.

$$\Delta RF^{cont} = \frac{arctan\left(1.9\Delta_{pn}^{0.74}\right)}{arctan(1.9)} \tag{3.18}$$

Table 3.3: Hydrogen and kerosene species adaptations for AirClim.

Fuel	Contrail RF Change (Soot)	$EICO_2$	EIH_2O
Kerosene	-	3.155	1.25
Hydrogen	- 69%	0	9

3.3.2. Future Traffic and Fleet Scenario

As suggested by Grewe et al. (2017a) it is important to define clearly the climate objective before setting an scenario. The climate objective is set to compare the climate impact of both the fleet of hydrogen aircraft and kerosene aircraft. Table 3.4 displays the flight scenario used in the study.

Table 3.4: Scenario assumptions used for the comparison of the climate change caused by the hydrogen and kerosene aircraft.

Scenario Parameters	**Value**	**Scenario Parameters**	**Value**
Simulation Start Year	2030	Simulation End Year	2130
B767S (ker) Start Year	2030	FMZ1G (hyd) Start Year	2030
Market Growth BAU (2019-2025)	6.0%	Market Growth BAU (2025-2050)	1.2%
Market Growth BAU (2050-2075)	1.0%	Market Growth BAU (2075-2130)	0.8%

The study is set to compare purely the technology, that is why the simulation start year coincides with the FZM1G and B767S start year. Moreover, to make it comparable to other studies, the simulation end year was set to 2130, to have ATR_{100} as a metric (described in Equation 2.5). Aviation market growth is understood as the change in Revenue Passenger Kilometer (RPK), assumed to grow by 6.0% from 2019 to 2025 according to ICAO, by 1% from 2050 to 2075 and by 0.8% from 2075 to 2130 when the simulation stops (Grewe et al., 2021) to maintain business as usual. It is important to note that we are not only interested on the growth for this analysis but more importantly on the fuel consumption, for that, fuel efficiency improvements over the years are included. Finally, in this study it is assumed that the aircraft entrance in the market is instantaneous, which will ease the calculation of the results and the direct comparison of the kerosene and hydrogen aircraft. Please note that, the aviation growth is assumed from 2019 because is the year for which the flight data was available.

A more realistic scenario can be drawn to observe the practicalities of a project of this magnitude, and how introducing the hydrogen technology later affects the final outcome. Table 3.5 displays the assumptions for the second study case. It can be observed that the starting year for the hydrogen technology is different from the first scenario, now the FMZ1G aircraft is introduced in the year 2050 according to the technology implementation road map of Hadnum et al. (2022). Both aircraft are introduced instantaneously, however it would be interesting to analyze the effects of progressively introducing the airplanes. It is obvious that the scenario is not fully realistic, since it is unlikely that the same aircraft would cover the whole market segment, however, it establishes different times of entrance in the market which will provide meaningful information.

Table 3.5: Scenario assumptions used for the second study case.

Scenario Parameters	**Value**	**Scenario Parameters**	**Value**
Simulation Start Year	2019	Simulation End Year	2150
B767S (ker) Start Year	2030	FMZ1G (hyd) Start Year	2050
Market Growth BAU (2019-2025)	6.0%	Market Growth BAU (2025-2050)	1.2%
Market Growth BAU (2050-2075)	1.0%	Market Growth BAU (2075-2130)	0.8%

4

Results & Discussion

This chapter elaborates and discusses the study results. Section 4.1 elaborates on the chosen routes and Section 4.2 presents the climate impact caused by the studied aircraft. Moreover, it details the climate change contribution from the species, the surface temperature trend over time and the geographical climate effects of contrails and emissions. It also presents two different study cases, the first one presenting the Flying-V as an alternative aircraft, and the second one introduces a scenario with different starting times for the hydrogen and kerosene aircraft. Finally, the uncertainties of the study are analyzed in a sensitivity analysis.

4.1. Flight Routes

Flight routes were selected with three requirements in mind, flight distance, flight frequency and global coverage. Using the Routing Design Model, flight routes which satisfy the requirements can be extracted. Figure 4.1 displays the great circle trajectories uniting the selected 1128 city-pairs that satisfy the requirements, for a total of 2.24 million flights. A similar trend to that in Figure 2.16 can be observed, where there is a higher concentration of flights in North America, Europe and Asia.

Figure 4.1: Global coverage of city pairs selected, the pink line represents the geodesic line from airport to airport and the intensity of the line the number of flights per year of each route.

A better way to examine the global coverage is by analyzing the flight occurrences per latitude and longitude as represented in Figure 4.2 and Figure 4.3. The figures show that almost all latitudes and longitudes are covered. The peak on the Figure 4.2 correspond to the 40-20 degrees north, these are mostly flights in Europe, United States and China. There are three peaks on Figure 4.3, these correspond to internal flights of United States, Europe and Asia. It can also be observed that, with the current route selection, there are slightly more flights connecting Europe with Asia than those connecting Europe with North America. This difference is due to the maximum distance (10 650 km) analyzed in the study, which deselects long transoceanic flights through the Atlantic Ocean, however, shorter connecting flights exist through the Middle East.

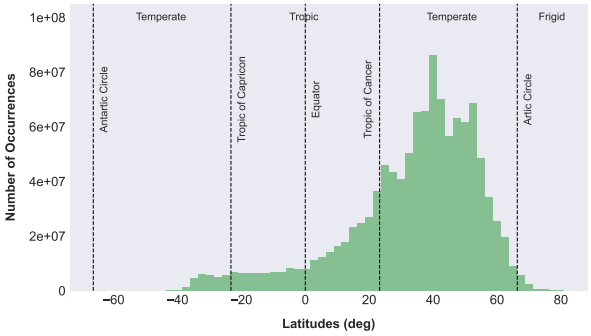

Figure 4.2: Latitude distribution of flight data points with marks on the temperate, the Tropics and frigid areas.

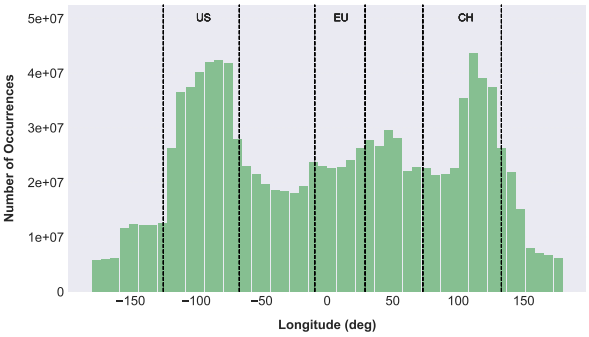

Figure 4.3: Longitude distribution of flight data points with marks on the United States, Europe and China.

Figure 4.4 displays the flight occurrences at different altitudes for the B767S aircraft. It can be observed that most of the flight points occur close at the cruise altitude (264 hPa). The rest of the flight points represent the aircraft climbing and descending, also included in the study.

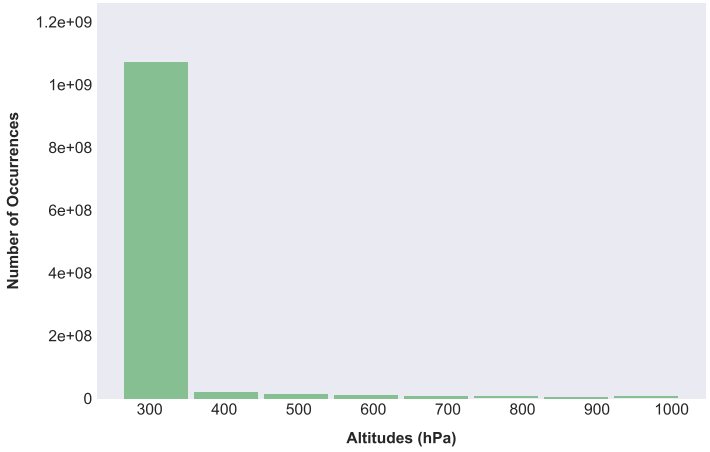

Figure 4.4: Altitude distribution of flight waypoints given in hectopascals.

Table 4.1 displays information about flown kilometers for the selected route and how those are distributed throughout the different latitudes. It can be observed that 78% of the flights are concentrated on temperate areas, 21 % on the Tropics and less than 1 % on frigid areas.

Table 4.1: Flown kilometers distributed by latitude for the selected routes.

	Flown Kilometers [km 10^6]			
City Pairs	**Total**	**Frigid**	**Temperate**	**Tropics**
1128	11453.77	91.312	8922.3	2440.1

4.2. Emissions and Climate Change

Once the selected routes have been analyzed, flight performance, emissions generated, and climate change can be studied. Section 4.2.1 represents how the aircraft designs investigated in the assignment align with the climate mitigation objectives set in the Paris Agreement. Section 4.2.2 and Section 4.2.3 investigate the individual contribution from emission species to climate change and how the relative contribution varies over time. Moreover, Section 4.2.4 analyzes the latitudinal variation of the emissions to understand the susceptibility to climate change. Two study cases were proposed in this study: the first one (Section 4.2.5) considers an alternative aircraft, the Flying-V, either kerosene powered (named FV8) or hydrogen powered (named FVHY). The second (Section 4.2.6) proposes a more realistic scenario, where the kerosene B767S and the FZM1G previously mentioned, are introduced in the market in 2030 and 2050 respectively. Finally, a sensitivity study is presented in Section 4.2.7 to understand other parameters that might change the outcome of the study.

4.2.1. Climate Mitigation Goal

To stop global warming and maintain an habitable Earth a consensus was reached, known as the *Paris Agreement*, to keep the rise of the mean global temperature well below 2°C (Delbeke et al., 2019) above the pre-industrial levels. It is important to question if any of the fleets analyzed in this study meet this climate objective.

Current temperature has risen about 1°C by 2022 [1] above pre-industrial levels; by 2030 the surface temperature increase is predicted to reach 1.5°C (Masson-Delmotte et al., 2021). The goal of aviation from 2030 onward should be to avoid the temperature increase by 0.5°C. Aviation is believed to be the cause of 3.5% of the current climate change (Ritchie, 2020). Therefore, for the aviation sector, the total emissions should not increase global surface temperature above 17.5 mK. The B767S aircraft, consumes a total of 48.7 billion kilograms of fuel, and the total fuel consumption in 2019 was 359.6 billion kilograms. This analysis accounts for roughly 13.5 % of the total aviation emissions. Table 4.2 displays the emissions caused by the hydrogen and kerosene aircraft relative to energy, flown distance and passengers displaced.

Table 4.2: Fuel used by the FZM1G and the B767S on all routes.

Aircraft Type	Fuel Burnt	Fuel Burnt per km	Energy Used per km	Fuel Burnt per km per Pax.
Unit	**Mt**	**kg/km**	**MJ/km**	**kg/km/pax**
FZM1G	16.7	1.45	174	0.0052
B767S	41.5	3.62	156	0.0130

From the table above we can observe that the kerosene aircraft (B767S) is consuming 2.5 times more fuel than the hydrogen aircraft (FZM1G). This difference is mainly caused by the difference between the hydrogen and kerosene energy density, being 2.79 times larger for the hydrogen fuel. This disparity can be observed in the energy used per km column, where the hydrogen aircraft requires a bit more energy to travel the same distance. This is caused by two reasons, the engine specific energy consumption, being slightly larger for the hydrogen aircraft (593 $MJ/s/N$E-6 vs 581 $MJ/s/N$E-6) and the larger OEW of the hydrogen aircraft, making the average thrust on the typical mission flight higher (35 kN/eng vs 32 kN/eng).

The influence on climate warming of the aircraft defined above can be observed in Figure 4.5. The ever increasing temperature is due the BAU scenario selected, where there is a continuous increase in demand and therefore in flights and fuel consumed.

[1] Lindsey, R. and Dahlman L. (2022, May 24) Climate Change: Global Temperature https://www.climate.gov/news-features/understanding-climate/climate-change-global-temperature

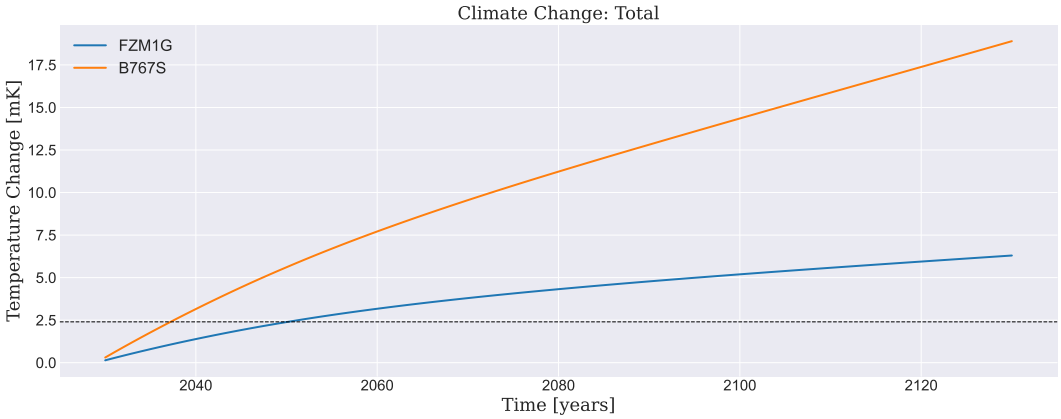

Figure 4.5: Change in surface temperature caused by the FMZ1G and B767S. The dashed line corresponds to the maximum temperature increase the fleet should cause to meet the climate objectives stated in the Paris Agreement.

The surface temperature increase after 100 years caused by the kerosene-fueled aircraft (B767S) is 18.9 mK, while for the hydrogen combustion aircraft (FMZ1G) is 6.3 mK (67% lower). Figure 4.5 draws the Paris Agreement goals represented by the dashed black line at 2.4 mK. It can be observed that both aircraft fail to keep the temperature increase below this number, however, whereas the B767S surpasses the 2.4 mK temperature increase only 3 years after its implementation, the hydrogen aircraft FMZ1G surpasses the line 20 years later. In Figure 4.5 the development of the temperature change over the years can be observed, however this will be treated further in Section 4.2.3 knowing more information on the climate effect from individual species. The next sections will provide an in-depth assessment on the reasons why such a deviation is observed.

4.2.2. Climate Effect from Individual Emissions

It is important to know the differences in emitted species between the B767S and the FMZ1G, as Table 4.2 only gives information about the fuel consumed. The kerosene emissions treated in this study are CO_2, NO_x and H_2O while for hydrogen no CO_2 is emitted. Table 4.3 displays the different emissions and emission indexes per aircraft. It can be observed that the emission index is now represented first as the emitted species per kilogram of fuel and secondly as the emitted species per energy consumed.

Table 4.3: Species emitted and fuel used by the FZM1G and B767S.

Aircraft	Fuel	NO_x	$EINO_x$		CO_2	$EICO_2$		H_2O	EIH_2O	
	Mt	kt	g/kg	g/MJ	Mt	kg/kg	kg/MJ	Mt	kg/kg	kg/MJ
FZM1G	16.7	179	10.8	0.0898	0	0	0	150	9	0.075
B767S	41.5	544	13.1	0.305	131	3.155	0.734	51.8	1.25	0.029

CO_2 and H_2O emissions were computed after the total flight emissions were simulated. NO_x was computed during the simulation using the methodology presented in Section 3.2.6. It can be observed that total NO_x emissions from kerosene are 3 times higher than emissions from hydrogen. However, it must be noted that NO_x was calculated based on fuel burnt, and thus 82% of the difference comes from the larger quantity of kerosene burnt compared with hydrogen. $EINO_x$ should reduce by 25% in hydrogen combustion by taking advantage of the lower lean limit of hydrogen, however, it is only reduced by 18% (which is the missing NO_x percentage).

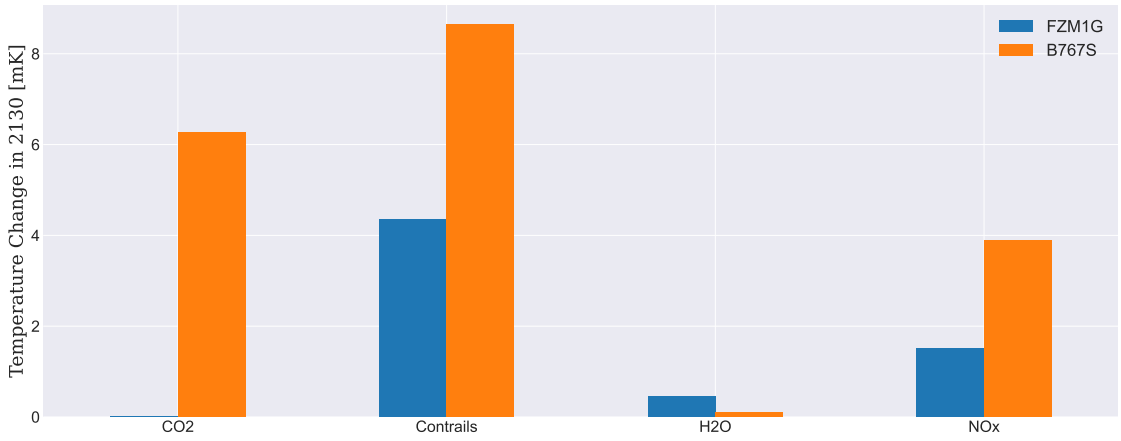

Figure 4.6: Contribution to surface temperature increase from each of the species per aircraft model.

Figure 4.6 displays how different species contribute to climate change by 2130. The sudden increase in temperature change in Figure 4.5 for both aircraft occurs due to the sudden introduction of the fleet in the market as explained in Section 3.3.2. As it can be observed, effects of hydrogen aviation on temperature rise are lower than those of kerosene aviation, with several considerations. Contrail effects are the largest individual contributor to surface temperature change for both kerosene and hydrogen aircraft. The temperature change due to contrails is considerably smaller for the hydrogen aircraft (50% lower). This reduction is caused mainly by the 69% reduction in radiative forcing due to soot elimination for hydrogen combustion as explained in Section 3.3, and due to the reduction in overall efficiency of the hydrogen aircraft (0.40 vs 0.41, affecting the contrail formation probability). Contrail effects on climate from the FZM1G could be lower, however, the higher cruise altitude causes an increase in surface temperature change. Moreover, the higher water vapour content on the hydrogen engine plume increases the contrail formation probability. CO_2 effects are only present for the kerosene aircraft (B767S), these effects will be better reflected in Section 4.2.3. H_2O climate effect is 4.7 times higher for the hydrogen aircraft, which has to do with the higher emission index of hydrogen combustion as seen in Table 4.3, but also with the higher altitude of the hydrogen aircraft, causing a larger temperature increase. Temperature increase from NO_x emissions is 2.6 times larger for kerosene aircraft. We can observe that the emissions of NO_x are 67% lower, however, the climate impact is only 61% lower. The difference is caused by the altitude, increasing the change in surface temperature the higher in the atmosphere NO_x is emitted (where the hydrogen aircraft is flying), this will be observed in Section 4.2.7.

4.2.3. Trend Over Time of Temperature Response for Individual Effect

It is important to understand how the different species affect climate over the years. Figure 4.7 displays the temporal climate change per kerosene emission species. It can be observed that initially CO_2 does not play a major role on the temperature rise (2035, 3.9% of total temperature increase), however, this effect increases over time (2130, 33% of total temperature increase). NO_x has the opposite effect, initially it is one of the largest contributors (2035, 41.1% of total temperature increase) but its percentage decreases over time (2130, 20.6% of total temperature increase). H_2O effects remain insignificant along the years. The relative contribution to climate change from contrail effects is 55% and it is maintained until 2050, contrails then start becoming slightly less important (2130, 45.7% of the total temperature increase) due to the cumulative behaviour of CO_2.

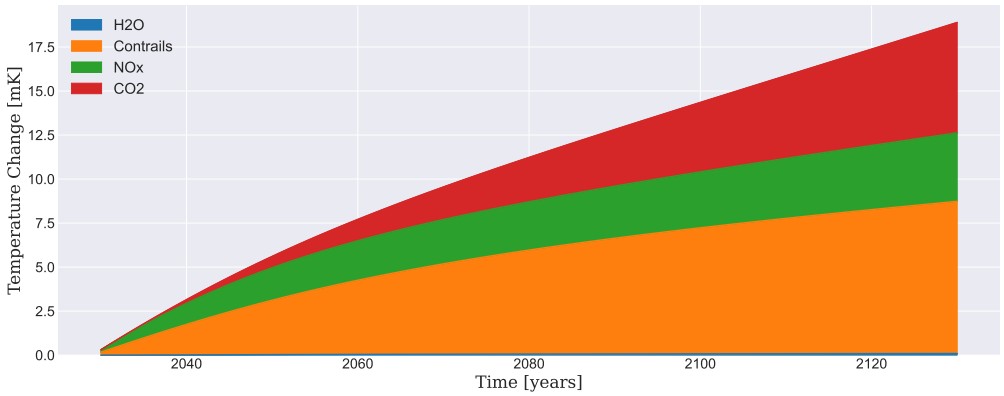

Figure 4.7: Contribution to surface temperature increase from each of the species caused by the B767S along the years.

In Figure 4.8 the temporal climate change for the hydrogen combustion aircraft case is displayed. Similarly to kerosene aircraft, NO_x influence on climate is reduced from 2030 to 2080. However, in this case the relative contribution is maintained from 2080 to 2130. H_2O contribution is more significant and increased over time (from 5.78% in 2035 to 7.05% in 2130). Since hydrogen does not produce CO_2, the cumulative behaviour of the emissions is reduced, causing the slope at which the temperature increases to decay.

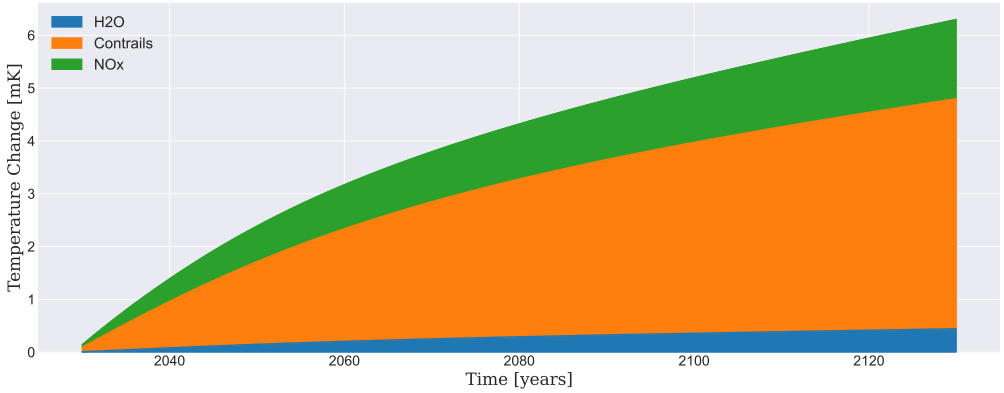

Figure 4.8: Contribution to surface temperature increase from each of the species caused by the FZM1G along the years.

Emissions can be differentiated on how fast they have an effect on climate and how long do they remain in the earth-system. CO_2 is a long-lived species, therefore it has an effect on climate years after of being emitted. Moreover, CO_2 effects on climate are not instantaneous, and some years might be required for the surface temperature change to start increasing (as shown in Figure 4.9). Contrails on the other hand have a shorter life. In Figure 4.10 it can be observed that the delta temperature increase of contrails is reduced with time, following the aviation market. This occurs because contrails dissipated hours-days after the formation (short-lived). NO_x effects are a bit more complicated, when released in the atmosphere NO_x causes both a production in ozone and a depletion of methane (causing consequently both an increase and a reduction in temperature). These compounds are very reactive, which causes a faster interaction with climate change at the beginning of the simulation than any other species (Figure 4.11). It can also be observed that NO_x follows a similar trend to that of contrails due to its short life. H_2O effects on temperature are similar to the contrail effects, with a fast reaction at the beginning and a non-cumulative behaviour.

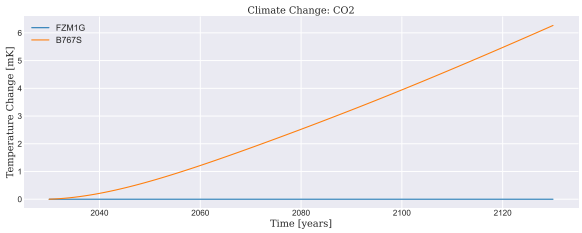

Figure 4.9: Surface temperature increase caused by CO_2 for the B767S and FZM1G.

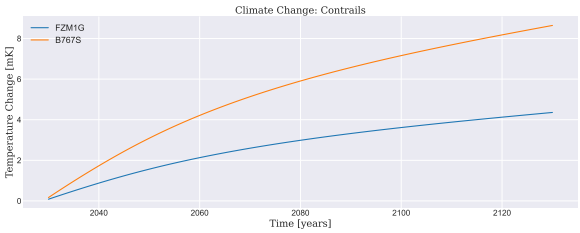

Figure 4.10: Surface temperature increase caused by contrails for the B767S and FZM1G.

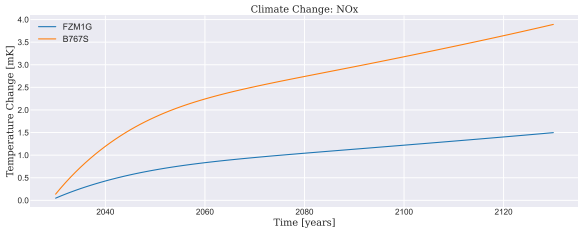

Figure 4.11: Surface temperature increase caused by NO_x emissions for the B767S and FZM1G.

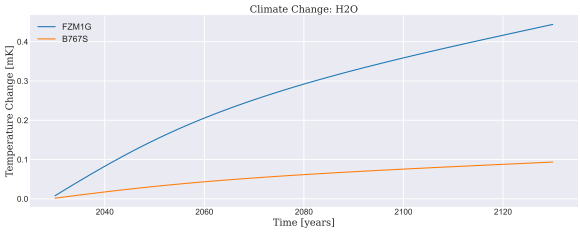

Figure 4.12: Surface temperature increase caused by water vapour emissions for the B767S and FZM1G.

These results lead to an important conclusion, hydrogen does not emit the species causing the largest cumulative behaviour (CO_2), this means that, if for any reason the hydrogen fleet is stopped, the surface temperature recovery should be faster for a hydrogen aircraft. Figure 4.13 demonstrates these effects.

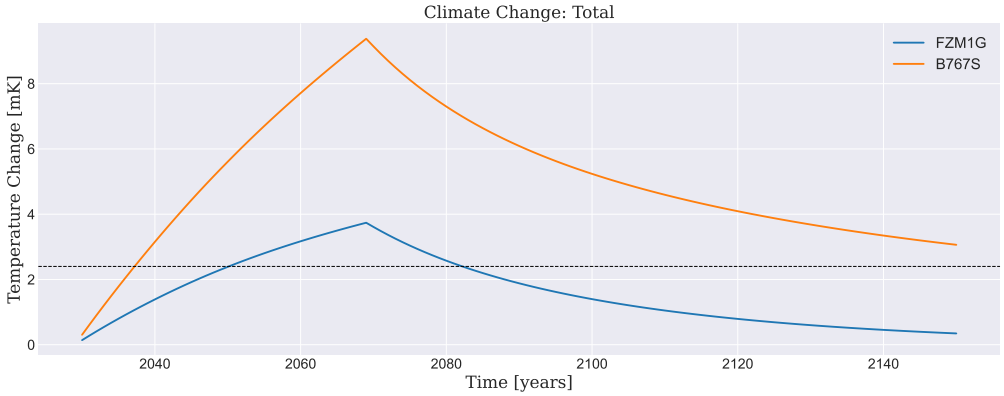

Figure 4.13: Temperature increase caused by the B767S and FZM1G and climate recovery when flights are stopped after 2070.

Until 2070, the same trend as in Figure 4.5 is observed. The trend differs once flights are stopped. Initially, the surface temperature change caused by the B767S reduces considerably. At the end of the simulation, temperature has been increased by 3.1 mK (CO_2 causes 2.4 mK). FZM1G also shows a similar initial surface temperature decay, however, at the end of the simulation, temperature has been increased only by 0.34 mK.

4.2.4. Non-CO_2 Geographical Effects

In Section 2.1.2 it was mentioned that emission climate effects depend greatly on the latitude at which the species are emitted. To investigate these effects, flight points were divided into three different zones, frigid latitudes greater than 66.34º North/South, temperate latitudes between 66.34º and 23.26º North/South, and tropical latitudes lower than 23.26º North/South. In Section 2.1, it was explained that CO_2 climate effects are not dependent on geographical location, as such, they will be excluded from

the analysis in this section. Please note that it will change the percentage of each non-CO_2 effect but it will help explaining the differences caused by local effects. Table 4.4 represents the fuel consumption, NO_x and H_2O released at different latitudes for the two aircraft. A slight deviation in NO_x emitted exits depending on the flight latitude (12.0 g/kg frigid B767S vs. 13.2 g/kg temperate B767S), this has to do with the fact that most of the flights are on cruise conditions when flying over the frigid areas, and thus emitting less NO_x due to the lower thrust setting compared to climb or take off. A lower latitudinal deviation is observed for the fuel consumption (3.48 kg/km frigid B767S vs. 3.64 kg/km temperate B767S) because fuel consumption has a lower dependency on thrust settings than NO_x. For the hydrogen FZM1G similar deviations are observed, fuel consumed and $EINO_x$ is slightly greater at temperate regions than at the Tropics or frigid areas.

Table 4.4: Emissions per flight latitude for the hydrogen FZM1G and kerosene B767S aircraft.

Latitude	Aircraft	Fuel		NO_x	$EINO_x$		H_2O	EIH_2O	
		Mt	kg/km	kt	g/kg	g/MJ	Mt	kg/kg	kg/MJ
Frigid	FZM1G	0.129	1.41	1.26	9.84	0.0820	1.16	9	0.075
	B767S	0.317	3.48	3.79	12.0	0.278	0.397	1.25	0.0104
Temperate	FZM1G	13.0	1.46	141	10.8	0.0902	117	9	0.075
	B767S	32.5	3.64	429	13.2	0.307	40.6	1.25	0.0104
Tropic	FZM1G	3.50	1.43	37.2	10.6	0.0886	31.5	9	0.075
	B767S	8.68	3.56	112	12.9	0.300	10.85	1.25	0.0104

Figure 4.14 represents the contribution to climate change of species emitted by the B767S in 2130 when varying the latitude from frigid areas to the Tropics. It can be observed that, over frigid latitudes, contrail effects are the governing factor on surface temperature increase. On the other hand, when tropical flights are analyzed, contrail effects almost disappear. This variation can be explained using Figure 2.13, at the current cruise altitude between 10 and 11 km, the contrail probability of formation is increased over polar latitudes and decreased towards the Tropics. The opposite is observed for NO_x effects, being more relevant over the Tropics and less relevant over the Poles. This variation occurs due to the accentuated ozone production from NO_x in the Tropics, due to the fast chemistry of the region as observed in Figure 2.11.

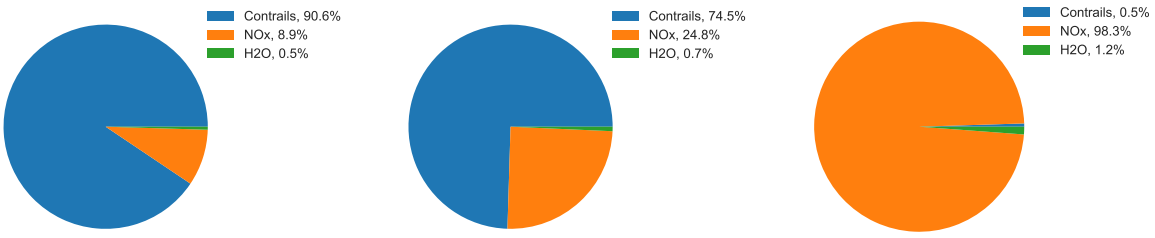

(a) Frigid latitudes. **(b)** Temperate latitudes. **(c)** Tropical latitudes.

Figure 4.14: Climate impact percentage contribution from species caused by the B767S aircraft at different latitudes.

Figure 4.15 represents the climate change contribution of the species emitted by the hydrogen aircraft (FZM1G) in 2130 when varying latitude. The results show a similar trend to that of the kerosene aircraft. Contrail effects are the governing factor over the frigid areas, with a considerably larger effect from H_2O. NO_x is also the most relevant factor at the Tropics however the contrail effects on climate are magnified due to the higher water vapour emission content. Moreover, hydrogen aircraft fly at a slightly higher altitude than the kerosene aircraft, increasing the probability of contrail formation and therefore the

influence on temperature change. That is why the contrail effects are more pronounced in the case of hydrogen aviation over the Tropics than those of kerosene aviation (Figure 2.13).

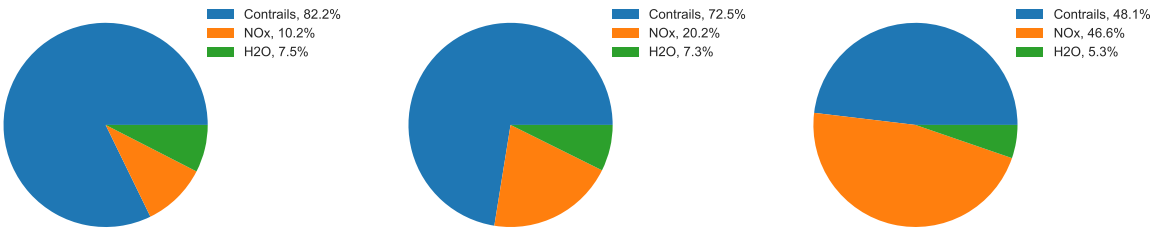

(a) Frigid latitudes. **(b)** Temperate latitudes. **(c)** Tropical latitudes.

Figure 4.15: Climate impact percentage contribution from species caused by the FZM1G aircraft at different latitudes.

Table 4.5 displays the total surface temperature change for the different latitudes and aircraft. The emitted species by the B767S flying over the frigid latitudes cause a 1.6% of the total temperature increase, however, for the FZM1G this percentage is 1.3%. The emitted species of the kerosene B767S flying over the tropical latitudes cause a 12.7% of the total temperature increase, however, for the FZM1G this percentage is increased to 14.0% due to the contrail effects. At tropical latitudes, hydrogen influence on climate is relatively more detrimental[2] than kerosene alternatives, however, at frigid latitudes, the opposite is observed.

Table 4.5: Surface Temperature Change (STC) caused by the B767S and FZM1G at different latitudes.

	Frigid		**Temperate**		**Tropics**	
Parameter	**STC**	**%**	**STC**	**%**	**STC**	**%**
Unit	**mK**	**-**	**mK**	**-**	**mK**	**-**
FZM1G	0.0820	1.3	5.34	84.7	0.883	14.0
B767S	0.309	1.63	16.2	85.6	2.41	12.7

Flying over the Tropics at low altitudes influences greatly the impact of the emissions on climate change, however, over frigid latitudes this altitude difference is less relevant. Nevertheless, it must be noted that these results are very dependent on the aircraft chosen. In this case the kerosene aircraft flies at 10 km, but, if it were to fly slightly higher, differences with hydrogen aviation would be negligible due to the increase in contrail formation probability.

4.2.5. Study Case 1: Flying-V Climate Analysis

The previous sections have demonstrated the climate advantages of using hydrogen combustion on conventional tube-and-wing aircraft. However, literature suggests that conventional aircraft will not be efficient on using hydrogen fuel due to volumetric constraints. In Chapter 2 the Flying-V was proposed as an alternative aircraft. A similar methodology can now be used to observe whether the Flying-V is able to improve the performance of the tube-and-wing B767S and FZM1G, and reduce the climate impact caused by their emissions. Table 4.6 displays the species emitted by each of the aircraft.

[2]Relatively detrimental because, even though the temperature increase caused by the FZM1G is lower than the kerosene alternatives (0.883 mK vs. 2.41 mK), the sensitivity to tropical latitudes is higher.

Table 4.6: Species emitted and fuel used by the tube-and-wing and Flying-V aircraft.

Aircraft	Fuel	NO_x	$EINO_x$		CO_2	$EICO_2$		H_2O	EIH_2O	
	Mt	kt	g/kg	g/MJ	Mt	kg/kg	kg/MJ	Mt	kg/kg	kg/MJ
FZM1G	16.7	179	10.8	0.0898	0	0	0	150	9	0.075
B767S	41.5	544	13.1	0.305	131	3.155	0.734	51.8	1.25	0.029
FV8	45.9	751	16.3	0.380	145	3.155	0.734	57.4	1.25	0.029
FVHY	19.5	265	13.6	0.113	0	0	0	176	9	0.075

The hydrogen Flying-V consumes 16.8% more fuel than the FZM1G, while the FV8 consumes 10.6% more than the B767S. This decrease in fuel efficiency is caused by the lower engine performance of the Flying-V aircraft, as (Beddoes et al., 2022) assumed optimistic improvements on the propulsion system. Similarly, NO_x emissions are 38% higher for the FV8 than for the B767s and 48% higher for the FVHY than for the FZM1G. The increase in NO_x for the Flying-V designs is caused by the lower engine performance, the larger mach cruise speed, and the lower aerodynamic performance. It is important to note that each aircraft is flying at a different altitude, which has an influence on the temperature response. Figure 4.16 displays the surface temperature change evolution along the years for each aircraft.

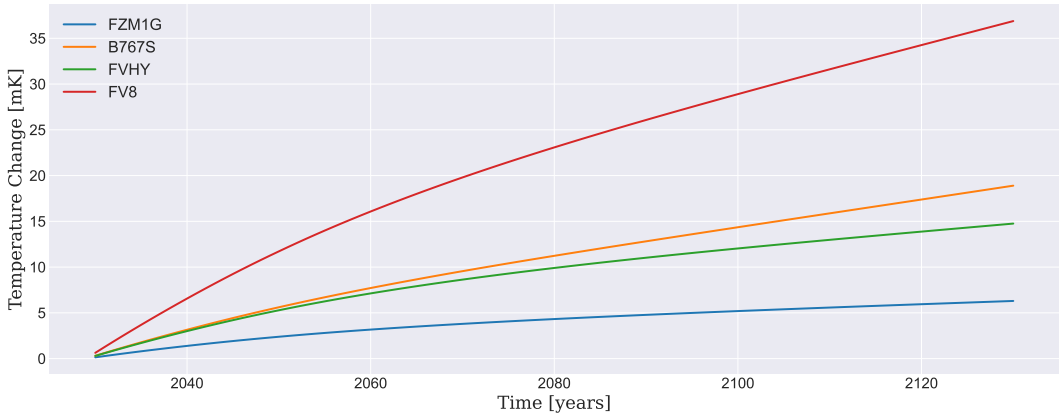

Figure 4.16: Change in surface temperature for hydrogen and kerosene tube-and-wing aircraft (FZM1G, B767S), and hydrogen and kerosene Flying-V aircraft (FVHY, FV8).

The FV8 generates an increase of 36.9 mK in surface temperature after 100 years, while the B767S increases the surface temperature by 18.9 mK (49% lower). The FVHY and the FZM1G cause an increase in surface temperature of 14.8 mK and 6.3 mK respectively (57%). The difference on climate impact for both kerosene and hydrogen aircraft is caused by the higher cruise altitude of the Flying-V designs. To test this hypothesis, the individual contribution from species can be observed in Figure 4.17. At higher altitudes, contrail and NO_x effects on climate are considerably larger than at lower altitudes. The FV8 emits 38% more NO_x than the B767S aircraft, however, the climate impact is increased by 100%. The FVHY emits 48% more NO_x, and the climate impact is increased by 168 %. Similarly the change in contrail climate effects due to the higher altitude of the FV8 when compared to the B767S (12.6 km vs. 10.0 km) corresponds to a 2.45 times larger surface temperature change. The change in contrail effects for the FVHY compared to the FZM1G (13.0 km vs. 10.7 mk) corresponds to a 1.52 times larger surface temperature change.

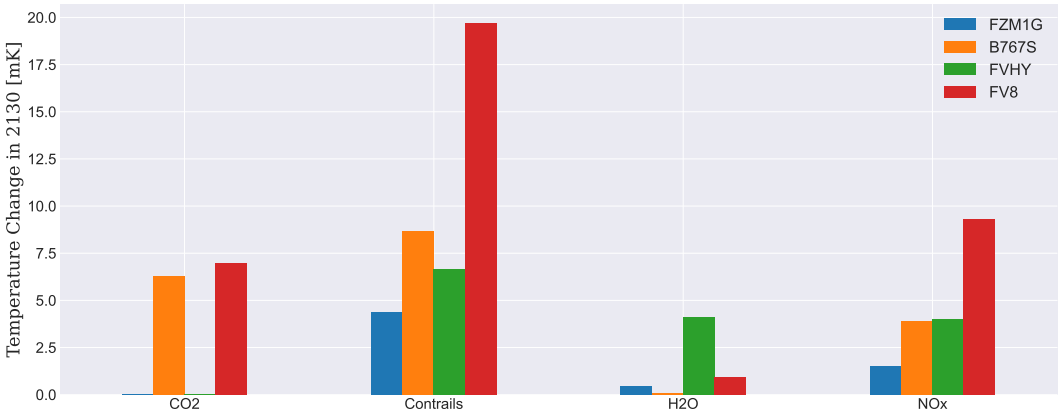

Figure 4.17: Contribution to surface temperature from each of the species caused by the tube-and-wing aircraft and the Flying-Vs.

The results however should be analyzed knowing that all the aircraft are still in design phase. Deviations in altitude, aircraft performance parameters and even aircraft weights will change the final results of the study case.

Same Engine Analysis

The Flying-V designs assume different engine performances than the tube-and-wing aircraft. To create a fairer comparison, the engine models[3] used by the tube-and-wing aircraft are used for the Flying-V designs. However, this study does not take into account the operative empty weight advantages caused by a reduced fuel weight, or the higher cruise altitude that the reduced weight might cause. The engines used for this section of the study are represented in Table 3.1, the FV8 will use the engine characteristics of the B767S engine and the FVHY will used the engine characteristics of the FZM1G. Table 4.7 displays the species emitted for the four aircraft. It can be observed that now the fuel consumed of the Flying-V designs are much closer to that of the tube-and-wing aircraft. NO_x emissions have been reduced for the Flying-Vs compared with Table 4.6, however, the difference with the tube-and-wing aircraft are still eminent. The greater cruise speed of the Flying-V designs increases NO_x production as mentioned in Section 3.2.6.

Table 4.7: Species emitted and fuel used by the tube-and-wing and Flying-V aircraft. The latter using the same engines as the tube-and-wing aircraft.

Aircraft	Fuel	NO_x	$EINO_x$		CO_2	$EICO_2$		H_2O	EIH_2O	
	Mt	kt	g/kg	g/MJ	Mt	kg/kg	kg/MJ	Mt	kg/kg	kg/MJ
FZM1G	16.7	191	11.5	0.0958	0	0	0	150	9	0.075
B767S	41.5	544	13.1	0.305	131	3.155	0.734	51.8	1.25	0.029
FV8	42.9	669	15.6	0.363	135	3.155	0.734	53.6	1.25	0.029
FVHY	16.2	206	12.7	0.106	0	0	0	146	9	0.075

Figure 4.18 displays the temperature change caused by the four aircraft over time, now with the engines used by the tube-and-wing aircraft mounted on the Flying-Vs. The surface temperature change caused by the FV8 and FVHY is 36.3 mK and 14.2 mK respectively. It can be observed that, even with the drop in fuel consumption for both aircraft, the climate effects have not decreased much. The reason can be explained using Figure 4.19 and Figure 4.17. It can be observed that NO_x and H_2O and CO_2 emissions drop significantly for the improved engine versions, however, the engine efficiency is increased, causing a higher temperature increase from contrails.

[3]The engine models will be sometimes refer to as improved engines as they show a better performance than the old Flying-V engines.

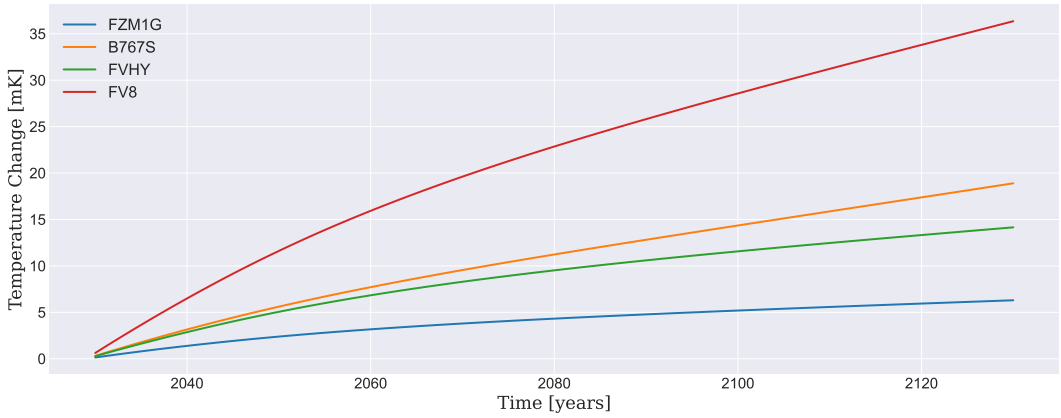

Figure 4.18: Change in surface temperature for hydrogen and kerosene tube-and-wing aircraft (FZM1G, B767S), and hydrogen and kerosene Flying-V aircraft with the improved engine (FVHY, FV8).

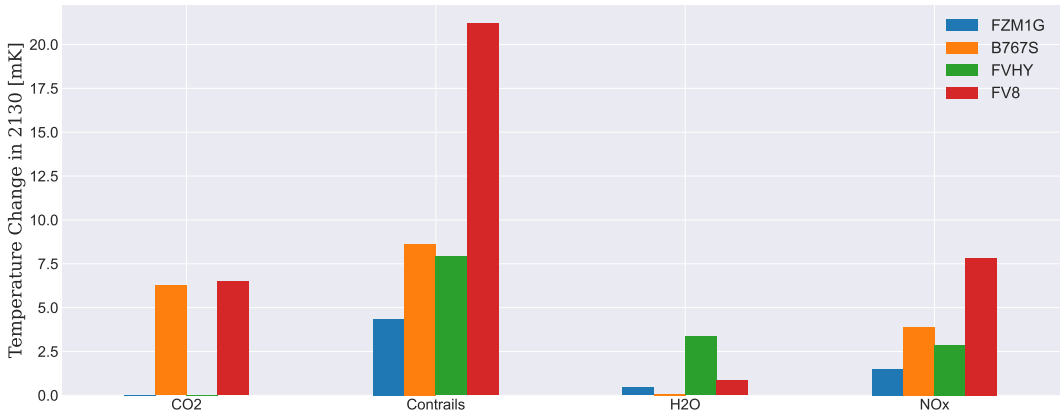

Figure 4.19: Contribution to surface temperature from each of the species for the tube-and-wing aircraft and the Flying-Vs using the same engine.

Something important to note is that the FV8 is able to carry 20% more payload overall, so, for a better final comparison the surface temperature increase can be divided by the payload carried (Table 4.8). It can be observed that, even with the higher transported payload weight, the FV8 is still worse for climate than the aircraft competitors.

Table 4.8: Temperature increase caused by each of the aircraft parameterized with respect to the payload weight transported.

Aircraft	FZM1G	B767S	FV8	FVHY
Temperature change per payload weight [mK/Gt]	0.188	0.564	0.898	0.422

With this in mind, and knowing that the tube-and-wing aircraft designs from Beddoes et al. (2022) are optimistic regarding the aerodynamic design, preliminary results have shown a better climate performance for the tube-and-wing aircraft (FZM1G and B767S) with and without engine improvements.

4.2.6. Study Case 2: Technology Introduction Year

In this section the second study case is analyzed, this scenario was described in Section 3.3.1 and is meant to represent a hypothetical situation rather than a direct comparison as in the previous sections. In this scenario the B767S technology is introduced in 2030, 11 years after the start of the simulation

and the hydrogen aircraft (FZM1G) is not introduced until 2050, 31 years after the beginning of the simulation. The baseline aircraft will be the B767-200ER (B767ER), used also as baseline by Beddoes et al. (2022). Table 4.9 displays the fuel emitted per aircraft in 2019.

Table 4.9: Species emitted and fuel used by the aircraft on the second study case.

Aircraft	Fuel	NO_x	$EINO_x$		CO_2	$EICO_2$		H_2O	EIH_2O	
	Mt	kt	g/kg	g/MJ	Mt	kg/kg	kg/MJ	Mt	kg/kg	kg/MJ
FZM1G	16.7	191	11.5	0.0958	0	0	0	150	9	0.075
B767S	41.5	544	13.1	0.305	131	3.155	0.734	51.8	1.25	0.029
B767ER	63.0	1145	18.17	0.422	199	3.155	0.734	78.8	1.25	0.029

Figure 4.20 displays the surface temperature change caused by the baseline and how the final temperature change would adapt if the B767S enters the market in 2030 and the hydrogen FZM1G enters the market in 2050. It can be observed that the FZM1G is an extension of the B767S, so it has been treated as a "storyline" where first the B767S is introduced and then it can be replaced by the FZM1G. The storyline concept has a major change with respect to the normal comparison, in 2030 the emissions from the B767ER are stopped, but the climate effects of the previous emissions still govern the temperature increase for the B767S and FZM1G after years of the simulation. This means that the climate "after-effects" of the B767ER were added to the B767S and FZM1G.

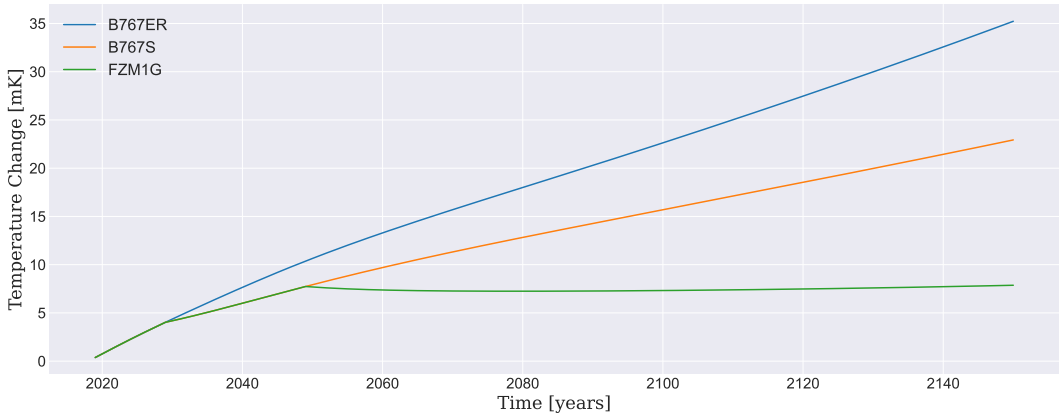

Figure 4.20: Surface temperature increase caused by the B767S, FZM1G and B767ER, where the B767S is introduced in 2030 and the FZM1G in 2050.

It must be noted that the results in this study case can not be compared to the results in Section 4.2.1 as the simulation start time differs from 2030 to 2019, and a new aircraft with higher emissions is introduced as a baseline. However, some interesting results can be observed. After 100 years of the introduction of the B767S (2130), the surface temperature change with respect to the baseline aircraft is 33% lower. Moreover, the hydrogen aircraft (FZM1G) causes a 78% lower temperature change with respect to the baseline after 100 years of flying (2050-2150).

4.2.7. Sensitivity Analysis

The sensitivity analysis is performed to understand the effects of uncertainties on the final results. The major flight performance uncertainty is the cruise altitude, strongly linked to climate effects. Furthermore, some parameters with high uncertainty related to hydrogen emissions and climate effects were mentioned in Chapter 2 and Chapter 3. The sensitivity study will be divided into the flight performance assessment and the hydrogen impact assessment.

Flight Performance Assessment

During the flight simulation, the cruise speed and cruise altitude define the flight time and the fuel consumed during the mission. The flight altitude has a clear relation to climate impact, and therefore the final results will change when tweaking it. Altitude and speed should not be separated, as they are dependent of each other. If an aircraft is flown at a higher cruise altitude, the cruise speed should be adapted to fly at the optimum lift coefficient. Mach speeds above 0.9 are removed from the study to avoid supersonic air regimes after critical mach speeds which can not be predicted with this model. Cruise altitudes above 11 km for this particular tube-and-wing aircraft designs require cruise mach speeds above 0.9. Table 4.10 displays the situations with the variable altitude and the resulting fuel consumed and Table 4.11 the surface temperature variation.

Table 4.10: Influence on fuel consumption caused by the sensitivity analysis flight performance situations.

Flight Performance Situations	**Fuel Consumed [Mt]**			
	FZM1G	**B767S**	**FV8**	**FVHY**
Baseline Altitude (10.7 km, 10 km, 13 km, 12.6 km)	16.7	41.5	45.9	19.5
Cruise Altitude 9 km	17.1	42.8	49.7	20.4
Cruise Altitude 10 km	16.8	41.5	48.3	50.8
Cruise Altitude 11 km	16.6	40.5	47.2	19.8

Table 4.11: Influence on fuel consumption caused by the sensitivity analysis hydrogen impact situations.

Flight Performance Situations	**Temperature Increase** $[mK]$			
	FZM1G	**B767S**	**FV8**	**FVHY**
Baseline Altitude (10.7 km, 10 km, 13 km, 12.6 km)	6.34	18.9	36.9	14.7
Cruise Altitude 9 km	3.58	14.7	15.8	3.34
Cruise Altitude 10 km	5.02	18.7	19.7	4.69
Cruise Altitude 11 km	7.34	22.4	23.36	6.86

The relation between altitude, fuel consumed and change in surface temperature is interesting. The higher the aircraft flies, the lower the fuel consumption is due to the lower air density and thus lower drag, however, the higher in the atmosphere the species are emitted, the larger climate effects. Please note that there is physical limits for the maximum altitude at which you can fly depending on cruise mach and wing loading.

The climate effects of the different altitudes can be observed visually in Figure 4.21. The plot also includes dotted lines connecting the surface temperature change per aircraft, displaying the relation between surface temperature change and altitude. The steeper line in the case of kerosene aviation indicates a higher surface temperature dependency on altitude. This is because of the higher emission index of kerosene aircraft and the higher radiative forcing of kerosene contrails, dependent on the cruise altitude.

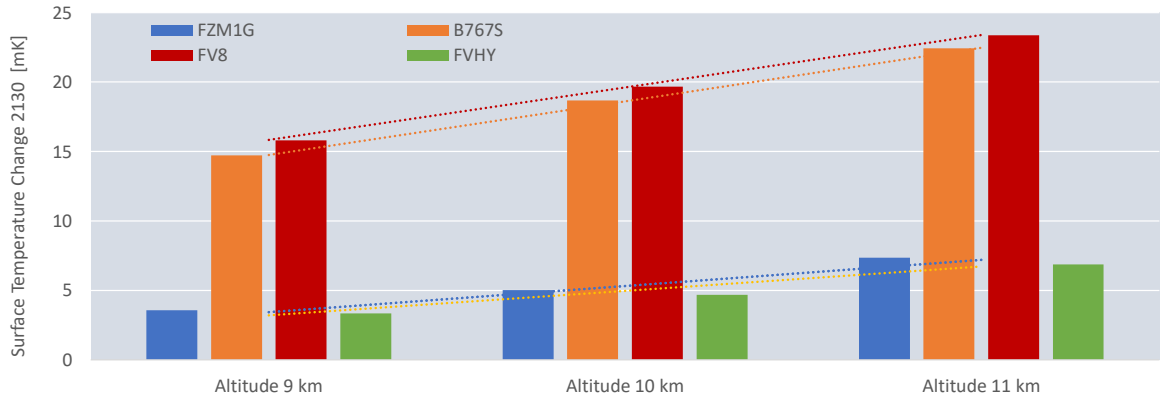

Figure 4.21: Surface temperature change with different altitudes.

Hydrogen Impact Assessment

The sensitivity analysis can also be performed with respect to hydrogen uncertainties. As explained in Section 3.3.1, the $EINO_x$ hydrogen ratio is subject to large uncertainties. The baseline situation uses a ratio of 0.75 (Equation 3.15). This parameter represents the $EINO_x$ change due to hydrogen combustion by taking advantage of the lower lean limit of hydrogen. However, Funke et al. (2019) states that it can be as low as 0.1 and as high as 1.3. Moreover, in Section 3.3.1 the contrail radiative forcing for hydrogen combustion was defined. It was explained that this parameter has a large variability. It would be interesting to analyze deviations in this parameter to observe if the final conclusion of the study still holds. Table 4.12 displays the variation in NO_x emissions when varying the $EINO_x$ ratio. For both hydrogen aircraft, NO_x reduces by 87% when $EINO_x$ ratio is set to 0.1, and increases by 72% when $EINO_x$ ratio is set to 1.3.

Table 4.12: NO_x emitted by the FZM1G and FVHY for the different situations analyzed in the sensitivity analysis.

Flight Performance Situations	NO_x Emissions [kt]	
	FZM1G	FVHY
Baseline (0.75 NO_x rat.)	179	265
1.3 NO_x ratio	308	455
0.1 NO_x ratio	23.7	35.0

Figure 4.22 displays the surface temperature increase in percentage for the situations described above. To support the graph, Table 4.13 is included below. If this study has overestimated the capacity of hydrogen to reduce NO_x emissions and $EINO_x$[4] is 1.3 times higher than for kerosene aviation, the surface temperature increases by 18% in the case of the tube-and-wing aircraft and 20% for the Flying-V. If on the other hand, this study has underestimated the hydrogen creation of NO_x and the ratio is 90% lower, the surface temperature would decrease by 20% for the hydrogen tube-and-wing and by 22% for the Flying-V.

The contrail RF ratio is the relation between the radiative forcing of hydrogen contrails versus kerosene contrails. For the baseline case is set to 0.31, which corresponds to a reduction of 69% in the RF of hydrogen contrails compared to kerosene contrails. If this ratio were to be 0.7 or even 1.3, the surface temperature change would increase. If the contrail radiative forcing ratio is increased to 0.7, the surface temperature change increases by 88% for the FZM1G and by 56% for the FVHY. When the contrail radiative forcing is increased to 1.3, the surface temperature change increases by 220% for the FZM1G and by 143% for the FVHY. The cause for the larger variation on contrail radiative forcing for the tube-and-wing aircraft is unknown, however, it might be related to a higher climate impact from contrails at lower altitudes.

[4]Note that $EINO_x$ increases with resepect to kerosene aviation, however NO_x is still lower due to the reduce fuel consumption.

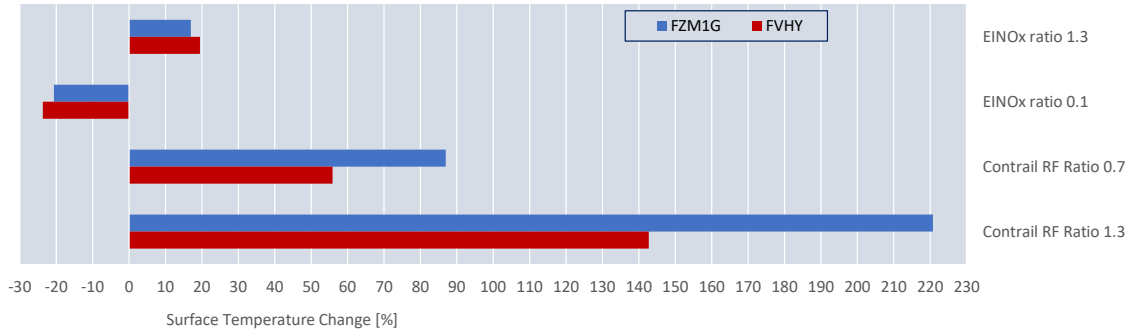

Figure 4.22: Surface temperature percentage change with different sensitive scenarios. For reference, the original $EINO_x$ ratio is set to 0.75 and the contrail RF ratio to 0.31.

Table 4.13: Situations for the hydrogen sensitivity analysis influence on surface temperature change.

Flight Performance Situations	**Temperature Increase** $[mK]$	
	FZM1G	**FVHY**
Baseline ($EINO_x$ ratio: 0.75, Contrail RF: 0.31)	6.34	14.7
$EINO_x$ ratio 1.3	7.37	17.6
$EINO_x$ ratio 0.1	5.00	11.3
Contrail Radiative Forcing Ratio 0.7	11.8	23.0
Contrail Radiative Forcing Ratio 1.3	20.2	35.8

For this study, it would also be interesting to know what could happen in the worst and best case scenario for hydrogen combustion, and compare that to the results in Figure 4.5. Figure 4.23 includes the best (FZM1G - BCS) and worst (FZM1G - WCS) estimate for the hydrogen tube-and-wing aircraft. The WCS includes the $EINO_x$ ratio of 1.3 and the contrail radiative forcing ratio of 1.3. The BCS includes the $EINO_x$ ratio of 0.1 and a contrail radiative forcing ratio of 0.31.

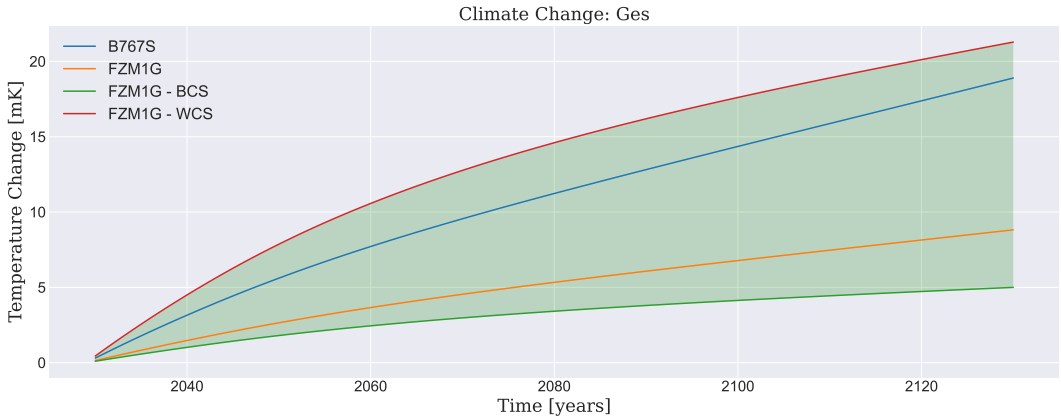

Figure 4.23: Temperature change distribution for the B767S and FZM1G, including a best and worst case scenario (BCS, WCS) for the hydrogen aircraft.

At the beginning of the simulation, the worst case scenario for the hydrogen aircraft creates a slightly larger climate warming than the B767S kerosene aircraft. However, the situation is reversed after 2105 due to the cumulative nature of the CO_2 emissions, as explained in Section 4.2.3. Even when assuming the worst case scenario, hydrogen aircraft causes a lower surface temperature increase that that of kerosene aircraft.

5

Conclusions

This study has developed a new methodology to model emissions and calculate the surface temperature change caused by the FZM1G and B767S tube-and-wing aircraft using hydrogen and kerosene combustion respectively. The chosen aircraft were flown over relevant flight routes, selected using the Routing Design Model, based on global coverage and aircraft mission specifications. An emission inventory, composed of consumed fuel and nitrogen oxide emissions per flight step, was calculated using the Flight Simulation Model. Using the Climate Impact Module, the surface temperature change for both hydrogen and kerosene aircraft was obtained. Furthermore, two study cases were analyzed. The first to understand the effects of the Flying-V on climate and the second to study the climate effects of different aircraft market introduction times. Finally, a sensitivity analysis was performed to assess the climate impact of best and worst case situations for hydrogen aircraft and the implications of changing the flight altitude.

Keeping in mind that all aircraft selected are still in the design phase, they help us draw important conclusions about the climate effects of hydrogen and kerosene aviation, specifically regarding surface temperature increase. The first conclusion is that hydrogen aviation consumes less fuel than kerosene aviation. The hydrogen fleet would only consume 16.7 megatons of hydrogen for the 2.2 million flights simulated, while the kerosene fleet would consume 41.5 megatons. The second conclusion comes from researching whether hydrogen emissions are less or more harming to the environment than kerosene emissions. Hydrogen aircraft cause a 67% lower surface temperature change than kerosene aircraft, 6.3 mK opposed to 18.9 mK. The improvement is achieved because of: the zero carbon emissions of burning hydrogen, the lower radiative forcing of hydrogen contrails, and the reduction in NO_x emissions due to the lower lean limit of hydrogen fuel. Furthermore, CO_2 is a long lived species and it has major climate effects years after its release in the atmosphere. Therefore, the effects on climate from kerosene aviation are far less controllable than hydrogen aviation. In the studied hypothetical situation where flights are halted, similarly to what happened during COVID-19, climate recovery occurred faster for hydrogen-powered aviation. Special attention should be paid when flying hydrogen aircraft at different latitudes, as hydrogen aircraft have shown lower susceptibility when flying over the Poles and higher susceptibility when flying over the Tropics. This observation is strongly linked to altitude, and different conclusions could result if the aircraft analysed were flying higher or lower.

Regarding the first study case, the kerosene Flying-V consumes slightly more fuel than the tube-and-wing B767S, while the hydrogen Flying-V consumes less than the FZM1G. However, when transforming the fuel consumption to climate impact, the higher altitude of the Flying-V designs results on a higher surface temperature increase. While the Flying-V designs might seem worse compared to the FZM1G and B767S, strong improvements over current aviation are expected, and specific emphasis should be given to the hydrogen design. The second study case showed interesting results, the B767S leads to a surface temperature change 23% lower than that of current aviation (B767ER). On the other hand, the temperature change caused by the hydrogen FZM1G is 57% lower than that of the B767ER. Finally, a sensitivity analysis was performed to assess the surface temperature change variability due to flight altitude and uncertainties on hydrogen emissions and climate effects. All aircraft were flown at 9, 10 and 11 kilometer altitudes. It was observed that, although the fuel consumption decreases at higher altitudes, the surface temperature change increases. The sensitivity to altitude was found to be higher

for kerosene aircraft than for hydrogen aircraft. When the uncertainties related to hydrogen emissions and contrails were investigated, the worst case situation induced a surface temperature change similar to the one of kerosene aviation. Nonetheless, surface temperature increase over time is lower for hydrogen aircraft, which favours hydrogen aviation in the long run.

Although aviation on its own will not solve the current environmental problems, I believe hydrogen combustion has the potential to become a new milestone in the development of a much more sustainable aviation. We have demonstrated that even the worst case situation for hydrogen aircraft is advantageous compared to kerosene aviation.

References

Abbot, D., Giannotta, A., Sun, X., Gauthier, P., & Sethi, V. (2021). Thermoacoustic Behaviour of a Hydrogen Micromix Aviation Gas Turbine Combustor Under Typical Flight Conditions [V006T03A013], *Volume 6: Ceramics and Ceramic Composites; Coal, Biomass, Hydrogen, and Alternative Fuels; Microturbines, Turbochargers, and Small Turbomachines*. https://doi.org/10.1115/GT2021-59844

Airbus Deutschland GmbH. (2003). Liquid Hydrogen Fuelled Aircraft - System Analysis. *Cryoplane*, (May 2003), 1–80.

Allen, M. R., Fuglestvedt, J. S., Shine, K. P., Reisinger, A., Pierrehumbert, R. T., & Forster, P. M. (2016). New use of global warming potentials to compare cumulative and short-lived climate pollutants. *Nature Climate Change*, *6*(8), 773–776. https://doi.org/10.1038/nclimate2998

Baklacioglu, T. (2015). Fuel flow-rate modelling of transport aircraft for the climb flight using genetic algorithms. *Aeronautical Journal*, *119*(1212), 173–183. https://doi.org/10.1017/S0001924000010320

Beddoes, S., Foster, M., James, D., Kay, E., Kay, O., Shawki, K., Stubbs, E., Thomas, D., Weider, K., & Wilson, R. (2022). *Flyzero-zero-carbon emission aircraft concepts*. Aerospace Technology Institute. https://www.ati.org.uk/flyzero-reports/

Benad, J. (2015). the Flying V - a New Aircraft Configuration for Commercial Passenger Transport. *Deutscher Luft- und Raumfahrtkongress*, (September), 1–8. https://doi.org/10.25967/370094

Boretti, A. (2021). Testing the hypothesis hydrogen jets may significantly contribute to global warming through jets contrails. *International Journal of Hydrogen Energy*, *46*(73), 36610–36618. https://doi.org/10.1016/j.ijhydene.2021.08.173

Brewer, G. D. (1991). *Hydrogen aircraft technology*. CRC Press.

Burkhardt, U., Bock, L., & Bier, A. (2018). Mitigating the contrail cirrus climate impact by reducing aircraft soot number emissions. *Climate and Atmospheric Science*, *1*. https://doi.org/10.1038/s41612-018-0046-4

Cadle, R. D. (2015). *Atmospheric chemistry* (Vol. 52). Elsevier Inc. https://doi.org/10.1029/EO052i006pIU368

Carter, R. (2021). Development of a liquid hydrogen combustion high bypass turbofan model in npss. *Mechanical Engineering and Materials Science Independent Study*.

Catling, D. C. (2015). *Planetary Atmospheres* (Vol. 10). Elsevier B.V. https://doi.org/10.1016/B978-0-444-53802-4.00185-8

Cecere, D., Giacomazzi, E., & Ingenito, A. (2014). A review on hydrogen industrial aerospace applications. *International Journal of Hydrogen Energy*, *39*(20), 10731–10747. https://doi.org/10.1016/j.ijhydene.2014.04.126

Chandrasekaran, N., & Guha, A. (2012). Study of prediction methods for NOx emission from turbofan engines. *Journal of Propulsion and Power*, *28*(1), 170–180. https://doi.org/10.2514/1.B34245

Chevron. (2007). Aviation Fuels Technical Review, 17.

Clean Sky. (2020). *Hydrogen-powered aviation - A fact-based study of hydrogen technology, economics, and climate impact by 2050*. https://doi.org/10.2843/766989

Dahlmann, K., Grewe, V., Frömming, C., & Burkhardt, U. (2016). Can we reliably assess climate mitigation options for air traffic scenarios despite large uncertainties in atmospheric processes? *Transportation Research Part D: Transport and Environment*, *46*(2), 40–55. https://doi.org/10.1016/j.trd.2016.03.006

Dedoussi, I. C. (2021a). *Aircraft emissions and climate effects - lecture 10* [University Lecture], Delft University of Technology.

Dedoussi, I. C. (2021b). *Aircraft emissions and climate effects - lecture 9* [University Lecture], Delft University of Technology.

Deidewig, F., Dopelheuer, A., & Lecht, M. (1996). Methods to Assess Aircraft Engine Emissions in Flight.

Delbeke, J., Runge-Metzger, A., Slingenberg, Y., & Werksman, J. (2019). The Paris Agreement. *Towards a Climate-Neutral Europe: Curbing the Trend*, 24–45. https://doi.org/10.4324/9789276082569-2

Demir, M. E., & Dincer, I. (2018). Cost assessment and evaluation of various hydrogen delivery scenarios. *International Journal of Hydrogen Energy*, *43*(22), 10420–10430. https://doi.org/10.1016/j.ijhydene.2017.08.002

Derakhshandeh, P., Ahmadi, A., & Dashti, R. (2021). Simulation and technical economic environmental optimization of the General Electric GE90 hydrogen turbofan engine. *International Journal of Hydrogen Energy*, *46*(5), 3303–3318. https://doi.org/10.1016/j.ijhydene.2020.10.182

Di Domenico, M., Gerlinger, P., & Aigner, M. (2010). Development and validation of a new soot formation model for gas turbine combustor simulations. *Combustion and Flame*, *157*(2), 246–258. https://doi.org/10.1016/j.combustflame.2009.10.015

Djojodihardjo, H. (2015). Space Monitoring of Cirrus Clouds and Contrails for Climate Change Correction and Control. *IAA Climate Change and Disaster Management Conference, Mexico City*, (September).

Elliott, D. (2015). Final report: Aviation Fuel Efficiency Technology Assessment. (604), 1–29.

Eurocontrol. (2004). User manual for the base of aircraft data (bada). *European Organisation for the Safety of Air Navigation, Eurocontrol*, *3.6*, 1. https://www.eurocontrol.int/publication/user-manual-base-aircraft-data-bada

European Union Aviation Safety Agency (EASA). (2020). Updated analysis of the non-CO2 climate impacts of aviation and potential policy measures pursuant to the EU Emissions Trading System Directive Article 30(4). European Union Aviation Safety (EASA), MOVE/E1/SER/2019-475/SI2.81706, Köln. *European Commission*, *30*. https://www.easa.europa.eu/sites/default/files/dfu/201119_report_com_ep_council_updated_analysis_non_co2_climate_impacts_aviation.pdf

Faggiano, F., Vos, R., Baan, M., & Van Dijk, R. (2017). Aerodynamic design of a flying V aircraft [Unpublished Master's Thesis]. *17th AIAA Aviation Technology, Integration, and Operations Conference, 2017*. https://doi.org/10.2514/6.2017-3589

Fahey, D. W., & Lee, D. S. (2016). Aviation and Climate Change: A Scientific Perspective. *Carbon & Climate Law Review*, *10*(2), 97–104.

Federal Aviation Administration (FAA). (2005). Aviation & emissions – A primer. *Aviation and Climate Change*, (January), 85–114.

Fuglestvedt, J. S., Berntsen, T. K., Isaksen, I. S., Mao, H., Liang, X., & Wang, W. (1997). Climatic effects of NO_x emissions through changes in tropospheric O_3 and CH_4: A global 3-D model study. *February 1997. Sciences-New York. Oslo, Norway. Houghton, J., Ding, Y., Griggs, D. J., and Noguer, M*, (10), 1–65.

Funke, H., Beckmann, N., & Abanteriba, S. (2019). An overview on dry low no x micromix combustor development for hydrogen-rich gas turbine applications. *International Journal of Hydrogen Energy*, *44*, 6978–6990. https://doi.org/10.1016/j.ijhydene.2019.01.161

Gauss, M., Isaken, I. S. A., Wong, S., & Wang, W. C. (2003). Impact of H2O emissions from cryoplanes and kerosene aircraft on the atmosphere. *Journal of Geophysical Research: Atmospheres*, *108*(10), 1–11. https://doi.org/10.1029/2002jd002623

Gierens, K., Kärcher, B., Mannstein, H., & Mayer, B. (2009). Aerodynamic contrails: Phenomenology and flow physics. *Journal of the Atmospheric Sciences*, *66*(2), 217–226. https://doi.org/10.1175/2008JAS2767.1

Gilani, M. (2019). Airline Weight Reduction to Minimize Direct Operating Cost Airline Weight Reduction to Minimize Direct Operating Cost. *University of Turkish Aeronautical Association*, (October 2019).

Gorbunov, B., Baklanov, A., Kakutkina, N., Windsor, H. L., & Toumi, R. (2001). Ice nucleation on soot particles. *Journal of Aerosol Science*, *32*(2), 199–215. https://doi.org/10.1016/S0021-8502(00)00077-X

Graver, B., Rutherford, D., & Zheng, S. (2020). CO2 emissions from commercial aviation: 2013, 2018, and 2019 | International Council on Clean Transportation. *International Council on Clean Transportation*, (October), 36. https://theicct.org/publications/co2-emissions-commercial-aviation-2020

Greene, D. L. (1992). Further 1992. 17:537-73. (1).

Grewe, V. (2021a). *Aircraft emissions and climate effects - atmospheric chemistry - lecture 2* [University Lecture], Delft University of Technology.

Grewe, V. (2021b). *Aircraft emissions and climate effects - climate responses and climate metrics - lecture 5* [University Lecture], Delft University of Technology.

Grewe, V., Bock, L., Burkhardt, U., Dahlmann, K., Gierens, K., Hüttenhofer, L., Unterstrasser, S., Rao, A. G., Bhat, A., Yin, F., Reichel, T. G., Paschereit, O., & Levy, Y. (2017a). Assessing the climate impact of the AHEAD multi-fuel blended wing body. *Meteorologische Zeitschrift*, *26*(6), 711–725. https://doi.org/10.1127/metz/2016/0758

Grewe, V., & Dahlmann, K. (2015). How ambiguous are climate metrics? And are we prepared to assess and compare the climate impact of new air traffic technologies? *Atmospheric Environment*, *106*, 373–374. https://doi.org/10.1016/j.atmosenv.2015.02.039

Grewe, V., Dahlmann, K., Flink, J., Frömming, C., Ghosh, R., Gierens, K., Heller, R., Hendricks, J., Jöckel, P., Kaufmann, S., Kölker, K., Linke, F., Luchkova, T., Lührs, B., van Manen, J., Matthes, S., Minikin, A., Niklaß, M., Plohr, M., … Ziereis, H. (2017b). Mitigating the climate impact from aviation: Achievements and results of the DLR WeCare project. *Aerospace*, *4*(3). https://doi.org/10.3390/aerospace4030034

Grewe, V., Gangoli Rao, A., Grönstedt, T., Xisto, C., Linke, F., Melkert, J., Middel, J., Ohlenforst, B., Blakey, S., Christie, S., Matthes, S., & Dahlmann, K. (2021). Evaluating the climate impact of aviation emission scenarios towards the Paris agreement including COVID-19 effects. *Nature Communications*, *12*(1), 1–10. https://doi.org/10.1038/s41467-021-24091-y

Grewe, V., & Stenke, A. (2008). AirClim: An efficient tool for climate evaluation of aircraft technology. *Atmospheric Chemistry and Physics*, *8*(16), 4621–4639. https://doi.org/10.5194/acp-8-4621-2008

Grouset, D., & Ridart, C. (2018). *Lowering energy spending together with compression, storage, and transportation costs for hydrogen distribution in the early market*. Elsevier Ltd. https://doi.org/10.1016/B978-0-12-811197-0.00006-3

Hadnum, L., Pacey, M., & Milne, K. (2022). *Technology roadmaps: Technology pathways to enable zero-carbon emission flight*. Aerospace Technology Institute. https://www.ati.org.uk/flyzero-reports/

Harris, C. D. (1990). Supercritical Aerofoils Design. *NASA Technical Paper*.

Herndon, S. C., Rogers, T., Dunlea, E. J., Jayne, J. T., Miake-Lye, R., & Knighton, B. (2006). Hydrocarbon emissions from in-use commercial aircraft during airport operations. *Environmental Science and Technology*, *40*(14), 4406–4413. https://doi.org/10.1021/es051209l

Hoffmann, P. (1981). *The forever fuel: The story of hydrogen* (1st ed.). Routledge. https://doi.org/10.4324/9780429311000

Hoffmann, P. (2001). *Tomorrow's energy: Hydrogen, fuel cells, and the prospects for a cleaner planet* (1st ed.). (The MIT Press.

Intergovernmental Panel on Climate Change (IPCC). (1999). *Climate Change 2013 - The Physical Science Basis*.

Intergovernmental Panel on Climate Change (IPCC). (2013). *Climate Change 2013 - The Physical Science Basis*.

International Civil Aviation Organization (ICAO). (2009). *Tenth session of the statistics division: Review of the classification and definitions used for civil aviation activities*.

International Energy Agency (IEA). (2019). The Future of Hydrogen The Future of Hydrogen. (June).

Iwabuchi, H., Yang, P., Liou, K. N., & Minnis, P. (2012). Physical and optical properties of persistent contrails: Climatology and interpretation. *Journal of Geophysical Research Atmospheres*, *117*(6), 1–18. https://doi.org/10.1029/2011JD017020

Jacob, D. J. (2000). Heterogeneous chemistry and tropospheric ozone. *Atmospheric Environment*, *34*(12-14), 2131–2159. https://doi.org/10.1016/S1352-2310(99)00462-8

Jain, P. C. (1993). Greenhouse effect and climate change: scientific basis and overview. *Renewable Energy*, *3*(4-5), 403–420. https://doi.org/10.1016/0960-1481(93)90108-S

Janić, M. (2014). Greening commercial air transportation by using liquid hydrogen (LH2) as a fuel. *International Journal of Hydrogen Energy*, *39*(29), 16426–16441. https://doi.org/10.1016/j.ijhydene.2014.08.011

Johansson, K. O., Head-Gordon, M. P., Schrader, P. E., Wilson, K. R., & Michelsen, H. A. (2018). Resonance-stabilized hydrocarbon-radical chain reactions may explain soot inception and growth. *Science*, *361*(6406), 997–1000. https://doi.org/10.1126/science.aat3417

Kahraman, N., Tangöz, S., & Akansu, S. O. (2018). Numerical analysis of a gas turbine combustor fueled by hydrogen in comparison with jet-A fuel. *Fuel*, *217*(August 2017), 66–77. https://doi.org/10.1016/j.fuel.2017.12.071

Kärcher, B. (2018). Formation and radiative forcing of contrail cirrus. *Nature Communications*, *9*(1), 1–17. https://doi.org/10.1038/s41467-018-04068-0

Köhler, M. O., Rädel, G., Dessens, O., Shine, K. P., Rogers, H. L., Wild, O., & Pyle, J. A. (2008). Impact of perturbations to nitrogen oxide emissions from global aviation. *Journal of Geophysical Research Atmospheres*, *113*(11). https://doi.org/10.1029/2007JD009140

Köhler, M. O., Rädel, G., Shine, K. P., Rogers, H. L., & Pyle, J. A. (2013). Latitudinal variation of the effect of aviation NOx emissions on atmospheric ozone and methane and related climate metrics. *Atmospheric Environment*, *64*(10), 1–9. https://doi.org/10.1016/j.atmosenv.2012.09.013

Lanza, G. R., Ye, X., Randhir, T., & Ries, J. B. (2014). Mechanisms and Effects of Acid Rain on Environment. *Journal of Earth Science & Climatic Change*, *05*(06). https://doi.org/10.4172/2157-7617.1000204

Larsson, J., Elofsson, A., Sterner, T., & Åkerman, J. (2019). International and national climate policies for aviation: a review. *Climate Policy*, *19*(6), 787–799. https://doi.org/10.1080/14693062.2018.1562871

Lee, D. S., Fahey, D. W., Skowron, A., Allen, M. R., Burkhardt, U., Chen, Q., Doherty, S. J., Freeman, S., Forster, P. M., Fuglestvedt, J., Gettelman, A., De León, R. R., Lim, L. L., Lund, M. T., Millar, R. J., Owen, B., Penner, J. E., Pitari, G., Prather, M. J., … Wilcox, L. J. (2021). The contribution of global aviation to anthropogenic climate forcing for 2000 to 2018. *Atmospheric Environment*, *244*(July). https://doi.org/10.1016/j.atmosenv.2020.117834

Lee, D. S., Pitari, G., Grewe, V., Gierens, K., Penner, J. E., Petzold, A., Prather, M. J., Schumann, U., Bais, A., Berntsen, T., Iachetti, D., Lim, L. L., & Sausen, R. (2010). Transport impacts on atmosphere and climate: Aviation. *Atmospheric Environment*, *44*(37), 4678–4734. https://doi.org/10.1016/j.atmosenv.2009.06.005

Lim, L., & Lee, D. S. (2006). Quantifying the effects of aviation on radiative forcing and temperature with a climate response model. *Proceedings of the TAC-Conference*, (1), 202–207.

Linke, F., Radhakrishnan, K., Grewe, V., Vos, R., Niklaß, M., Lührs, B., Feijia, Y., & Dedoussi, I. (2020). GLOWOPT-A new approach towards global-warming-optimized aircraft design. (1). https://www.researchgate.net/publication/343306431

Marquart, S., Ponater, M., Strom, L., & Gierens, K. (2005). An upgraded estimate of the radiative forcing of cryoplane contrails. *Meteorologische Zeitschrift*, *14*(4), 573–582. https://doi.org/10.1127/0941-2948/2005/0057

Mason, R. S. (2013). *Atmospheric photochemistry* (R. C. Evans, P. Douglas, & H. D. Burrow, Eds.). Springer Netherlands. https://doi.org/10.1007/978-90-481-3830-2_5

Masson-Delmotte, V. P., Zhai, A., Pirani, S., Connors, C., Péan, S., Berger, N., Caud, Y., Chen, L., Goldfarb, M., Gomis, K., M. Huang, Leitzell, E., Lonnoy, J., Matthews, T., T.K. Maycock, Waterfield, O., Yelekçi, R., Yu, B., & (eds.), Z. (2021). *Summary for policymakers. in: Climate change 2021: The physical science basis. contribution of working group i to the sixth assessment report of the intergovernmental panel on climate change*. Cambridge University Press. https://doi.org/10.1017/9781009157896.001

Meinshausen, M., Raper, S. C. B., & Wigley, T. M. L. (2011). Emulating coupled atmosphere-ocean and carbon cycle models with a simpler model, MAGICC6 - Part 1: Model description and calibration. *Atmospheric Chemistry and Physics*, *11*(4), 1417–1456. https://doi.org/10.5194/acp-11-1417-2011

Naeem, M., Singh, R., & Probert, D. (1998). Implications of engine deterioration for fuel usage. *Applied Energy, Elsevier*.

Najjar, Y. S. (2013). Hydrogen safety: The road toward green technology. *International Journal of Hydrogen Energy*, *38*(25), 10716–10728. https://doi.org/10.1016/j.ijhydene.2013.05.126

Norris, G., & Wagner, M. (1998). *Boeing*. Osceola, Wis.

Omidvarborna, H., Kumar, A., & Kim, D. S. (2015). Recent studies on soot modeling for diesel combustion. *Renewable and Sustainable Energy Reviews*, *48*, 635–647. https://doi.org/10.1016/j.rser.2015.04.019

Ommi, F., & Azimi, M. (2012). Most effective combustion technologies for reducing Nox emissions in aero gas turbines. *The International Journal of Multiphysics*, *6*(4), 417–424. https://doi.org/10.1260/1750-9548.6.4.417

Onorato, G. (2021). *Fuel tank integration for hydrogen airliners delft university of technology [unpublished master's thesis]* [University Master Thesis], Delft University of Technology.

Oosterom, W. J. (2021). Flying-V Family Design [Unpublished Master's Thesis]. http://resolver.tudelft.nl/uuid:9e8f9a41-8830-405d-8676-c46bf6b07891

Osigwe, E. O., Gad-Briggs, A., Nikolaidis, T., Jafari, S., Sethi, B., & Pilidis, P. (2021). Thermodynamic performance and creep life assessment comparing hydrogen-and jet-fueled turbofan aero engine. *Applied Sciences (Switzerland)*, *11*(9). https://doi.org/10.3390/app11093873

Petzold, A., Gysel, M., Vancassel, X., Hitzenberger, R., Puxbaum, H., Vrochticky, S., Weingartner, E., Baltensperger, U., & Mirabel, P. (2005). On the effects of organic matter and sulphur-containing compounds on the CCN activation of combustion particles. *Atmospheric Chemistry and Physics*, *5*(12), 3187–3203. https://doi.org/10.5194/acp-5-3187-2005

Planès, T., Delbecq, S., Pommier-Budinger, V., & Bénard, E. (2021). Simulation and evaluation of sustainable climate trajectories for aviation. *Journal of Environmental Management*, *295*. https://doi.org/10.1016/j.jenvman.2021.113079

Proesmans, P., & Vos, R. (2021). Airplane design optimization for minimal global warming impact. *AIAA Scitech 2021 Forum*, 1–25. https://doi.org/10.2514/6.2021-1297

Prussi, M., O'Connell, A., & Lonza, L. (2019). Analysis of current aviation biofuel technical production potential in EU28. *Biomass and Bioenergy*, *130*(August), 105371. https://doi.org/10.1016/j.biombioe.2019.105371

Rao, A. G. (2019a). *Aero engine technology flight performance and propulsion - lecture 2: Thermodynamics* [University Lecture], Delft University of Technology.

Rao, A. G. (2019b). *Aero engine technology flight performance and propulsion - lecture 4: Aero engine efficiencies and classification* [University Lecture], Delft University of Technology.

Rao, A. G., Yin, F., & Van Buijtenen, J. P. (2014). A hybrid engine concept for multi-fuel blended wing body. *Aircraft Engineering and Aerospace Technology*, *86*(6), 483–493. https://doi.org/10.1108/AEAT-04-2014-0054

Reekers, M. (2021). Climate Effects of the Flying V [Unpublished Master's Thesis]. *TU Delft University*.

Reider, R., & Edeskuty, F. J. (1979). Hydrogen Satery Problems. *International Journal of Hydrogen Energy*, *4*, 41–45.

Ritchie, H. (2020). Climate change and flying: What share of global co2 emissions come from aviation? *Our World in Data*. Retrieved May 4, 2022, from https://ourworldindata.org/co2-emissions-from-aviation

Samset, B. H., Myhre, G., Schulz, M., Balkanski, Y., Bauer, S., Berntsen, T. K., Bian, H., Bellouin, N., Diehl, T., Easter, R. C., Ghan, S. J., Iversen, T., Kinne, S., Kirkeväg, A., Lamarque, J. F., Lin, G., Liu, X., Penner, J. E., Seland, O., … Zhang, K. (2013). Black carbon vertical profiles strongly affect its radiative forcing uncertainty. *Atmospheric Chemistry and Physics*, *13*, 2423–2434. https://doi.org/10.5194/acp-13-2423-2013

Schumann, U. (1996). On Conditions for Contrail Formation from Aircraft Exhausts. *Meteorol. Zeitschrift*, 4–23.

Seymour, K., Held, M., Georges, G., & Boulouchos, K. (2020). Fuel Estimation in Air Transportation: Modeling global fuel consumption for commercial aviation. *Transportation Research Part D: Transport and Environment*, *88*(October), 102528. https://doi.org/10.1016/j.trd.2020.102528

Slayton, R., & Spinardi, G. (2016). Radical innovation in scaling up: Boeing's Dreamliner and the challenge of socio-technical transitions. *Technovation*, *47*, 47–58. https://doi.org/10.1016/j.technovation.2015.08.004

Sorokin, A., Arnold, F., & Wiedner, D. (2006). Formation and growth of sulfuric acid-water cluster ions: Experiments, modelling, and implications for ion-induced aerosol formation. *Atmospheric Environment*, *40*(11), 2030–2045. https://doi.org/10.1016/j.atmosenv.2005.11.053

Ström, L., & Gierens, K. (2002). First simulations of cryoplane contrails. *Journal of Geophysical Research Atmospheres*, *107*(18), AAC 2–1–AAC 2–13. https://doi.org/10.1029/2001JD000838

Svensson, F. (2005). Potential of Reducing the Environmental Impact of Civil Subsonic Aviation by Using Liquid Hydrogen. (April).

Thatcher, D. R., & Jablonowski, C. (2016). A moist aquaplanet variant of the Held-Suarez test for atmospheric model dynamical cores. *Geoscientific Model Development*, *9*(4), 1263–1292. https://doi.org/10.5194/gmd-9-1263-2016

The Group of Twenty (G20). (2021). G20 Leaders Declaration. (June), 1–20.

Turgut, E. T., & Usanmaz, O. (2017). An assessment of cruise nox emissions of short-haul commercial flights. *Atmospheric Environment*, *171*, 191–204. https://doi.org/10.1016/j.atmosenv.2017.10.013

van Woensel, C. W. C. (2021). *Integration of a liquid hydrogen fuel tank into the concept of the flying-v [unpublished master's thesis]* [University Master Thesis], Delft University of Technology.

Voigt, C., Kleine, J., Sauer, D., Moore, R. H., Bräuer, T., Le Clercq, P., Kaufmann, S., Scheibe, M., Jurkat-Witschas, T., Aigner, M., Bauder, U., Boose, Y., Borrmann, S., Crosbie, E., Diskin, G. S., DiGangi, J., Hahn, V., Heckl, C., Huber, F., … Anderson, B. E. (2021). Cleaner burning aviation fuels can reduce contrail cloudiness. *Communications Earth & Environment*, *2*(1). https://doi.org/10.1038/s43247-021-00174-y

Vos, R. (2019). *Advanced aircraft design i - lecture 7: Reynolds effects* [University Lecture], Delft University of Technology.

Wei, P. S., Chiu, H. H., Hsieh, Y. C., Yen, D. L., Lee, C., Tsai, Y. C., & Ting, T. C. (2019). Absorption coefficient of water vapor across atmospheric troposphere layer. *Heliyon*, *5*(1), e01145. https://doi.org/10.1016/j.heliyon.2019.e01145

Whelan, G. M., Cawkwell, F., & Mannstein, H. (2017). The use of Meteorological Data to Improve Contrail Detection in Thermal Imagery over Ireland . (September 2009), 8–11.

Whiteley, M. (2018). European Aviation Fuel Burn and Emissions Inventory System for the European Environment Agency (for data from 2005, Version 2018.01). *Eurocontrol*, *01*. https://www.eurocontrol.int/publication/european-aviation-fuel-burn-and-emissions-inventory-system-feis-european-environment

Wilcox, L. J., Shine, K. P., & Hoskins, B. J. (2012). Radiative forcing due to aviation water vapour emissions. *Atmospheric Environment*, *63*, 1–13. https://doi.org/10.1016/j.atmosenv.2012.08.072

Yahya, M. Z. W., Azami, M. H., Savill, M., Li, Y. G., Khan, S. A., & Warimani, M. S. (2019). Modelling of a three-shaft high-bypass-ratio engine performance and emission prediction using hydrogen fuels. *International Journal of Innovative Technology and Exploring Engineering*, *8*(6), 484–490.

Zheng, X. S., & Rutherford, D. (2020). Fuel burn of new commercial jet aircraft: 1960 to 2019. *The International Council on Clean Transportation*, (September).

A

Data Filtering

The following list contains the aircraft ICAO from scheduled aviation. The ICAO code selection was conservative, as the type of aircraft should not be the bottle neck of the data. In the list, not only the main models of passenger aircraft are found, but also old and outdated models which are still flown in less developed countries.

A124, A140, A148, A158, A19N, A20N, A21N, A225, A306, A30B, A310, A318, A319, A320, A321, A332, A333, A337, A338, A339, A342, A343, A345, A346, A359, A35K, A388, A3ST, A400, AT72, AT73, AT75, AT76, ATP, B37M, B38M, B39M, B3XM, B461, B462, B463, B703, B712, B720, B721, B722, B732, B733,B734, B735, B736, B737, B738, B739, B741, B742, B743, B744, B748, B74D, B74R, B74S, B752, B753, B762, B763, B764, B772, B773, B778, B779, B77L, B77W, B788, B789, B78X, BCS1, BCS3, BLCF, C30J, C919, CONC, CRJ1, CRJ2, CRJ7, CRJ9, CRJX, DC10, DC85, DC86, DC87, DC91, DC92, DC93, DC94, DC95, DH8A, DH8B, DH8C, DH8D, E135, E145, E170, E190, E195, E290, E295, E75L, E75S, F100, F28, F50, F70, IL18, IL62, IL76, IL86, IL96, K35R, L101, MD11, MD81, MD82, MD83, MD87, MD88, MD90, P8, RJ1H, RJ70, RJ85, SU95, T134, T154, T204

The initial flight file contained the following information about each flight: flight number, callsign, operator ICAO code, operator name, airline ICAO code, aircraft ICAO code, aircraft registration, origin ICAO code, origin and destination IATA code, origin and destination airport name, origin and destination city name, origin and destination country, take off and landing date, take off and landing time, flight time and the flight radar 24 id number. Only the aircraft ICAO code, origin and destination IATA code, origin and destination country and flight time were kept.

B

Verification

The verification of the tool is a crucial step to ensure the correctness of any tool that has been used during the study. In this case the verification will be divided into different modules. Section B.1 verifies the techniques to ensure that no flight outliers existed on the created route data set. Section B.2 verifies one of the most complex modules of the study, which comprises the flight simulation and emission inventory creation, comparing the results to a commonly used software capable of achieving similar results. Finally, Section B.3 compares the final results to the results from Clean Sky (2020) to ensure that the climate module is working correctly.

B.1. Routing Design Verification

During the data processing the information was heavily modified. It is important to satisfy the requirements on flight distance, flight frequency and global coverage. The flight distance was verified using google, the distance between random airports in a sample was found. The distance from São Paulo airport (GRU) to Miami airport (MIA) for example is found to be 6553 km. From online references[1][2] it was observed 6554-6574 km. The same verification was performed for other flights and all yielded similar results, however when observing the maximum and minimum distances flown by different aircraft (using the "Max and Min Range" checkbox in Figure 3.3) an error was observed in one of the airports. The airport LIY in the US was written as LHW (an airport in China) making the distance between two points in Asia unrealistic. Same happened with the airport of UTH in Vietnam, it was confused with the Salt Lake regional airport. The last requirement is set on the global coverage of the flights. It will be verified by looking at the world graph generated by the program. Lines will represent the flights and it will make it possible to observe if the globe is being enfolded by the selected routes (Figure 4.1).

B.2. Verification of Flight Simulation

In this subsection, the most relevant modules of the flight simulation will be verified, the modules are: the flight planner, the auto pilot, the engine model, and the flight dynamics model. Finally, the complete code will be verified to ensure the weight loop is working correctly.

B.2.1. Flight Planner & Auto Pilot

The flight planner and the auto pilot control the time of the flight, and the altitude of the aircraft. The flight altitude was verified with Piano-X[3]. Piano-X is a software which calculates the flight performance

[1] Air Miles Calculator (2022, January 17) Distance between São Paulo (GRU) and Miami, FL (MIA), https://www.airmilescalculator.com/distance/gru-to-mia/

[2] Airport Distance Calculator (2022, January 17) Distance From Guarulhos International Airport to Miami International Airport (GRU - MIA Distance), https://www.airportdistancecalculator.com/flight-gru-to-mia.html#.YeWpi_go-3A)

[3] Lissys (2021, November 23) Piano-X, https://www.lissys.uk/PianoX.html

of a chosen aircraft. The chosen aircraft in this case was the A350-900 with the Trent XWB-84 engine model and the flight distance was set to 15000 km. The results displayed in Table B.1 compare the flight times for both the Piano-X and the developed tool (FS-tool).

Table B.1: FS tool verification for the climb and descent times of the A359.

Flight Phase	**Climb time [s] 0 - 11 km**	**Cruise time [s] @ 11 km**	**Descent time [s] 11 - 0 km**	**Total time [s]**
FS-Tool	1001	58319	1056	60375
Piano-X	1315	57886	1326	60527
Error	23.87 %	0.74 %	20.36 %	0.25 %

The observed difference is more pronounced during the climb and descent phases. This is because of the differences on the flight profile. During climb, the Piano-X tool accelerates on level flight, while the FS tool accelerates the aircraft while climbing, as observed in real flights on FlightRadar24. The climbing flight profile also diverges on the number of climb steps. Piano-X uses four different climb steps: from 0 to 1500 ft, from 1500 ft to FL100, from FL100 to Mach 0.82, from Mach 0.82 to FL360. The FS-tool uses three steps, as observed in Figure 3.6. The time to climb calculated by the Piano-X tool is larger due to the lower rate of climb in the different phases. In addition, the higher descent rates on the Piano-X tool cause the longer calculated descent time on the FS-tool. When changing the flight profile to match the profile of Piano-X the difference in flight time was reduced as shown in Table B.2.

Table B.2: FS tool verification for the climb and descent times of the A359.

Flight Phase	**Climb time [s] 0 - 11 km**	**Cruise time [s] @ 11 km**	**Descent time [s] 11 - 0 km**	**Total time [s]**
FS-Tool	1326	57468	1328	60122
Piano-X	1315	57886	1326	60527
Error	0.83 %	0.74 %	0.18 %	0.75 %

B.2.2. Engine Model Verification

It is important to identify the different blocks on the engine model, these are the engine model itself, the engine deck interpolation and the $EINO_x$ equations used. To verify the engine model the fuel flow of a certain point in flight from the previously mentioned A350-900 Trent XWB-84 can be compared with the engine model used in the tool. Different thrust settings and altitudes will be tested to verify the engine model. As it can be observed Table B.3 the engine model is very accurate around the design conditions but it is less accurate on off-design conditions. Moreover, the engine pressure ratios were chosen to match the fuel flow of the cruise, decreasing the accuracy on the climb and descent phases. During the descent phase, if the engine needs to provide negative thrust, the engine is set to idle conditions, where it needs to provide 4% of the maximum thrust. This percentage was calculated to match the fuel flow of Piano-X during the descent (4.63% error on the table).

Table B.3: FS engine model verification for different flight phases of the A359.

Flight Condition Fuel Flow	Cruise Alt: 11 km F = 57 kN M = 0.85	Climb Alt: 2.63 km F = 191 kN M = 0.441	Climb Alt: 0.457 km F = 224 kN M = 0.388	Descent Alt: 2.91 km F = 14 kN M = 0.445
Engine Model [kg/s]	0.84487	2.34501	2.76764	0.1805
Piano-X [kg/s]	0.84036	2.26834	2.54444	0.1725
Error w.r.t Piano-X	0.53 %	3.38 %	8.77 %	4.63%
Engine Deck [kg/s]	0.84659	2.34638	2.76772	0.1806
Error w.r.t Piano-X	0.74 %	3.44 %	8.77 %	4.69 %

The engine model is used to generate an engine deck and interpolate the fuel flow value. Therefore it is important to verify the functioning of the interpolation tool and the engine deck. The last row on Table B.3 displays the values obtained during the interpolation. It can be observed that the difference between the interpolation and the engine model is minimal. Although the error is more significant during the descent and climb phases the error is between bounds and will not affect the cruise phase.

B.2.3. Flight Dynamics Verification

The flight dynamics module calculates the required thrust at different stages of the flight. To verify that the module is working correctly the thrust required to climb, cruise and descent the aircraft can be calculated. Figure B.1 demonstrates that the thrust calculated at every step of the flight is correct, meaning that the aerodynamics and physics equations must be correct.

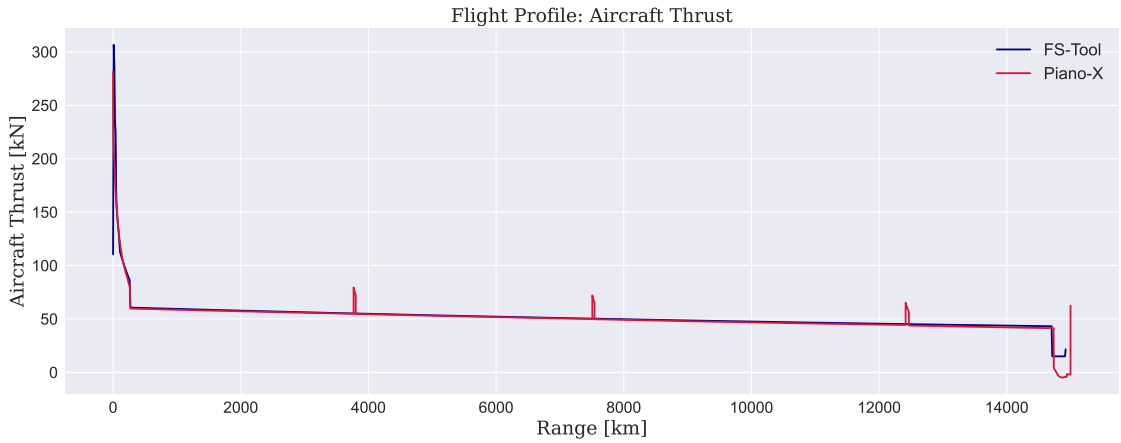

Figure B.1: Aircraft thrust for Piano-X and the FS-tool.

The peaks on thrust along the cruise phase on the Piano-X model correspond to the cruise climb steps. The FS-tool does not include these cruise steps.

B.2.4. Code Assembly verification

The final code assembly can be verified comparing the total weight of the aircraft along the flight. Figure B.2 compares the weight of the aircraft for both models, it can be observed that the fuel consumption of the FS-tool is slightly larger than the fuel consumption of the Piano-X model, this was already observed in the verification of the engine model. The total fuel consumed in the mission is 91560 kg for Piano-X and 92363 kg for the FS-tool. The total error is 1.47%, however, this error will increase for shorter flights were the cruise phase is not as relevant.

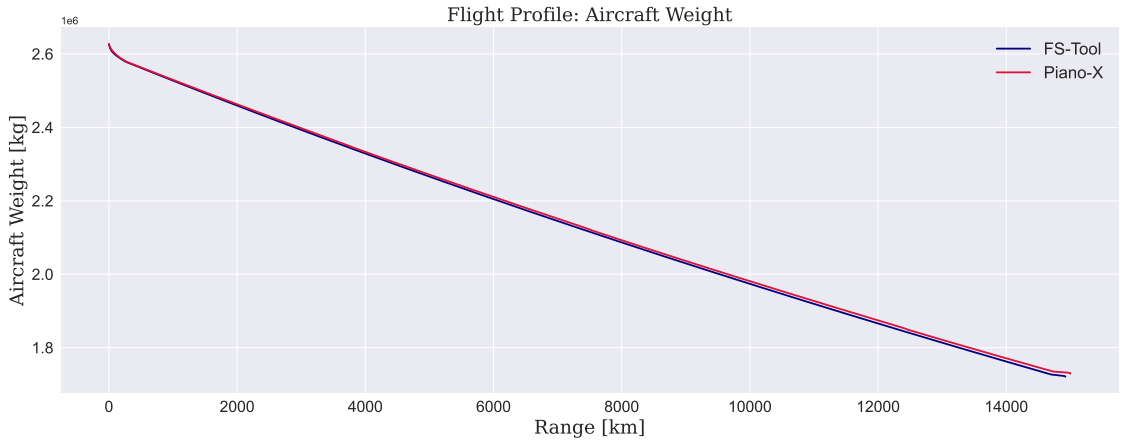

Figure B.2: Aircraft weight for Piano-X and the FS-tool.

If the fuel remaining after the flight is larger than the flight required for contingencies (loiter, diversion and contingency fuel), the new fuel weight should be added to the initial dry weight of the aircraft and the loop should start again. After a few iterations Figure B.3 displays a lower initial weight and thus a lower fuel consumption along the flight. In the last iteration, the fuel consumed during the mission is 89913 kg.

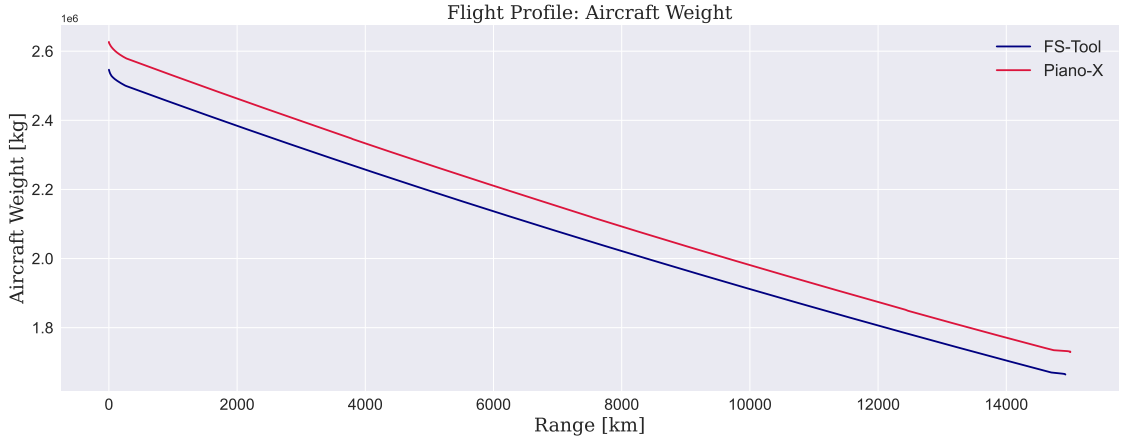

Figure B.3: Aircraft weight for Piano-X and the FS-tool including fuel weight iteration.

B.2.5. Hydrogen Consumption Verification

Hydrogen has an energy content per kilogram of 120 MJ, while kerosene has an energy content of 43 MJ. The ratio, and the expected fuel consumed during the mission for hydrogen should be around 2.79 times higher for kerosene. Table B.4 displays the kerosene FV and hydrogen FV fuel consumption for the different flight stages.

Table B.4: FS tool verification for hydrogen fuel consumption of the B767S and the FZM1G for the typical flight mission.

Flight Phase	Fuel during climb [kg] 0 - 11 km	Fuel during cruise [kg] @ 11 km	Duel during descent [kg] 11 - 0 km	Total fuel [kg]
B767S	2664	21673	392.4	24857
FZM1G	935	8853	124.8	9958
Ratio	2.84 %	2.45 %	3.14 %	2.49 %

It can be observed that the FZM1G is less efficient than the B767S as the ratio of fuel consumed is slightly lower than the energy ratio of hydrogen and kerosene. This is due to the engine overall efficiency being slightly higher for kerosene 0.412 than for hydrogen 0.404. During cruise, the hydrogen engine consumes less fuel due to the lower weight of hydrogen aircraft and the higher altitude.

B.2.6. NO_x Emission Verification

In this section the method to predict NO_x emissions will be verified using the values from Turgut and Usanmaz (2017). NO_x are difficult to model and predict, however, the values obtained for kerosene aviation in the study should be between certain bounds, as displayed in Table B.5.

Table B.5: NO_x emissions index literature estimations.

Description	$EINO_x$ g/kg fuel	Description	$EINO_x$ g/kg fuel
Global fleet (1991-1992)	16.8	Global fleet (2002–2025)	12.3 - 10.1
Global fleet (2000–2005)	13.8-14.3	Global fleet (±25%)	13.8
China domestic flights	12.7	Cruise (10 km; 0.82 Ma)	11.7–18.8
Cruise (B747-400)	10.0–13.0	Cruise (long range)	12.3–30.4

The $EINO_x$ obtained for the B767S in normal flight conditions is equal to 13.1 g/kg, which is between bounds of many of the estimations listed by Turgut and Usanmaz (2017). We can conclude that the model BFFM2 used predicts correctly the NO_x emissions.

B.3. Climate Impact Assessment Verification

The verification of the climate module is more challenging than the other modules. This section will compare the results with expected results from literature. Clean Sky (2020) reported the change on climate impact per emitted species, these are listed in Table B.6 next to the values obtained during the study. It must be mentioned that Clean Sky (2020) based their values on current aircraft technology.

Table B.6: Verification of the reduction of hydrogen combustion surface temperature change with respect to current kerosene technology with Clean Sky (2020).

Specie	CO_2	Contrails	NO_x	H_2O	Total
Clean Sky Hydrogen Combustion	-100 %	-30 to -50%	-50 to -80%	+150%	-50 to -75%
Hydrogen Aircraft	-100%	-50%	-62%	+374%	-67%

It can be observed that all the values are between bounds of the Clean Sky (2020) report except for the water vapour surface temperature change. The report assumes that the hydrogen aircraft emits 2.55 times more water vapour than the kerosene aircraft, while this study assumes an increase in 7.2. This number was achieved balancing the combustion equations as explained in Section 3.3.1.